PACIFIC EARTHQUAKE ENGINEERING RESEARCH CENTER

Blind Prediction of Shaking Table Tests of a New Bridge Bent Design

Selim Günay
Fan Hu
Khalid M. Mosalam

Department of Civil and Environmental Engineering
University of California, Berkeley

Arpit Nema
Jose Restrepo

Department of Civil and Environmental Engineering
University of California, San Diego

Adam Zsarnoczay
Jack Baker

Department of Civil and Environmental Engineering
Stanford University

PEER Report 2020/09
Pacific Earthquake Engineering Research Center
Headquarters, University of California, Berkeley

November 2020

PEER 2020/09
November 2020

Blind Prediction of Shaking Table Tests of a New Bridge Bent Design

Selim Günay

Fan Hu

Khalid M. Mosalam

Department of Civil and Environmental Engineering
University of California, Berkeley

Arpit Nema

Jose Restrepo

Department of Civil and Environmental Engineering
University of California, San Diego

Adam Zsarnoczay

Jack Baker

Department of Civil and Environmental Engineering
Stanford University

PEER Report 2020/10
Pacific Earthquake Engineering Research Center
Headquarters at the University of California, Berkeley

November 2020

ABSTRACT

Considering the importance of the transportation network and bridge structures, the associated seismic design philosophy is shifting from the basic collapse prevention objective to maintaining functionality on the community scale in the aftermath of moderate to strong earthquakes (i.e., resiliency). In addition to performance, the associated construction philosophy is also being modernized, with the utilization of accelerated bridge construction (ABC) techniques to reduce impacts of construction work on traffic, society, economy, and on-site safety during construction.

Recent years have seen several developments towards the design of low-damage bridges and ABC. According to the results of conducted tests, these systems have significant potential to achieve the intended community resiliency objectives. Taking advantage of such potential in the standard design and analysis processes requires proper modeling that adequately characterizes the behavior and response of these bridge systems.

To evaluate the current practices and abilities of the structural engineering community to model this type of resiliency-oriented bridges, the Pacific Earthquake Engineering Research Center (PEER) organized a blind prediction contest of a two-column bridge bent consisting of columns with enhanced response characteristics achieved by a well-balanced contribution of self-centering, rocking, and energy dissipation.

The parameters of this blind prediction competition are described in this report, and the predictions submitted by different teams are analyzed. In general, forces are predicted better than displacements. The post-tension bar forces and residual displacements are predicted with the best and least accuracy, respectively. Some of the predicted quantities are observed to have coefficient of variation (COV) values larger than 50%; however, in general, the scatter in the predictions amongst different teams is not significantly large.

Applied ground motions (GM) in shaking table tests consisted of a series of naturally recorded earthquake acceleration signals, where GM1 is found to be the largest contributor to the displacement error for most of the teams, and GM7 is the largest contributor to the force (hence, the acceleration) error. The large contribution of GM1 to the displacement error is due to the elastic response in GM1 and the errors stemming from the incorrect estimation of the period and damping ratio. The contribution of GM7 to the force error is due to the errors in the estimation of the base-shear capacity. Several teams were able to predict forces and accelerations with only moderate bias. Displacements, however, were systematically underestimated by almost every team. This suggests that there is a general problem either in the assumptions made or the models used to simulate the response of this type of bridge bent with enhanced response characteristics. Predictions of the best-performing teams were consistently and substantially better than average in all response quantities. The engineering community would benefit from learning details of the approach of the best teams and the factors that caused the models of other teams to fail to produce similarly good results.

Blind prediction contests provide: (1) very useful information regarding areas where current numerical models might be improved; and (2) quantitative data regarding the uncertainty of analytical models for use in performance-based earthquake engineering evaluations. Such blind prediction contests should be encouraged for other experimental research activities and are planned to be conducted annually by PEER.

ACKNOWLEDGMENTS

The blind prediction contest was supported by the Transportation Research Program (TSRP) of the Pacific Earthquake Engineering Research Center (PEER). Graduate student Yingjie Wu and PEER staff provided valuable help in the preparation and conduct of the shaking table tests. Erika Donald, PEER Communications Specialist, prepared the blind prediction website and PEER Associate Director, Amarnath Kasalanati, and Communications Director, Grace Kang, contributed to the announcement of the competition and supported other logistics. All these contributions are greatly acknowledged.

Any opinions, findings, and conclusions or recommendations expressed in this material are those of the authors and do not necessarily reflect those of PEER or the Regents of the University of California.

CONTENTS

LIST OF TABLES

LIST OF FIGURES

1 Introduction

1.1 MOTIVATION FOR THE BLIND PREDICTION CONTEST

As reported by the U.S. Geological Survey (USGS) [2014], at least 40% of the U.S. can experience earthquakes with the potential to damage highway bridges within their lifetime. This hazard has the potential to turn to a disaster considering that 54,560 bridges across the country are already considered structurally deficient as of 2017 and the U.S. bridge infrastructure scored a C+ grade in American Society of Civil Engineers' 2017 Infrastructure Report Card (*https://www.infrastructurereportcard.org/*). These bridges often serve as key links in the local and national transportation networks. Their potential closures lead to financial losses beyond the costs of repair or replacement, including: (1) economic losses related to medium- and long-term interruption of local businesses; and (2) and disruption of local communities [Palermo and Pampanin 2008]. Additionally, the importance of these bridges increases significantly in the aftermath of any seismic event in terms of emergency response and recovery.

Considering the importance of these structures, the associated design philosophy is shifting from the basic collapse prevention objective to maintaining functionality in the aftermath of moderate to strong earthquakes, i.e., the concept of resiliency. In addition to performance, the associated construction philosophy is also being modernized with the utilization of accelerated bridge construction (ABC) techniques to reduce impacts of construction work on traffic, society, economy, and on-site safety during construction.

Recent years have seen several developments towards the design of low-damage bridges and ABC. According to the results of conducted tests, these systems have significant potential to achieve the intended resiliency objectives. Taking advantage of such potential in the standard design and analysis processes requires proper modeling that adequately characterizes the behavior and response of these systems.

To evaluate the current practices and abilities of the structural engineering community to model this type of resiliency-oriented bridges, the Pacific Earthquake Engineering Research Center (PEER) organized a blind prediction contest of a two-column bridge bent consisting of columns with enhanced response characteristics achieved by a well-balanced contribution of self-centering, rocking, and energy dissipation. This two-column bridge bent was tested on the UC Berkeley's six-degrees-of-freedom (DOF) shaking table in September 2017. The contestants of the competition were provided with all the data required to develop an analytical model and conduct nonlinear time-history analysis. Provided data included the ground motions measured on the table, geometry of the columns, footing and the cap beam, reinforcement details, material properties obtained from tests of steel and concrete samples, geometry and mass of the weight blocks, post-tension details, and construction drawings. Using the analysis results obtained from their developed analytical models, contestants were expected to predict different response quantities that included peak and residual horizontal displacements, vertical uplift of the cap beam, lateral and vertical inertia forces, overturning moment, and peak and residual post-tension bar forces.

Expected outcomes and benefits of the conducted blind prediction exercise include:

1. To highlight the gap between analysis and experiments.
2. To identify the sources of the differences between analytical and experimental results and evaluate the sources of any systematic errors.
3. To test the capabilities of simulation software to model actual behavior observed in experiments.
4. To enhance the predictive capabilities of models by exercising them in new ways.
5. To encourage modelers to understand and deal with the complexities of real experiments and real-life conditions.
6. To evaluate the modeling and analysis errors for different performance levels.
7. To develop methods for systematically improving analytical predictions.
8. To provide suggestions for future blind prediction contents.

1.2 ORGANIZATION OF THE REPORT

The report contains seven chapters. Chapter 2 describes the experimental program of the two-column bridge bent with enhanced response characteristics. The test setup is described along with the utilized innovative features, descriptions of the columns, cap beam and the footing, material properties, and the utilized ground motions and test matrix. Chapter 3 elaborates on the test results in terms of the measured response quantities and the behavior of the specimen after each ground motion.

Chapter 4 describes the organization and rules of the contest, the criteria used to score the predictions, the winners of the contest and their predictions compared against the experimental results, and the results of the other teams. In addition, it reports the statistics of the conducted survey.

Chapter 5 presents the results of statistical analysis including: mean and median error, coefficient of variation, bias, accuracy estimated error, lognormal distribution of average error over the nine ground motions for all predicted quantities, and histograms that show the error of the predicted displacement and acceleration quantities for different ground motions. This chapter also focuses on the evaluation of single and combined model performances, and evaluates the predicted error bounds.

Chapter 6 studies the effects of different modeling aspects on the predictions. Finally, Chapter 7 presents a summary of the main findings and conclusions.

2 Description of the Experimental Program

The specimen used for the blind prediction contest was tested dynamically on the PEER shaking table located at the UC Berkeley Richmond Field Station. The primary objective of the experiment was the study of a multi-column bridge bent designed for hybrid re-centering behavior. As a secondary objective, the study also focused on the development of an alternate precast (automated) construction technique for ABC. This study continues the research performed under the PEER Transportation Systems Research Program (TSRP) by Guerrini et al. [2013; 2015] where single column bents were tested under cyclic and dynamic loading. The design and construction details of the experiment are presented in this chapter.

2.1 DESIGN AND CONSTRUCTION

The prototype bent for the experiment was derived from Bent 3 of the Massachusetts Avenue Over Crossing (MAOC) bridge, located within 5.8 km (3.6 miles) of the San Andreas Fault. The existing bridge consists of four bents, each with four cast-in-place, fixed-end columns spaced at 3.067 m (120.5 in.) on center. Each column is reinforced with 22 No. 36 (Imperial size #11) Gr 60 bars, for a longitudinal reinforcement ratio (ρ_l) of 1.9%. Bent 3 of the bridge has a clear height of 9.6 m (378 in.), with a foundation size of 13 m × 3.45 m × 1.22 m (512 in. × 136 in. × 48 in.) and a bent cap size of 14.85 m × 1.83 m × 1.37 m (585 in. × 72 in. × 54 in.). Complete details of the bridge are presented in Nema [2018].

For the hybrid column design of the prototype re-centering bent, a portion of the longitudinal steel in the MAOC bridge columns (A_{st}) was replaced with unbonded post-tensioning steel (A_{sPT}) and steel bars for energy dissipation (A_{sED}). This replacement was conducted while maintaining equal levels of steel strength between the original and innovative columns, following Equation (2.1). Additional criteria for the replacement of mild steel with post-tensioning steel are given in Equation (2.2a) and (b), developed in Guerrini et al. [2015]. The limit on the re-centering coefficient (Λ_C) ensures the closure of the opening in the rocking interface to achieve the re-centering of the system by keeping the total nominal force capacity of steel bars for energy dissipation, $F_{ED,o}$, smaller than the sum of the axial force on the column determined from factored load combination (P_u) and the initial elastic post-tensioning force ($F_{PT,e}$). The limit on the energy-dissipation coefficient (Λ_D) ensures sufficient energy-dissipation capacity in the system to avoid the development of large lateral displacement and acceleration demands.

$$A_{st}f_y = A_{sED}f_{yED} + A_{sPT}f_{yPT} \tag{2.1}$$

$$\Lambda_{\mathrm{C}} = \frac{F_{ED,o}}{P_u + F_{PT,e}} \leq 1.0 \tag{2.2a}$$

$$\Lambda_{\mathrm{D}} = \frac{F_{ED,o}}{P_u + F_{PT,e} + F_{ED,o}} \geq 0.1 \tag{2.2b}$$

In addition to changes in the steel reinforcement for the prototype, the bridge gradient (2%) and skew were ignored for simplicity, and the number of columns was reduced from four in the bridge to two in the prototype. The reduction in the number of columns was required to optimize the experimental setup for the force and displacement capabilities of the shaking table while maintaining a suitable scale for the test specimen. This change required adjustments to the bent geometry—specifically the distance between columns in the prototype—to achieve similar levels of stresses in the prototype columns and the two end columns in the four-column bridge bent. For this purpose, a preliminary parametric study was conducted using analytical models of the prototype and the bridge as detailed in Nema [2018].

The final prototype consisted of two hybrid re-centering columns spaced 4.2 m (58 in.) on center. Post-tensioning was provided by a 10.82 m (275 in.) unbonded length of 8 × 4-15 mm (0.6-in.) Gr 270 strands (f_{pu} = 1860 MPa = 270 ksi) with an initial prestress of 40% f_{pu} (GUTS), assumed to span from mid-depth of the foundation to mid-depth of the bent cap. The expected strength of concrete was assumed to be 46 MPa (6.7 ksi), which is equivalent to the expected concrete strength used in the analytical bridge model. Mild-steel reinforcement in each column consisted of ten No. 36 (#11) ASTM A706 Grade 60 bars, which were debonded from the concrete over a height of 0.5 m (19.69 in.) at each rocking interface. For analytical purposes, the bar-bond development length was assumed to be 10-bar diameters on each end of the debonded bar resulting in an effective debonded length of 1.22 m (48.03 in). An illustration of this concept is shown in Figure 2.1. The debonding is required to prevent early dissipator fracture since the gap opening results in large inelastic deformations in the mild-steel reinforcement crossing the rocking interface.

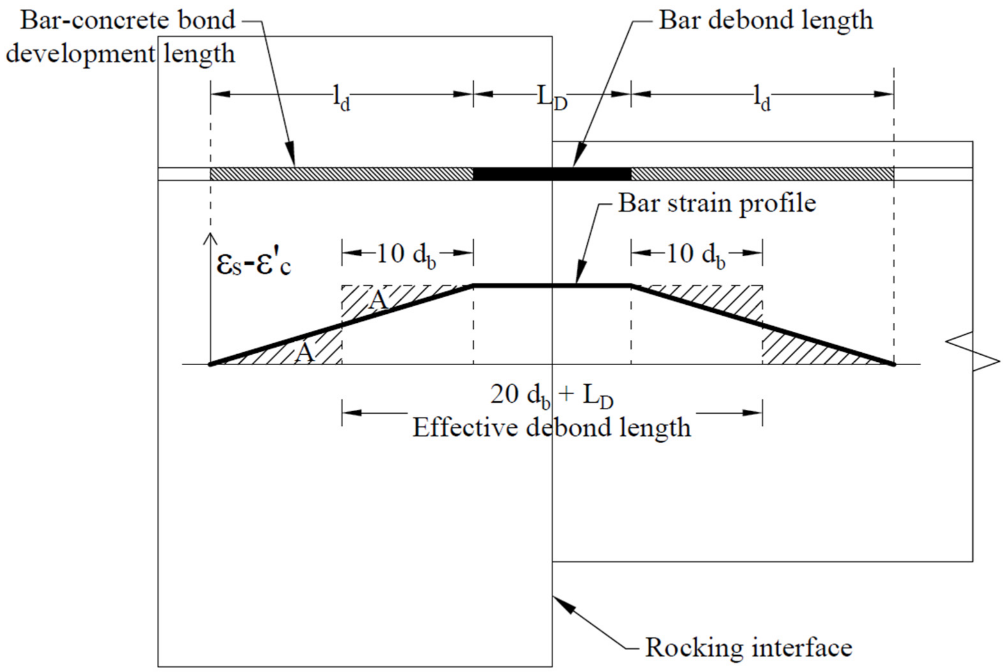

Figure 2.1 **Reinforcement bar debonding at rocking interface.**

Table 2.1 **Comparison of re-centering (Λ_C) and energy-dissipation (Λ_D) coefficients between prototype and Guerrini et al. [2015].**

	Mild Steel	PT Steel	Λ_C	Λ_D
Prototype	10 × No. 36	32 × 15 mm	0.84	0.46
Guerrini et al. [2015], Unit 1A	6 × 14.3 mm	4 × 35 mm	0.42	0.29
Guerrini et al. [2015], Unit 1B	6 × 12.7 mm	4 × 35 mm	0.60	0.37

The dimensions of the cross section of the foundation and the bent cap are the same as those in the bridge. The effective inertial and gravity loads applied to the prototype bent are 2.55 MN (573 kip), estimated from the tributary length of the bridge deck corresponding to Bent 3. Table 2.1 compares the parameter values given by Equation (2.2a) and (b) for the prototype and the test specimen in Guerrini et al. [2015].

The test specimen was obtained by scaling down the prototype by a factor of $S_l = 0.35$ to limit the expected forces and displacements within the shaking table limits. An important objective is to maintain similarity in terms of stresses between the prototype and the specimen, which called for the provision of additional seismic mass in the specimen and required applying compression in time of the ground-motion histories. The seismic mass was provided by the bent cap and six concrete blocks post-tensioned to the bent cap, representing the bridge superstructure. This splitting of the seismic mass was needed so that components could be safely picked up by the indoor crane in the laboratory.

The joints between the columns and the foundation/bent cap were formed using socket connections. This eliminated the need for a mortar layer at the rocking interface, which could be a limiting factor for the column response; see Restrepo et al. [2011]. Details of the scaling procedure and the design and construction of the columns, foundation, and bent cap are presented in the following sections.

2.1.1 Scaling

The specimen scaling procedure involved mass substitution in addition to geometrical scaling. The additional mass was required for similitude between stresses in the specimen and the prototype. Scaling in the model space without mass substitution is derived from the length scale, defined as the ratio of the model unit length to the prototype unit length, as defined by Equation (2.3a). The remaining scale factors are derived from the length scale factor assuming consistent mass density and mass material modulus between the prototype and the specimen, and are listed in Equations (2.3b) to (2.3g).

Length
$$S_l = \frac{l_m}{l_p} = 35\% \tag{2.3a}$$

Area
$$S_A = \frac{A_m}{A_p} = \frac{l_m^2}{l_p^2} = S_l^2 \tag{2.3b}$$

Volume
$$S_V = \frac{V_m}{V_p} = \frac{l_m^3}{l_p^3} = S_l^3 \tag{2.3c}$$

Mass
$$S_M = \frac{M_m}{M_p} = \frac{\rho V_m}{\rho V_p} = S_l^3 \tag{2.3d}$$

Force
$$S_F = \frac{F_m}{F_p} = \frac{M_m g}{M_p g} = S_l^3 \tag{2.3e}$$

Stress
$$S_\sigma = \frac{\sigma_m}{\sigma_p} = \frac{F_m/A_m}{F_p/A_p} = S_l \tag{2.3f}$$

Stiffness
$$S_K = \frac{K_m}{K_p} = \frac{EA_m/l_m}{EA_p/l_p} = S_l \tag{2.3g}$$

As can be observed from Equation (2.3f), the stresses in the model space are scaled by the factor S_l. To impose similitude in terms of stresses, additional mass is added to the system such that Equation (2.3f) with the total modified mass results in a scale factor of 1. The additional mass required can then be obtained from the total model space mass necessary for stress similitude. This relation is expressed in Equation (2.4a). Finally, the time-scale factor can be obtained using the masses and stiffnesses in the model and prototype space; see Equation (2.4b). Accordingly, the resulting acceleration scale factor is 1.

$$S'_{\sigma} = 1 = \frac{M'_{m}g/A_m}{M_p g/A_p} \Rightarrow M'_m = M_p S_l^2 = \frac{M_m}{S_l} \tag{2.4a}$$

$$\Delta \mathrm{M_m} = M'_m - M_m = M_m \frac{(1 - S_l)}{S_l}$$

Time

$$S'_T = \frac{T_m^2}{T_P^2} = \frac{\sqrt{M'_m/K_m}}{\sqrt{M_p/K_p}} = \sqrt{S_l} \tag{2.4b}$$

Acceleration

$$S'_a = \frac{l_m/T_m^2}{l_m/T_P^2} = 1 \tag{2.4c}$$

2.1.2 Column

Specimen overview, including the columns, bent cap, foundation, and the mass blocks, is shown in Figure 2.2. The column design was based on the scaled prototype column. Each column had an external diameter of 406 mm (16 in.). Ten #4 (12.7 mm dia.) A706 Grade 60 reinforcing bars provided the longitudinal reinforcement; a 152 mm (6 in.) length of each reinforcing bar at the rocking interface was debonded from the surrounding concrete using duct tape to prevent large strains. Three separate #3 (9.5-mm diameter) A706 Grade 60 spirals were used to hold the longitudinal reinforcement together; the splitting of the spiral was necessary to prevent the transverse spirals from contributing to energy dissipation by yielding at the rocking interface. The use of spirals was only for construction purposes since the column outer shell provided the majority of shear and confining reinforcement.

Due to the difficulty in sourcing 9.5-mm- (3/8 in.) diameter strands, and to aid in monitoring post-tensioning forces, the strands in the prototype were replaced by a single 36-mm- (1-3/8-in.-) diameter ASTM A722 Grade 150 threaded post-tensioning bar, which had a yield strength capacity equal to that of ten (10) 9.5-mm- (3/8-in.-) diameter strands. The bar anchorage was embedded inside the column bottom before the pouring of concrete, and the PT bar itself was enclosed inside a 51-mm- (2-in.-) inner-diameter (ID) PVC sleeve to debond it from the concrete. The PT bar was left inside the sleeve during the pouring of concrete to help keep the PVC sleeves aligned. The top end of the bar was extended from the top of the column for the placement of a concentric load measuring cell resting on the bent-cap. This extension also proved helpful in guiding the bent cap in place during assembly.

The use of a dry-socket connection to connect the columns to the foundation and the bent cap allowed for an innovative construction method. The entirety of each column was formed by inserting the reinforcement cage inside a segmented steel shell, assembled from 6.4-mm- (0.25-in.-) thick ASTM A53 Grade B pipe, followed by the pouring of 41.4 MPa (6 ksi) concrete. The steel pipe served as a permanent formwork, provided a force transfer mechanism between the column and end beams; it also served as confinement to ensure satisfactory rocking performance. To allow rocking at the beam–column interface, the pipe was segmented into five sections: (1) two end sections embedded inside the socket connection were provided with weld beads outside and inside for developing composite action; (2) one central section over the column clear height; and

(3) finally two thin removable open strips: one strip between the central section and each of the two end sections. The five segments were spot-welded together at a few locations to form the single pipe unit used for casting each column. These spot welds were ground off, and the thin strip segments removed to form the rocking interface in the assembled specimen. Some photographs from the column construction process are shown in Figure 2.3 and Figure 2.4.

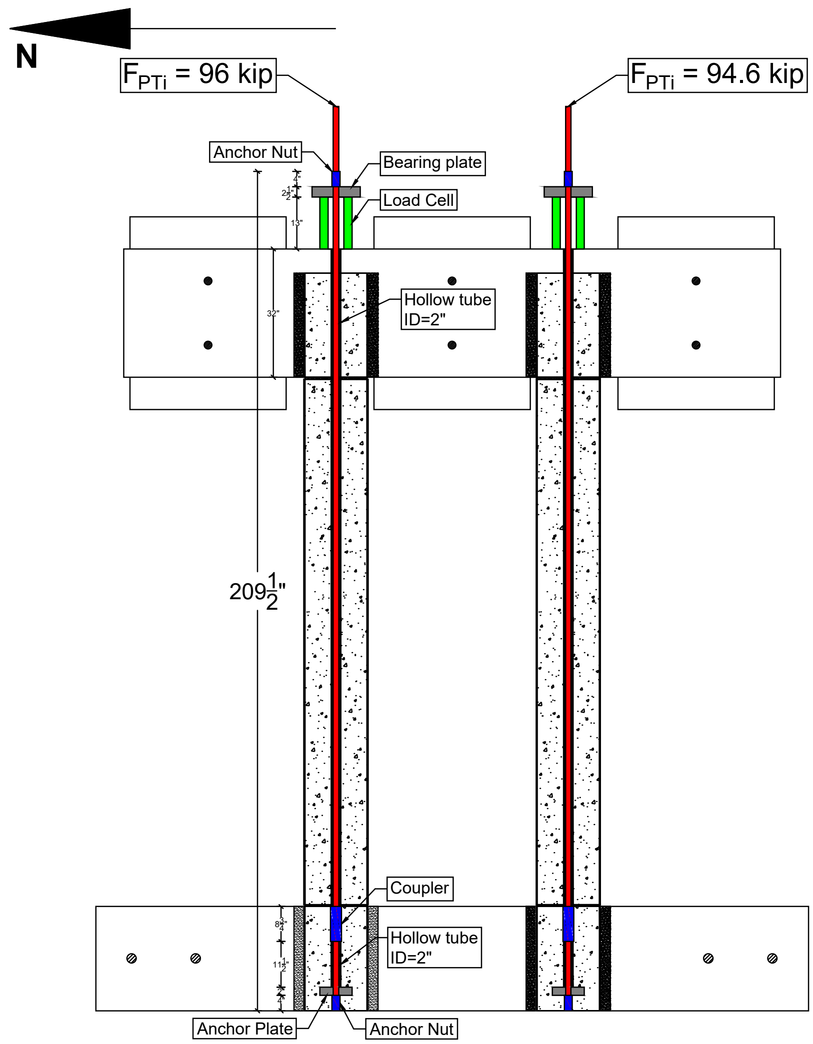

Figure 2.2 **Specimen overview.**

(a)

(b)

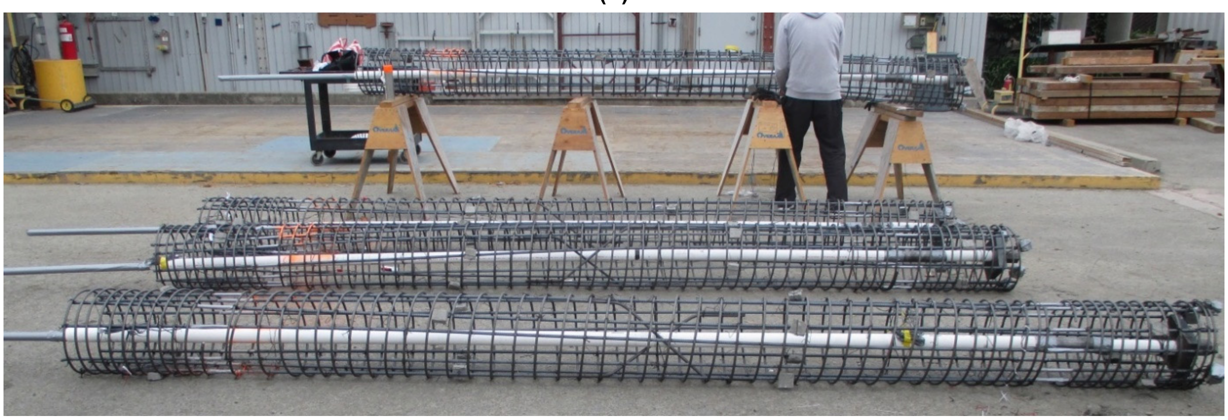

(c)

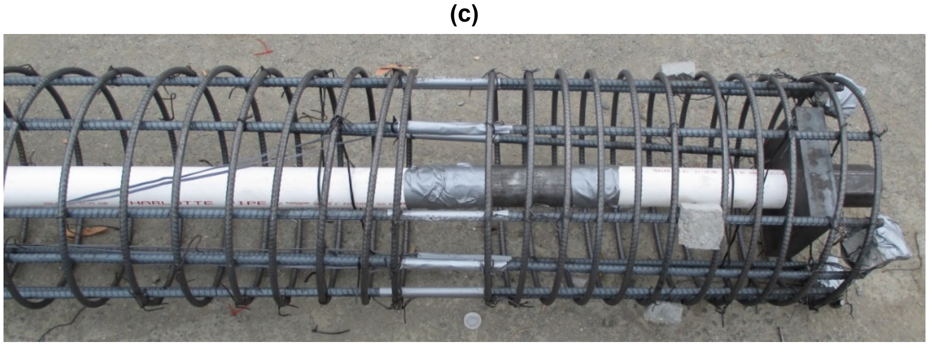

(d)

Figure 2.3 Column reinforcement details: (a) column steel shells; (b) weld beads at column ends; (c) column reinforcement cages; and (d) mild steel debonding detail.

Figure 2.4 Column casting setup.

2.1.3 Foundation

The foundation was designed around the socket connection. The socket for accommodating each column was formed out of a 559-mm- (22-in.-) ID corrugated metal pipe (CMP). The foundation width was set to 965 mm (38 in.) to allow 203 mm (8 in.) of space on either side for placing reinforcement and provide cover. The foundation depth was set to 660 mm (26 in.) for bond development between the column and the foundation in the socket. Finally, a foundation length of 4521 mm (178 in.) was selected to accommodate tie-downs for securing the foundation to the shaking table.

Primary reinforcement design was done following the strut-and-tie method as prescribed in § 5.6.3 of *AASHTO LRFD Bridge Design Specifications*, 7th ed. [2012]. The column axial load was assumed to be transferred directly to the shaking table, while lateral loads were assumed to be transferred by lateral bearing at the top and bottom of the socket. The strut and tie model indicated that the socket-type of joint requires extra crossties around the connection to prevent splitting of the foundation in the longitudinal direction due to the bearing forces arising from the transfer of column shears to the foundation. Additional staples were provided around the socket to prevent any splitting due to out-of-plane forces. This reinforcement, while not necessary for the specimen, is necessary for the bridge foundations. A picture of the foundation reinforcement around the socket connection detail is shown in Figure 2.5.

Figure 2.5 Socket detail in foundation.

2.1.4 Bent Cap

The bent-cap design revolves around the socket connection. The socket was formed from 559-mm- (22 in.) ID, 660-mm- (26 in.) deep CMP, and the beam width was 965 mm (38 in.). Unlike the foundation, vertical loads need to be transferred from the bent cap to the columns; therefore, a 152-mm- (6-in.-) thick layer of reinforced concrete (RC) was placed on top of the column sockets for a total bent-cap depth of 813 mm (32 in.). The contribution of the bond development in the socket was ignored as a safety measure. The bent-cap length was set at 4166 mm (164 in.) to accommodate the six concrete blocks needed to simulate the superstructure mass.

The reinforcement design was done using the strut-and-tie method, in a manner similar to the foundation design. The vertical load was transferred from the bent cap to the column via bearing against the top layer of concrete, strengthened by straight- and bent-hanger reinforcement. As in the foundation, additional crossties and staples were provided to prevent the beam from splitting in the longitudinal and transverse direction.

A 51-mm (2-in.) ID opening was allowed in the 152.4-mm (6-in.) top layer above each socket to allow the PT bars to pass through. Additional smaller openings were provided near the socket periphery to allow the pouring of the grout. Additional 51-mm (2-in.) ID sleeves were provided through the vertical faces of the bent cap at the three locations where the six concrete blocks were anchored. Photographs of the bent-cap reinforcement and the socket-connection detail are shown in Figure 2.6(a) and (b).

(a)

(b)

Figure 2.6 Bent cap reinforcement: (a) socket reinforcement detail in bent cages; and (b) assembled reinforcement cage.

2.1.5 Superstructure Mass

The superstructure mass in the specimen was provided by the bent cap and six concrete blocks measuring 1219 mm × 1219 mm × 991 mm (48 in. × 48 in. × 39 in.). This split in the superstructure mass was done to limit the weight of the bent cap and the blocks to within the lifting capability of the indoor crane at the shaking table. Each block had a mass of nearly 3550 kg, and blocks were installed in pairs on each side of the bent cap at three locations. Minimum reinforcement was provided for each block and was distributed as skin reinforcement on each face of the blocks. The blocks were installed at mid-height on the bent cap to avoid introducing artificial rotational mass moment of inertia.

2.1.6 Specimen Assembly

The precast columns, foundation, and bent cap were manufactured offsite by a precast concrete fabricator and delivered to the UC Berkeley Richmond Field Station Laboratory for assembly and testing. Before starting the assembly, the 6.4 mm (0.25 in.) steel strips located at the column rocking interface were removed by grinding off the spot welds and prying apart the strips; see Figure 2.7. The PT bars extending out from the top of the columns were covered with a few layers of duct tape to prevent any bonding to the grout in the sockets. At the same time, the foundation was installed on a bed of gypsum on the shaking table and tied down with a total force of 1.33 MN (300 kips) exerted through three tie-down bars. Once the foundation was installed, the shaking table was calibrated to the input ground motions for accurate reproduction of the response spectra.

With the foundation installed and the shaking table calibrated, columns were leveled inside the foundation socket, anchored down to maintain their level (Figure 2.8) and non-shrink grout was poured in the gap between each column and the CMP forming the foundation socket; see Figure 2.9. The grout was then allowed to set for three days before beginning the placement of the bent cap on top. This time was spent creating wooden formwork support for the bent cap.

In preparation of bent-cap installation, 12.7-mm (0.5-in.) shim blocks were placed on top of the columns, and the column tops covered with wet rags to ensure proper setting of the grout. The bent cap was then lifted above the columns and brought down carefully until it was lightly resting and centered on the columns; see Figure 2.10. The centering of the bent cap was aided by the PT bars extending out from the top of the columns. The bent cap was leveled on top of the columns by adjusting the wooden support, after which the supports were strengthened further by cross braces. With the bent cap in place and leveled, the bottoms of the sockets were sealed up (Figure 2.11) and grout was poured from the top; see Figure 2.12. Typically, a thin layer of grout should be first poured into each socket and allowed to harden for a day before completely filling the sockets with grout. This measure is to further strengthen the seal at the bottom of the socket and prevent any leaks due to the weight of the grout.

(a) (b)

Figure 2.7 Steel strip removal from columns: (a) removal of shell strip; and (b) strip removed.

Figure 2.8 Column placement.

Figure 2.9 Grouting of columns in foundation socket.

Figure 2.10 Bent-cap placement.

Figure 2.11 Sealing bent cap socket bottom.

Figure 2.12 Grouting bent cap socket

The grout in the bent cap was allowed to set for three days, after which the PT bars extending out from the top were moderately tensioned. The concrete blocks were post-tensioned to the bent cap with a total force of 445 kN (100 kips) for each set of two blocks, exerted through two 25.4-mm (1-in.) PT bars passing through the blocks and the bent cap; see Figure 2.13

Since the specimen was designed to be tested under transverse and vertical shaking only, two restraint frames, each consisting of two A-frames connected by a diagonal and horizontal W section for lateral stability, were erected to limit any twisting or motion in the longitudinal (out-of-plane) direction; see Figure 2.14. The specimen was allowed to slide on low-friction surfaces formed by greased wooden shims attached to the concrete blocks and the horizontal W-section beam connecting the A-frames. The frame installation was done concurrently with the installation of the concrete blocks. When the installation of the blocks and restraining frames was finished, the column PT bars were tensioned to the target stress of 40% GUTS, for a target force of 422 kN (94.8 kips) on each bar.

Figure 2.13 Superstructure mass block installation.

Figure 2.14 Completed specimen.

2.2 MATERIAL PROPERTIES

2.2.1 Concrete

The specified strength of concrete for the foundation, bent cap, and the columns was 41.4 MPa (6 ksi). The actual compressive strength was measured using 152-mm- (6-in.-) diameter and 305-mm- (12-in.-) high standard concrete cylinders. The foundation and bent cap were cast from the same batch of concrete, while the columns were cast together from a different batch. The same mix design was used for both concrete batches, with a large aggregate size of 25.4 mm (1 in.).

Before the testing of the specimen, six cylinders were tested on different two days to track the development of concrete strength. Additionally, on the first day of testing six cylinders from each batch of concrete were tested using a compressometer to obtain their stress–strain profile in addition to the crushing strength. The average strengths measured on each day of testing are listed in Table 2.2 and the average stress-strain response from the compressometer tests are shown in Figure 2.15. A comparison of the measured modulus of elasticity to the value calculated following Eq. 19.2.2.1.b, ACI 318-14 shows that the ACI equation underestimates the initial concrete stiffness.

Table 2.2 Measured compressive strength of cementitious materials

Material	Age (days)	Compressive strength		Young's modulus, measured		Young's modulus, ACI	
		(MPa)	(ksi)	(GPa)	(ksi)	(GPa)	(ksi)
Foundation / bent-cap concrete	14	31.1	4.51	n/a		n/a	
	32	37.6	5.45				
	73 (DOT)	41.9	6.08	36.0	5220	30.6	4440
Column concrete	7	30.5	4.42	n/a		n/a	
	22	34.6	5.02				
	48 (DOT)	47.5	6.89	39.6	5750	32.6	4731
Infill grout	22 (DOT)	47.4	6.87	n/a		n/a	

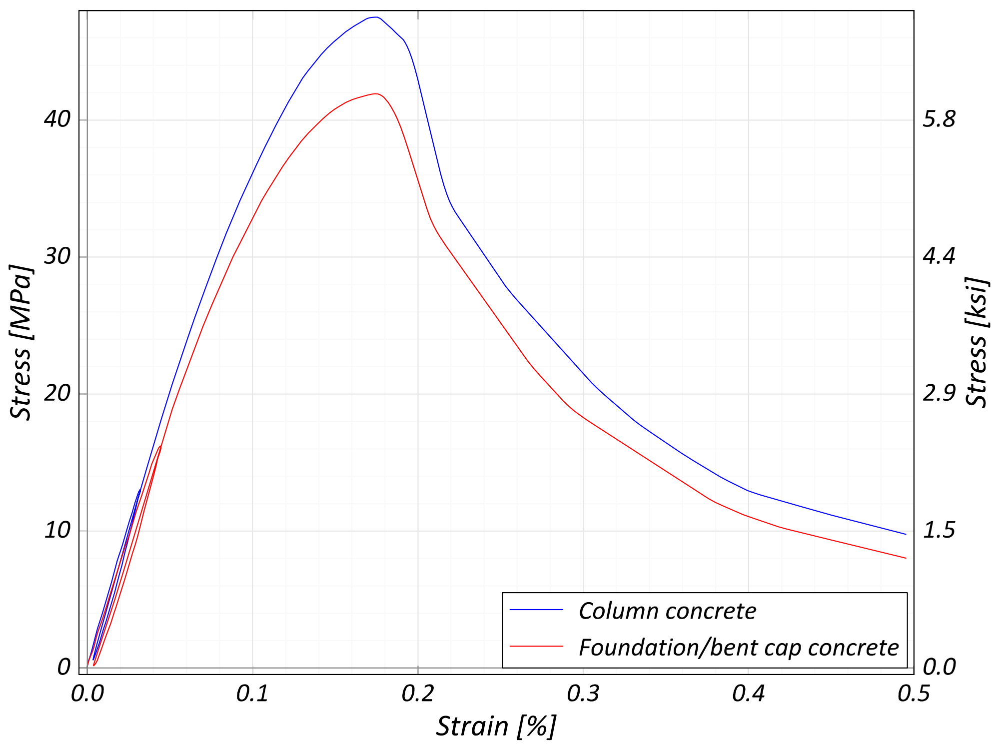

Figure 2.15 Concrete material stress–strain response.

2.2.2 Infill Grout

BASF MasterFlow® 928 non-shrink grout, mixed to a fluid consistency, was used for grouting the gap between the columns and the CMP socket walls. Compressive strengths were measured on the day of the test on 51-mm- (2-in.-) diameter and 102-mm- (4-in.) tall standard cylinders. The average strength from three cylinders is reported in Table 2.2.

2.2.3 Longitudinal Reinforcement (Hysteretic Energy Dissipators)

Three samples, each 457 mm (18 in.) long, of the A706 Grade 60 #4 bar used in the column reinforcement were tested under monotonic tension to characterize the material. The average properties of the three samples are reported in Table 2.3, and the full stress–strain relation is shown in Figure 2.16 Note that the uniform strain is taken as the minimum strain at peak stress from among the three samples.

2.2.4 Prestressing Steel

Three specimens, each 610 mm (24 in.) long, of the ASTM A722 Grade 150 threaded bar used for post-tensioning the columns were tested under monotonic tension to characterize the material. The average properties of the three samples are reported in Table 2.3, and the full stress–strain relation is shown in Figure 2.17.

2.2.5 Shell Steel

Three A53 samples obtained by straightening some of the 6.4-mm (0.25-in.) strips removed from the column outer steel shell at the rocking interface were tested under monotonic tension to characterize the material. The average properties of the three samples are reported in Table 2.3, and the full stress–strain relation is shown in Figure 2.18. For the strips, the strain recording was stopped at 1.8% strain, and only the ultimate strength was reported beyond that point.

Table 2.3 Measured steel mechanical properties.

Material	Elastic nodulus		Yield stress		Yield strain (%)	Peak stress		Uniform strain (%)
	(MPa)	(ksi)	(MPa)	(ksi)		(MPa)	(ksi)	
A706	192,000	27,900	489	70.9	0.45	681	98.8	10
A722	217,000	31,400	939	136	0.63	1,100	160	7.0
A53	188,000	27,200	339	49.2	0.38	461	66.9	n/a

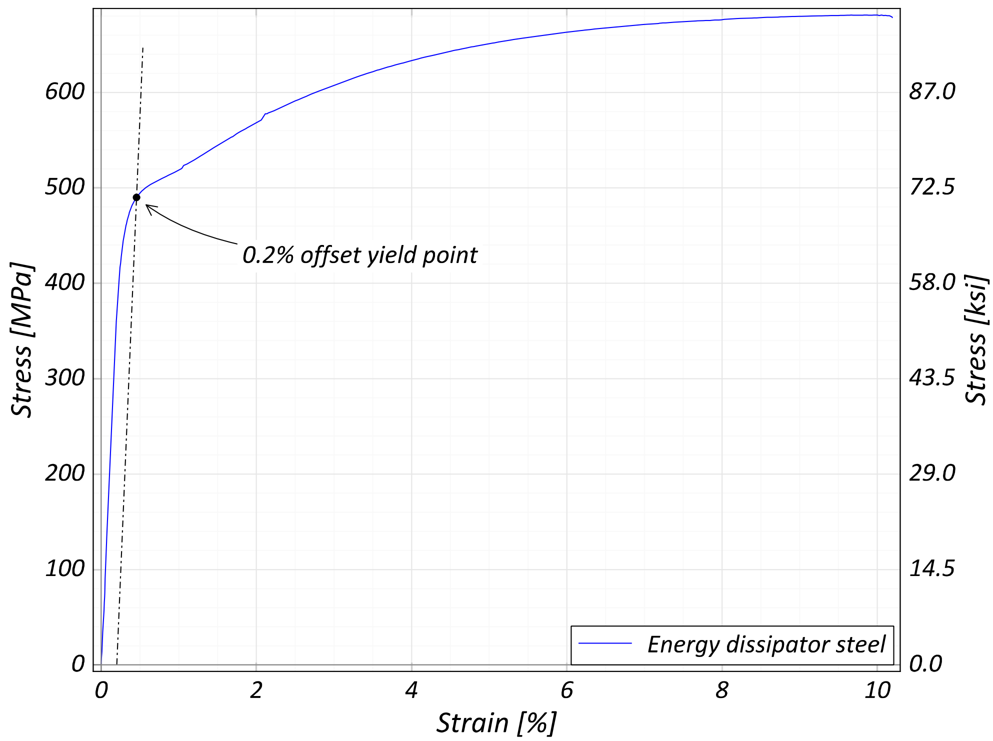

Figure 2.16 Mild steel material stress–strain response.

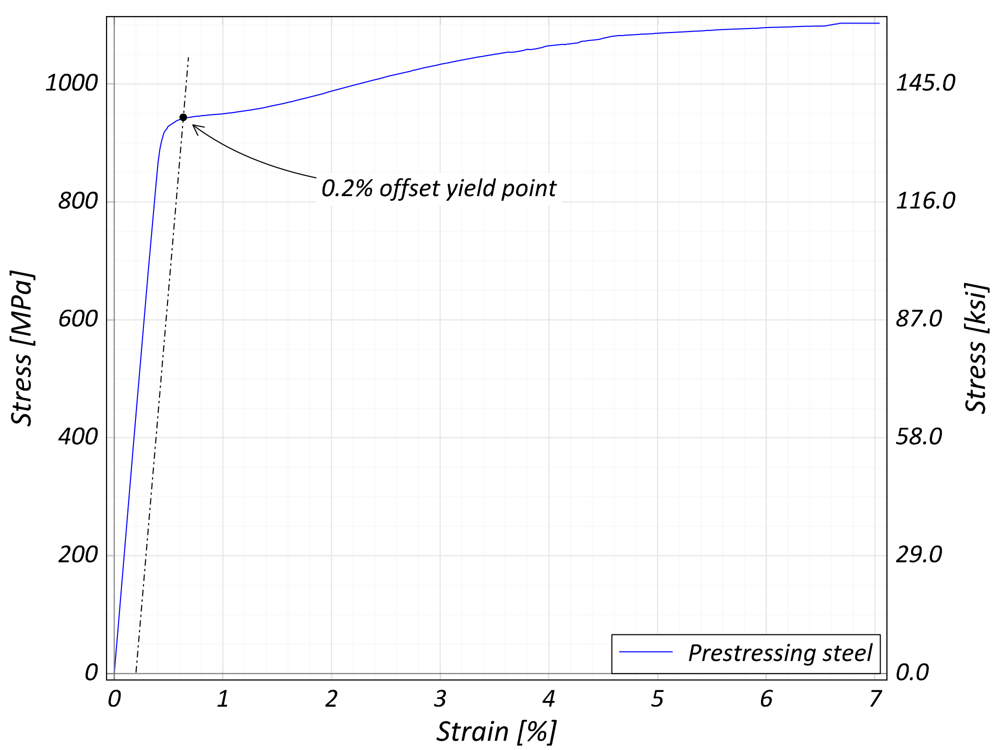

Figure 2.17 Prestressing steel material stress–strain response.

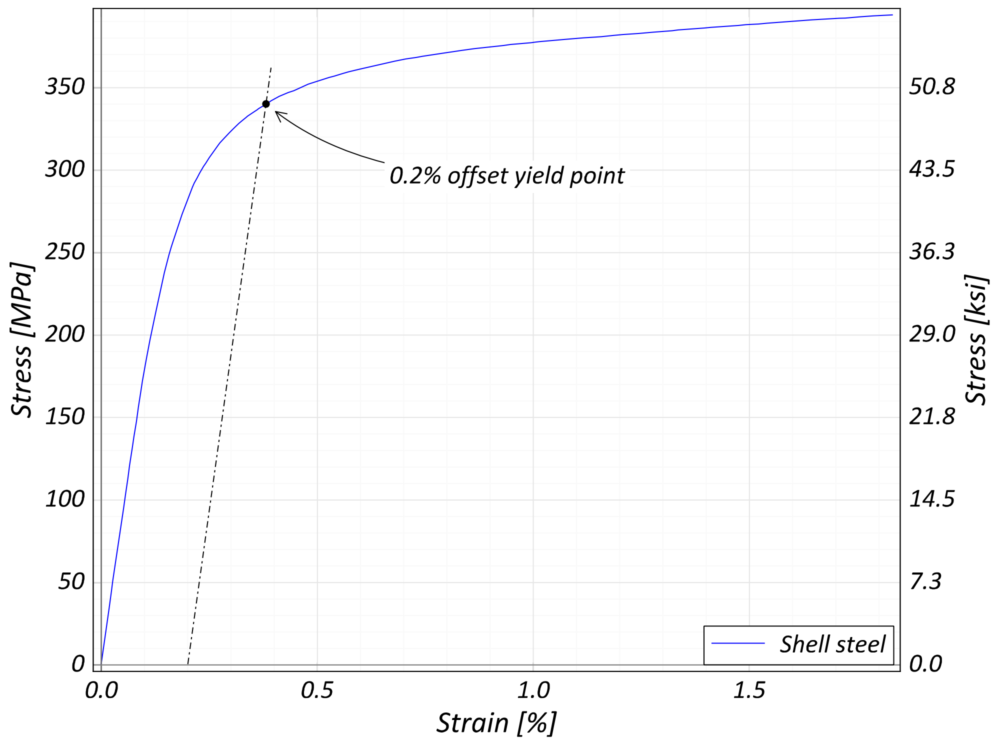

Figure 2.18 Column steel shell material stress–strain response.

2.3 INSTRUMENTATION

A wide array of instruments was installed to monitor the response of the specimen. All the sensor data was sampled at 200 Hz. Twelve (12) accelerometers installed on the shaking table and the foundation measured the input accelerations in three directions at the ends of the foundation, while twenty-six (26) accelerometers on the bent cap and the concrete blocks helped measure the inertia forces experienced in the specimen along all six DOFs.

Nine (9) string potentiometers were anchored at one end to frames off the table and connected to the foundation and the bent cap at the other end to get a measure of absolute displacements. These, coupled with two curtains of two (2) diagonal and two (2) vertical string potentiometers measuring relative displacement between the foundation and the bent cap, were used for measurements of relative displacements between the two. Four (4) linear potentiometers were installed at each rocking interface to measure the gap openings and end rotations in the columns. One last linear potentiometer was used to monitor the shaking table vertical displacement by suspending it from a stiff frame anchored to a location off the table.

Ten (10) strain gauges, with a gauge length of 5 mm each, were installed in the debonded lengths of three energy dissipaters at each rocking interface and in each column to measure the strains experienced during shaking. To measure the strains produced by the transfer of axial forces between the columns and the end beams, four (4) 5-mm (0.2-in.) strain gauges were installed in the CMP in each of the sockets, and two (2) each at a location 203 mm (8 in.) from the top and the bottom of the socket along the direction of shaking.

For the south column, the shell segments embedded inside the sockets were fitted with four (4) 5-mm (0.2 in.) rosette gauges at each end: one gauge at each point 51 mm (2 in.) from the end of the embedded segment and on diametrically opposite points along the shaking direction. Additional non-yielding gauges installed on this segment were in the specimen out-of-plane direction at each location, corresponding to the strain gauges applied to the CMP. Four (4) strain gauges, measuring circumferential strains, were also installed 51 mm (2 in.) and 102 mm (4 in.) above each rocking interface in the same column and along the direction of shaking to obtain an indication of the steel shell behavior.

For each socket in the bent-cap, a 5-mm (0.2-in.) strain gauge was installed in the 45° segments of two hanger reinforcement bars to get a measure of the force transferred between the bent cap and the columns through bearing instead of socket shear. Two (2) strain gauges were installed in each of the PT bars, located on the portion of the bar above the bent cap and inside the load cells, which were installed to measure the PT bar forces.

In addition to the sensors, video recordings of the specimen response during the shaking were also made from various locations. Four (4) GoPro cameras recorded high-quality videos of the rocking interfaces at the foundation level for each of the two columns, while two additional GoPro cameras and two Canon T5i DSLR cameras were used to record the specimen overall response. The videos were synchronized to the sensor data using a system of LEDs set to blink at the beginning and end of the tests, with the input voltage being monitored at one of the data channels.

2.4 INPUT GROUND MOTIONS

A numerical model of the test specimen was developed in OpenSees using the expected member geometries and expected material properties as per the Caltrans *Seismic Design Criteria* [Caltrans 2013]. This model was then used to select a suite of near-fault earthquakes to be imposed on the specimen for dynamic testing. Details of the model are presented in Nema [2018]. The selection was made based on the expected peak drift as calculated by the numerical model relative to the design drift capacity of the system defined by the yielding of the PT bars, which was calculated to be 7%. The selected motions represent very mild (0.6% drift), mild (1.8% drift), moderate (4% drift), and large (>5% drift) events.

Nine (9) earthquake simulations were planned in the initial loading protocol. To investigate the effects of lower intensity aftershocks, the test sequence was not conducted with continually increasing demands; instead, a larger motion was followed by the smaller intensity of shaking until a peak drift of 4% was reached. The resulting protocol called for tests to be capable of producing the following sequence of drifts: 0.6%, 0.6%, 1.8%, 0.6%, 4%, 1.8%, 4%, 5%, and 7%. For larger drifts, ground-motion polarity was occasionally switched to avoid damaging the specimen in only one direction. A 120-sec-long, 2.5% RMS noise signal, bound by an upper frequency of 75 Hz, was applied in the horizontal excitation direction after each earthquake to monitor the dynamic properties of the specimen.

Details of the nine ground motions are listed in Table 2.4 in the order they were imposed on the specimen, and the response spectra for the two components are shown in Figure 2.19 and Figure 2.20.

Table 2.4 Input ground motion sequence for dynamic test.

GM #	Event name	Station name	Unscaled PGA (*g*)	Scale factor	Expected drift (%)
01	Landers, 1992	Lucerne	0.72	0.9	0.6
02	Landers, 1992	Lucerne	0.72	0.9	0.6
03	Tabas, 1978	Tabas	0.85	-0.9	1.8
04	Kocaeli, 1999	Yarimca	0.3	1	0.6
05	Northridge, 1994	RRS	0.85	0.81	4
06	Duzce, 1999	Duzce	0.51	1	1.8
07	Northridge, 1994	NFS	0.72	-1.2	4
08	Kobe, 1995	Takatori	0.76	-0.8	5
09	Kobe,1995	Takatori	0.76	0.9	7

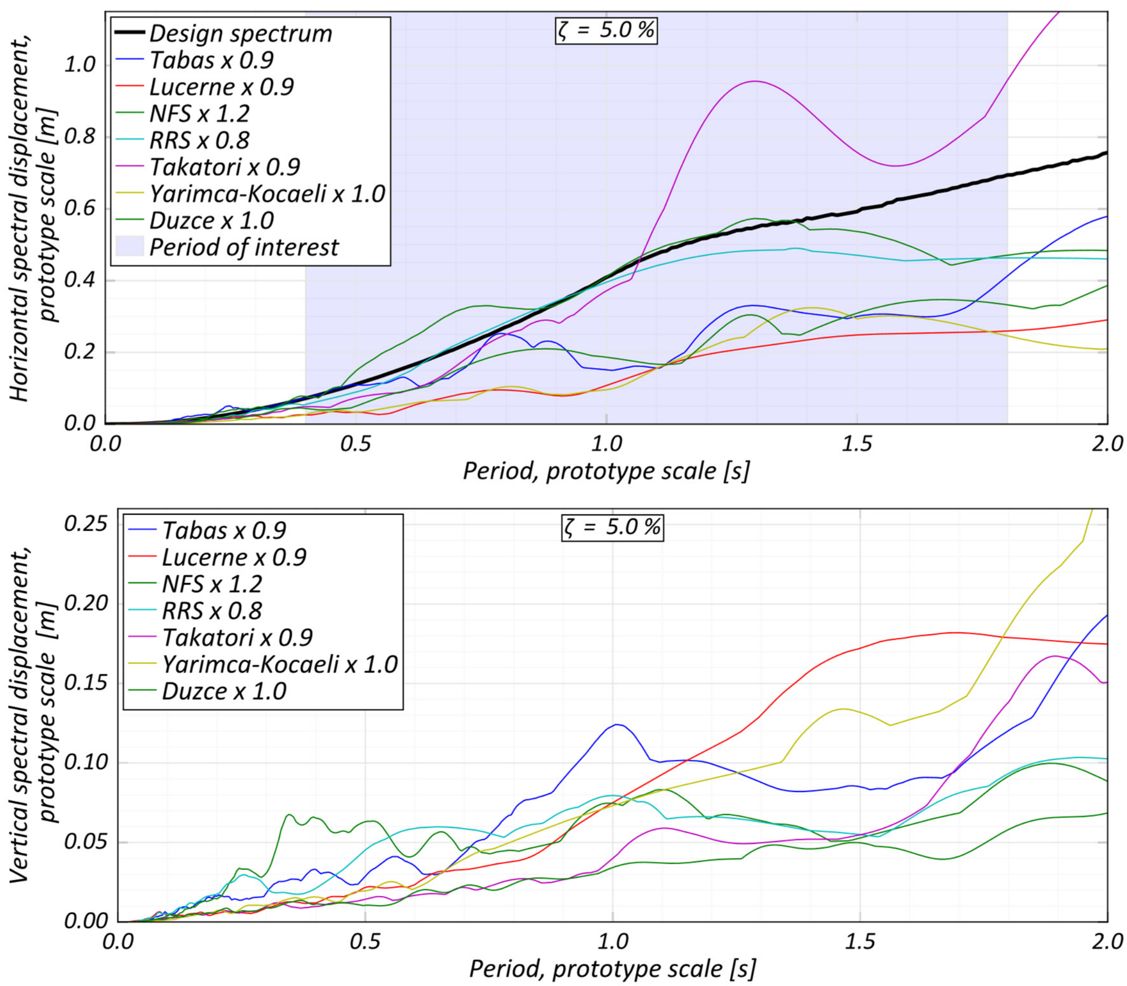

Figure 2.19 Spectral displacement response of input ground motions for dynamic test.

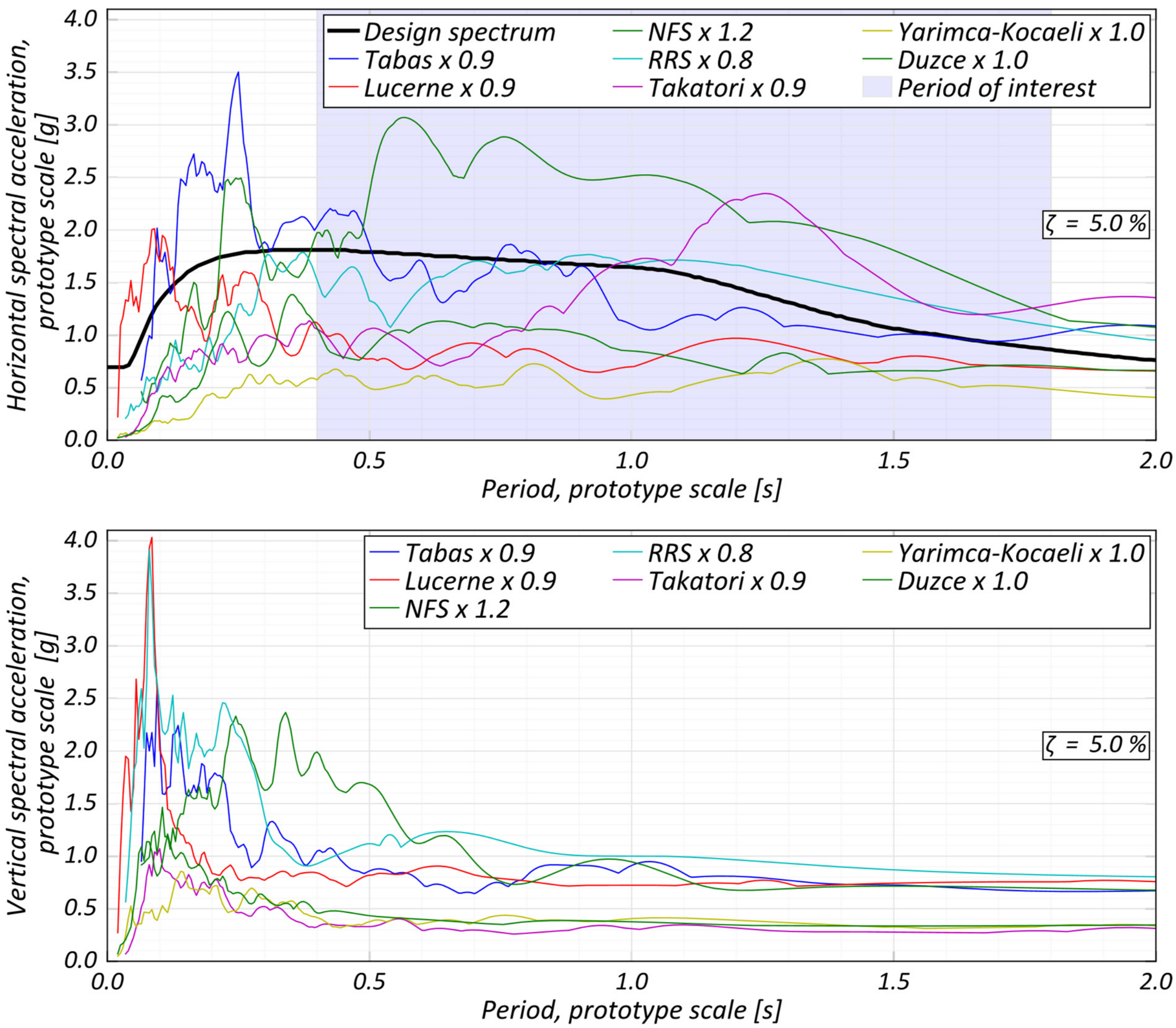

Figure 2.20 Spectral acceleration response of input ground motions for dynamic test.

3 Test Results

In the test results presented below, lateral displacements were normalized by the clear height of the columns and expressed as drift ratios. Lateral forces were normalized by the specimen superstructure weight, 303 kN (68.1 kips), taken as the weight above half the clear height and were expressed as base-shear coefficients. Post-tensioning forces were normalized by the ultimate force capacity of the bars (1120 kN) and were expressed as a percentage of the measured ultimate stress in the prestressing bars (f_{pu}, 1100 MPa, 160 ksi). Positive transverse drifts and accelerations were defined to be towards the south, while positive rotations were defined along the east. All the results presented were filtered through a high-order (2000 point) low-pass filter with a cut-off frequency of 25 Hz.

3.1 LATERAL RESPONSE

The hysteretic responses observed during the tests are shown in Figure 3.1. In each sub-figure, a background plot in gray represents the specimen response to all the preceding excitations, and a red dot marks the specimen base shear and drift ratio at the end of the excitation. Overlaid hysteretic responses during all tests are plotted in Figure 3.2.

GM01 and GM02 were repetitions of the same excitation, serving as a test run to check the correct behavior of the specimen and instrumentation, and to induce any settlements or cracking. This proved useful since the NW concrete block was found to be not seated properly and showed twisting during GM01. Additionally, the restraint frame was found to be bearing against the specimen and providing lateral resistance. Both these issues were corrected before GM02 by increasing the clamping force on the concrete mass blocks to 890 kN (200 kips) and pushing the restraint frames slightly away from the specimen. GM02 can be observed to have a slightly softer response compared to GM01.

GM03 represented an earthquake inducing mild drift demands on the specimen, with GM04 acting as an aftershock. The hysteresis response shows a small amount of energy dissipation, indicating possible rocking at the base. It can be seen from the hysteresis response of GM03 and GM04 that the specimen response has softened, indicating that the concrete at the base has cracked.

GM05 induced moderate drift demands on the specimen, with GM06 serving as an aftershock with mild drift demands. The pinched shape of hysteresis seen in GM05 is behavior characteristic of hybrid recentering systems, indicating rocking behavior under this excitation. GM06 and GM03 were expected and found to have mild (~1.8%) drift demands; however, comparing the responses under the two excitations showed reduced energy dissipation and softer response under GM06.

GM07, GM08, and GM09 formed the final three motions in the planned loading protocol, with increasingly larger demands. The direction of each excitation was carefully chosen to avoid larger drifts on only one side of the specimen. It can be seen from the response under GM08 and GM09 that the specimen maintained its recentering behavior under the large demands imposed. The peak force observed under GM09 is slightly smaller than that under GM08, indicating a small loss in force capacity resulting from the yielding of the prestressing bars.

A summary of peak and residual lateral drifts observed during different excitations is presented in Table 3.1 and shown graphically in Figure 3.3. Also included in Table 3.1 are the rotations measured at the rocking interfaces of the south column, which are shown graphically in Figure 3.4(a) and (b). The recentering behavior of the system is evident in the residual drifts and rotations seen at the end of each motion. The rotations at the column top are slightly smaller than at the bottom; which can be attributed to the larger moments at the bottom of the column. Additionally, the column base rotation time histories for GM08 and GM09 are shown in Figure 3.5 where the rotation response closely follows the drift response, indicating that the column behaved nearly like a rigid body over the clear height.

The prestressing forces measured during the tests in each of the two bars are presented in Table 3.2 and Figure 3.6. Additionally, the stress–strain response measured during GM08 and GM09 shown in Figure 3.7(a) and (b) indicates light yielding of the bars. It is likely that the yielding is concentrated at the rocking interfaces, resulting from the potential development of "kinks" or yield curvatures at these locations.

The maximum and residual gap opening at the bottom interface of the south column at the north and south faces is shown at the end of this chapter in Figure 3.18, Figure 3.19, Figure 3.20, and Figure 3.21. Also shown below each face is the specimen's overall deformation at the instance of maximum gap opening in that face, with the corresponding drift listed in the sub-caption. The rocking interface naturally forms at the location of the strip removed from the column outer shell, and the gap closes completely at the end of each excitation, with only minor spalling seen in GM08.

Table 3.1 Summary of lateral drift, uplift, and south column interface rotation response.

Excitation	Lateral drift ratio (%)		Peak uplift (mm)	Bottom rotation (%)		Top rotation (%)	
	Peak	Residual		Peak	Residual	Peak	Residual
GM01	0.35	0.01	0.7	0.26	0.007	0.25	0.006
GM02	0.77	0.01	0.8	0.66	0.026	0.59	0.005
GM03	1.78	0.06	2	1.60	0.068	1.45	0.028
GM04	1.11	0.06	0.9	0.99	0.070	0.88	0.031
GM05	3.81	0.16	5.3	3.51	0.160	3.28	0.114
GM06	1.74	0.15	2.3	1.60	0.139	1.44	0.094
GM07	4.55	0.15	6.4	4.29	0.135	4.16	0.104
GM08	7.22	0.3	6.9	6.75	0.249	6.44	0.171
GM09	7.51	0.15	7.3	7.16	0.111	7.00	0.055

Table 3.2 Summary of peak and residual prestressing ratios.

Excitation	Peak stress (%f_{pu})		Residual stress (%f_{pu})	
	North bar	South bar	North bar	South bar
GM01	39.5	38.2	37.9	37.3
GM02	42.2	40.0	37.8	37.1
GM03	50.0	47.4	37.7	36.9
GM04	44.5	43.3	37.7	36.8
GM05	64.5	64.1	36.8	35.3
GM06	47.5	46.8	36.7	35.1
GM07	64.9	70.5	37.3	33.9
GM08	84.2	70.0	30.9	31.1
GM09	71.7	81.6	28.5	23.6

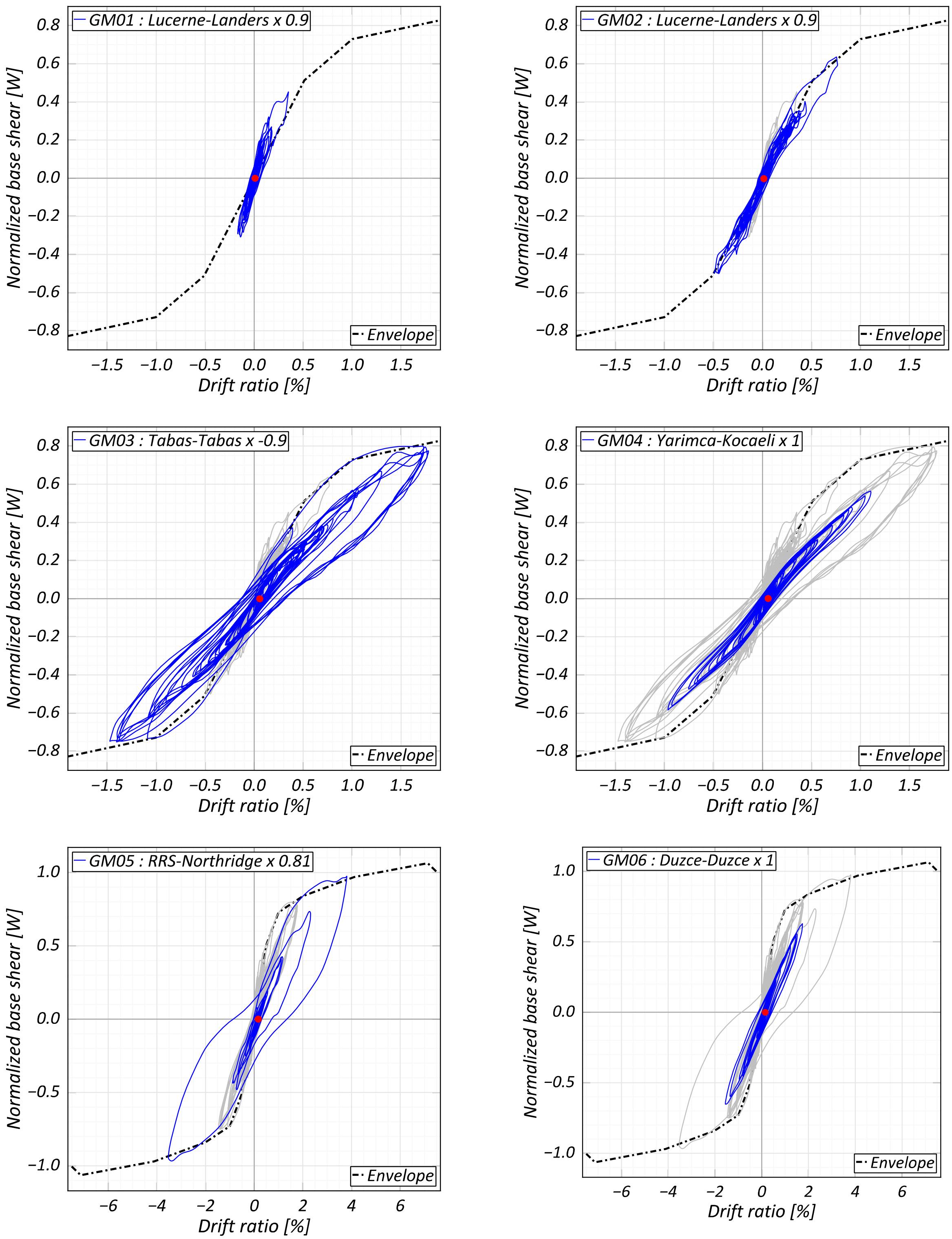

Figure 3.1 Hysteretic responses.

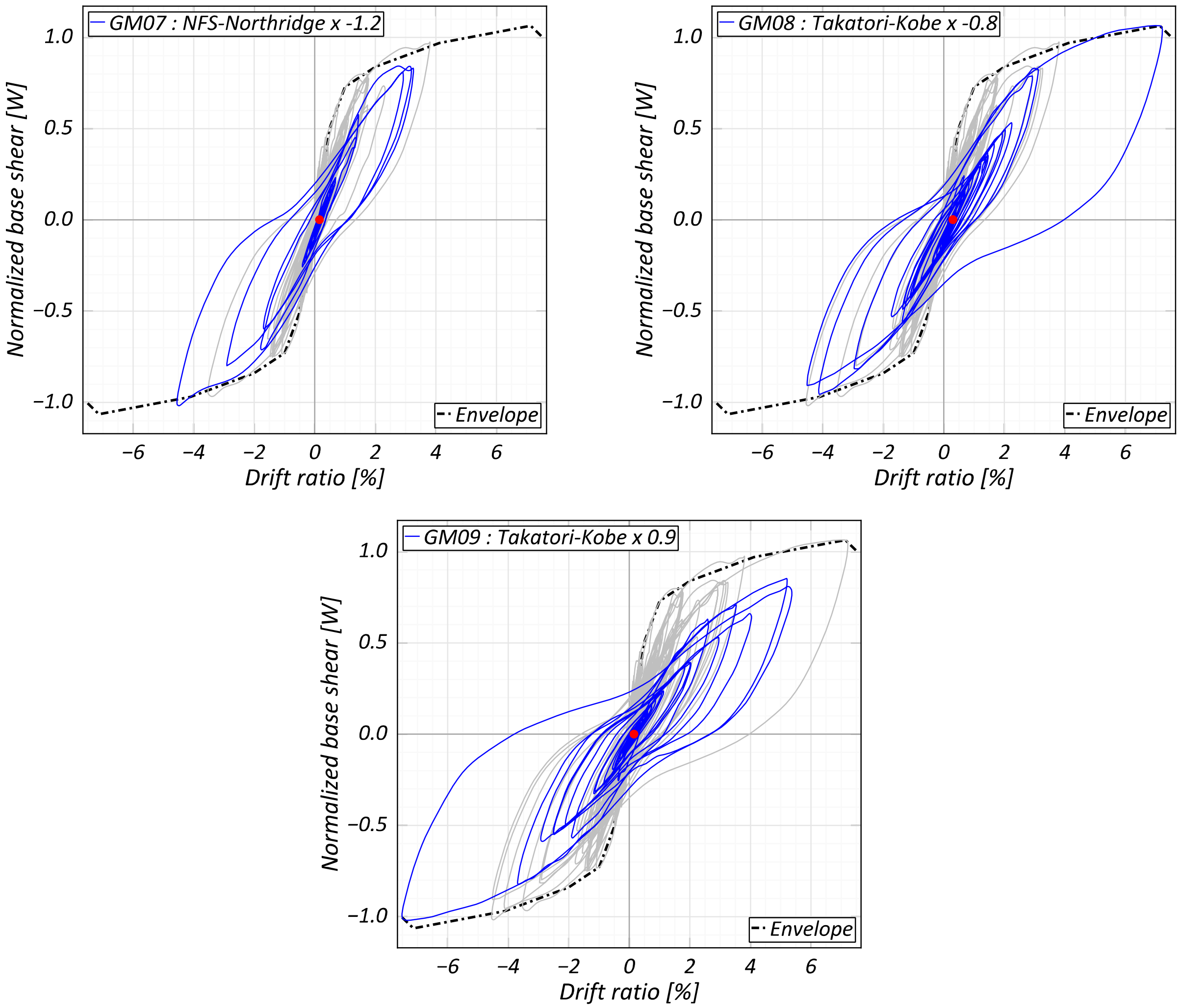

Figure 3.1 (continued).

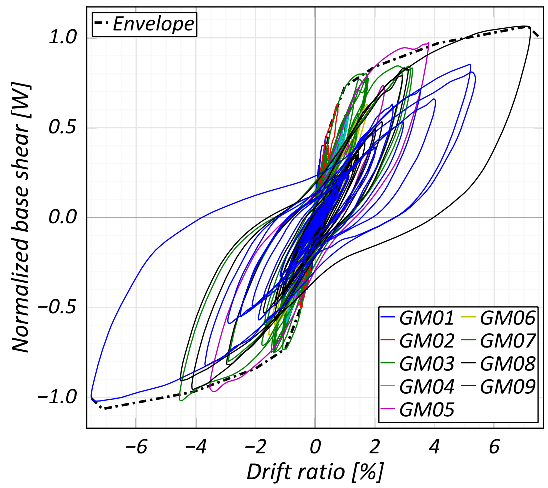

Figure 3.2 **Overlaid hysteretic responses.**

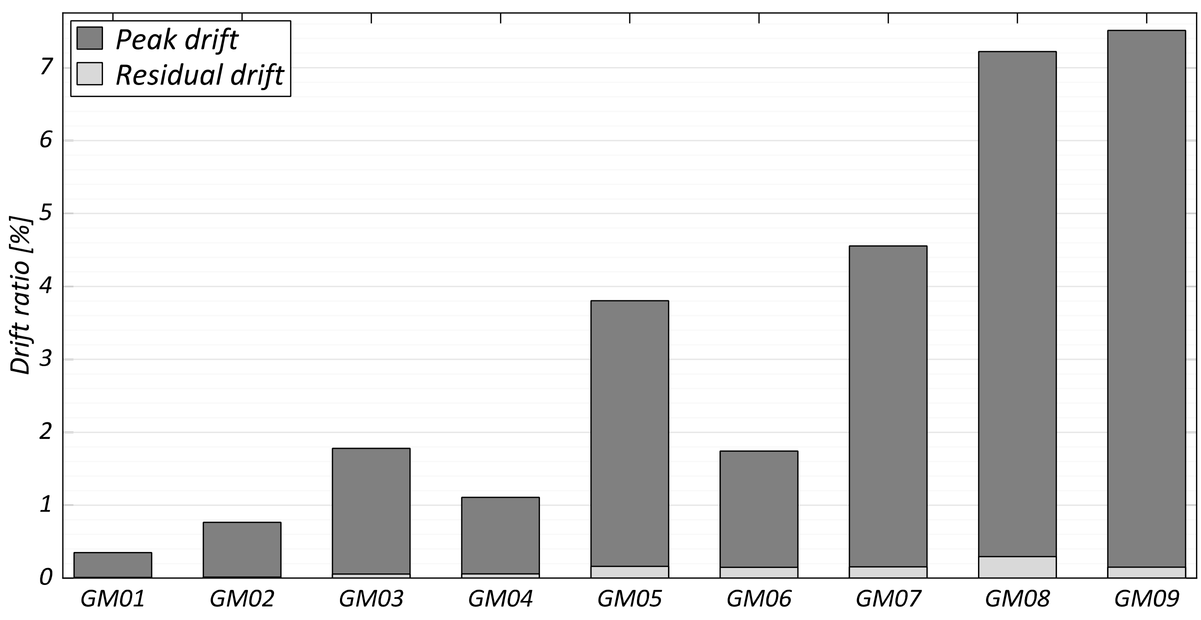

Figure 3.3 **Peak and residual lateral drifts.**

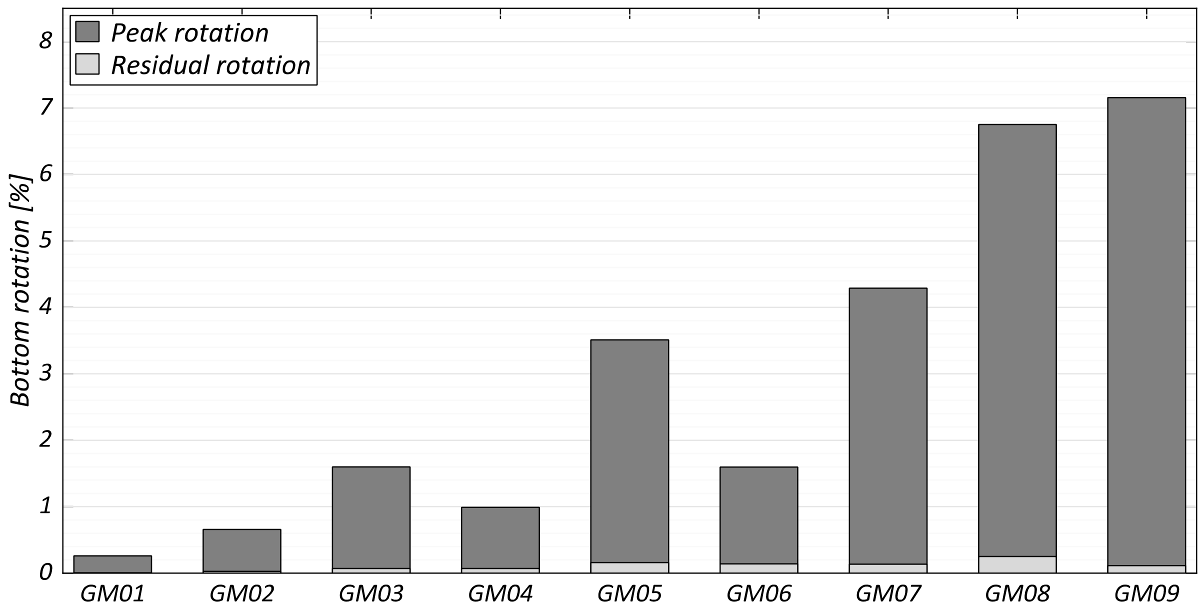

(a)

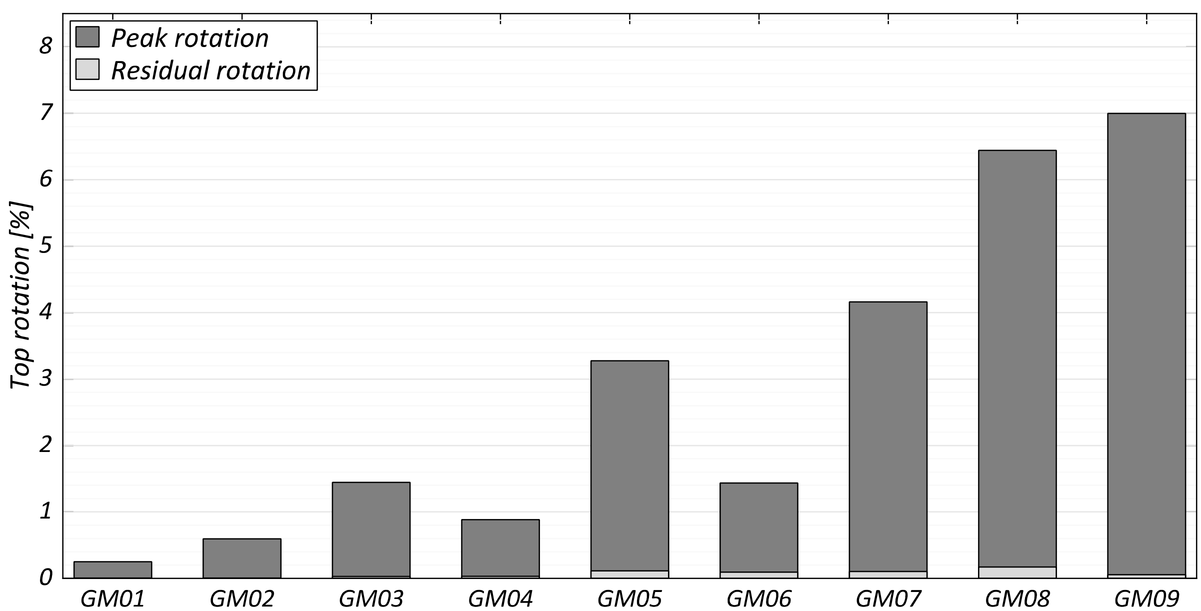

(b)

Figure 3.4 **Peak and residual column interface rotations: (a) south column bottom; and (b) south column top.**

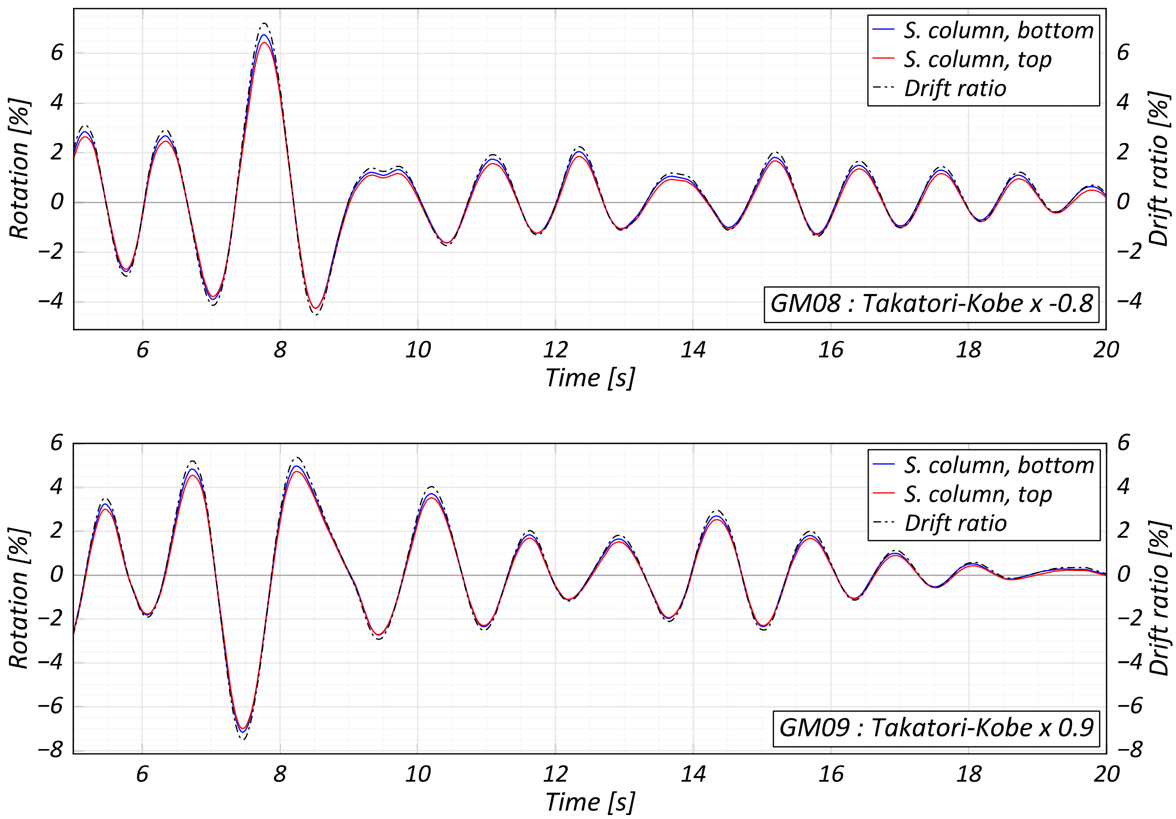

Figure 3.5 Column base rotations measured in GM08 and GM09.

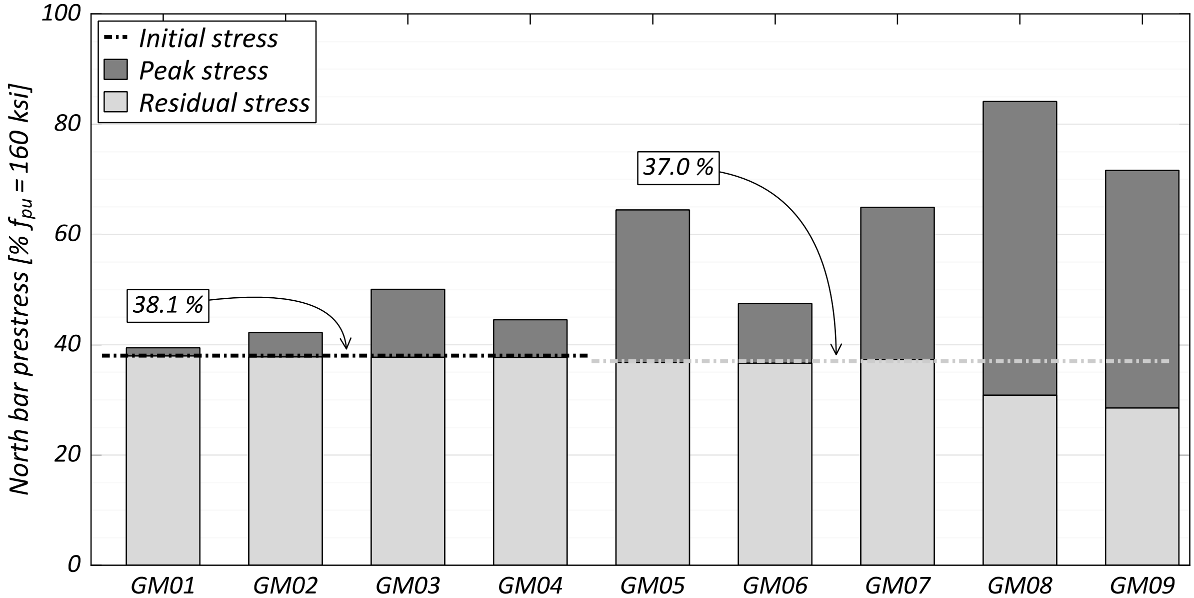

(a)

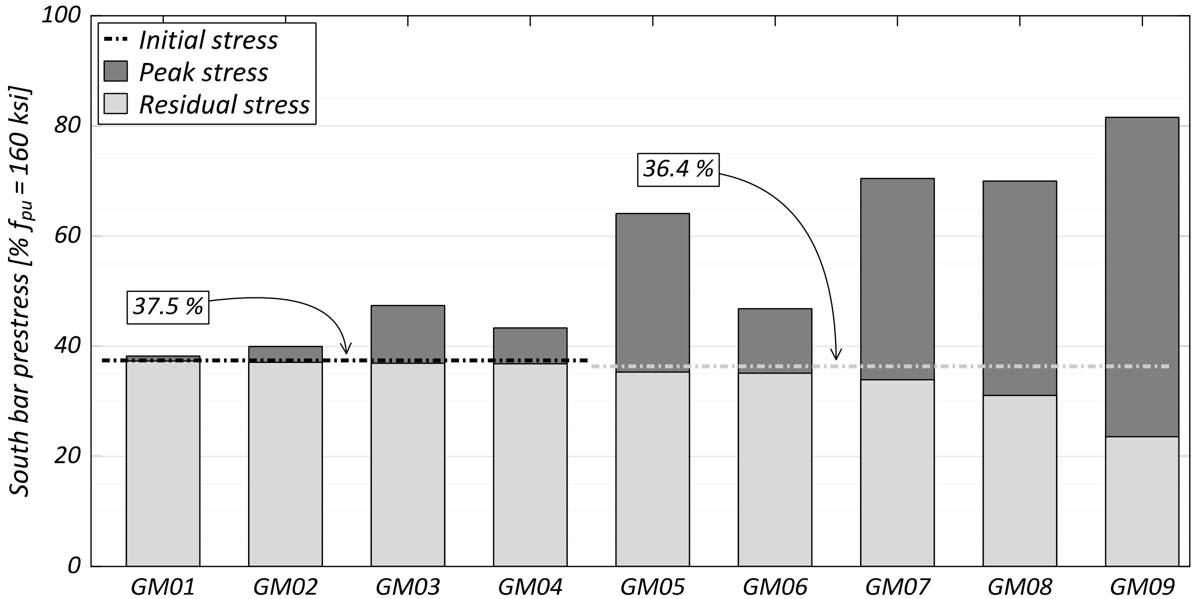

(b)

Figure 3.6 Peak and residual prestress ratios: (a) north bar; and (b) south bar.

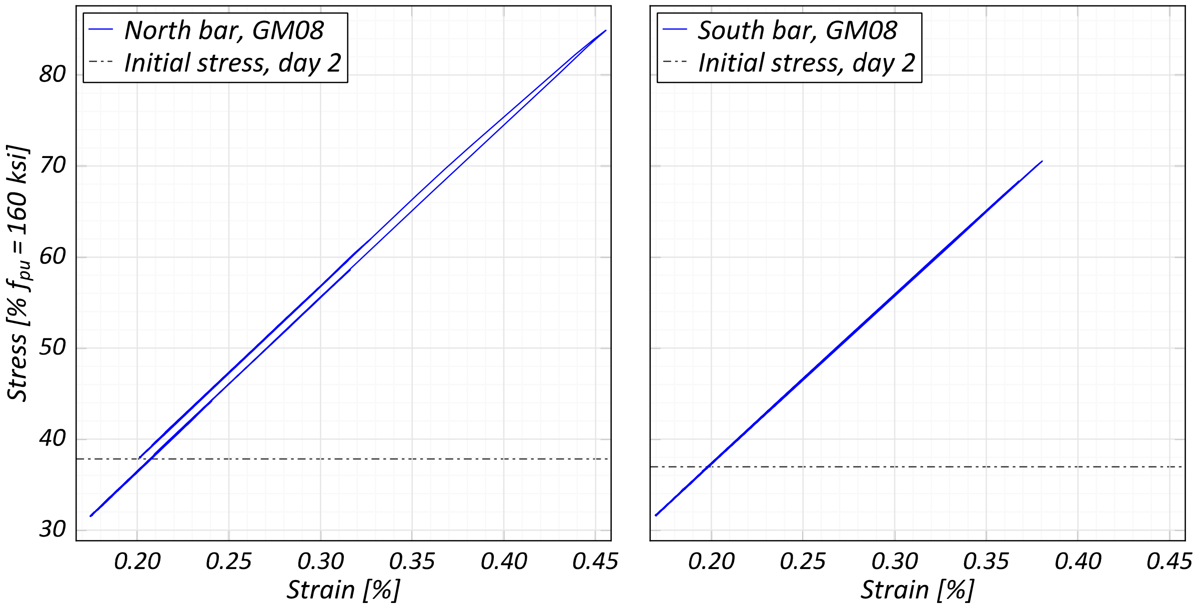

(a) GM08

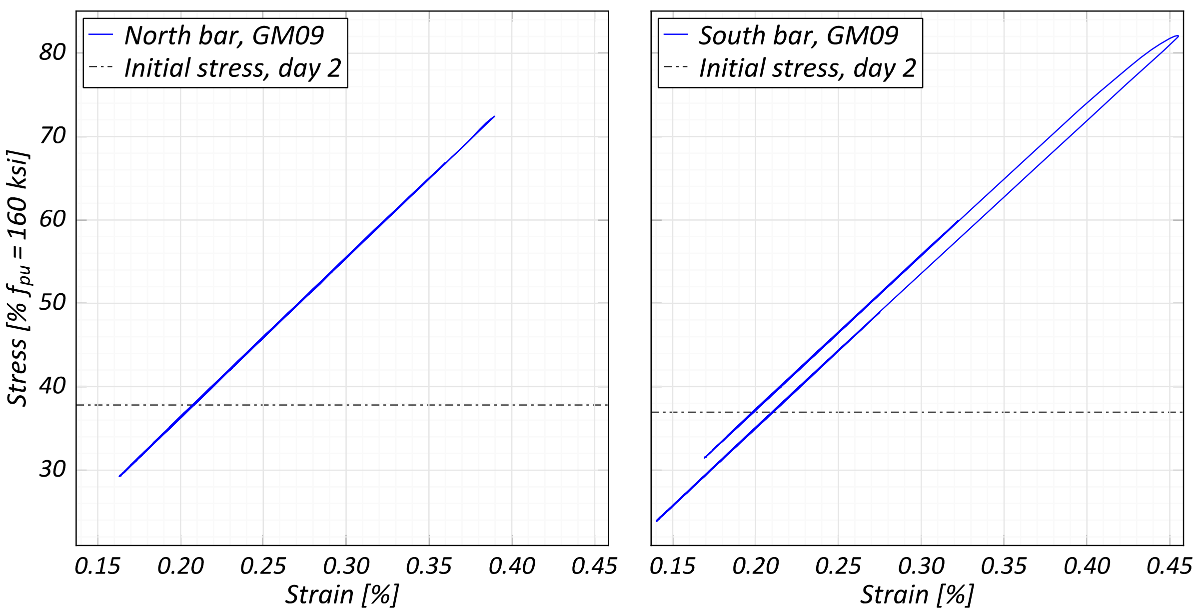

(b) GM09

Figure 3.7 Stress-strain behavior of prestressing bars: (a) GM08; and (b) GM09.

3.2 STRAIN MEASUREMENTS

Figure 3.8 shows the strain time history measured during GM05 from one dissipator bar (longitudinal reinforcement) in each of the two columns. Also marked in the time history is the point of peak strain rate. Note the strain rate value is given in specimen time since the strain rate affects the dynamic behavior of the mild steel dissipator bars. Strain data from the dissipators is not available beyond GM05 since most of the strain gauges installed on the dissipators ceased functioning at the end of day 1 of testing, and the remaining strain gauges failed during GM06. A similar strain history for the prestressing bars from GM09 is presented in Figure 3.9.

The peak circumferential strains measured in the steel shell near the rocking interfaces of the south column are tabulated in Table 3.3. Comparing the values to the stress–strain response seen for the shell material demonstrates that the shell underwent plastic deformation under GM08. The strain history for this earthquake is presented in Figure 3.10. Note that the marked yield line corresponds to the 0.2% offset yield strain, while the nonlinear material response begins at a significantly smaller strain value of 1 millistrain.

The longitudinal strain histories measured during GM09 in the corrugated metal pipe forming the foundation socket of Column 1 are shown in Figure 3.11. The measured strain values are small and predominantly in compression. The compression measurements likely resulted from Poisson effects caused by the circumferential elongation of the CMP under increased column compression and socket compressive stresses.

The strain history from one of the hanger reinforcement bars in the bent cap is shown in Figure 3.12. From the small strain values seen, it can be concluded that this reinforcement is not necessary, and the CMP socket connection is likely sufficient for transferring vertical forces.

Table 3.3 South column shell circumferential strain.

Excitation	North face strain (%)		South face strain (%)	
	Bottom	Top	Bottom	Top
GM01	-0.014	0.017	-0.006	-0.017
GM02	0.027	0.037	0.020	0.014
GM03	0.064	0.067	0.075	-0.024
GM04	0.056	0.041	0.054	-0.030
GM05	0.120	0.178	0.138	-0.044
GM06	0.081	0.115	0.085	0.023
GM07	0.136	0.151	0.138	0.043
GM08	0.127	0.403	0.315	0.062
GM09	0.218	0.371	0.327	0.110

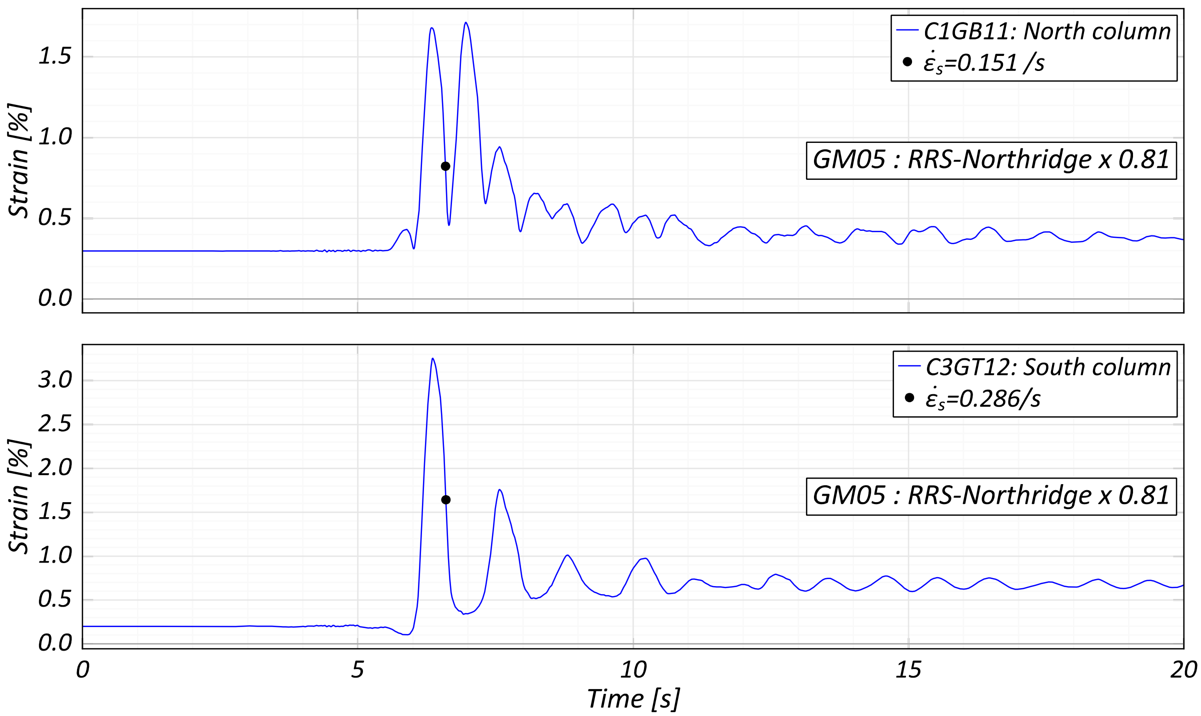

Figure 3.8 Energy dissipator strain history, GM05.

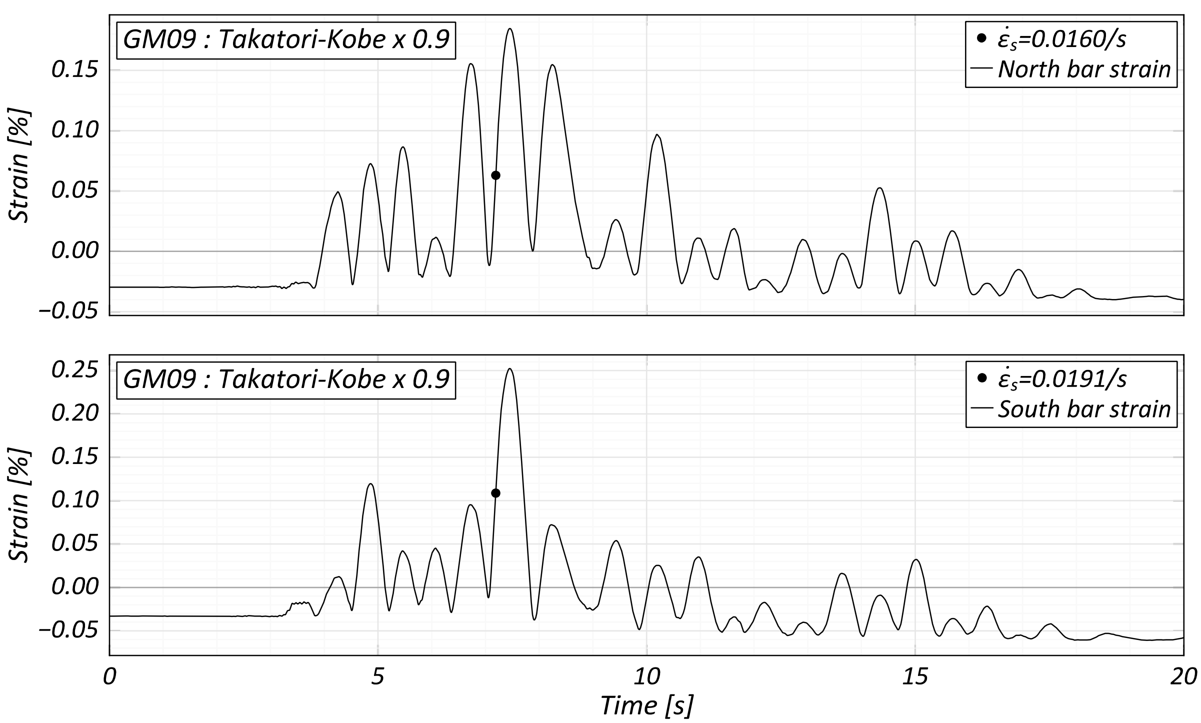

Figure 3.9 Prestressing bar strain history, GM09.

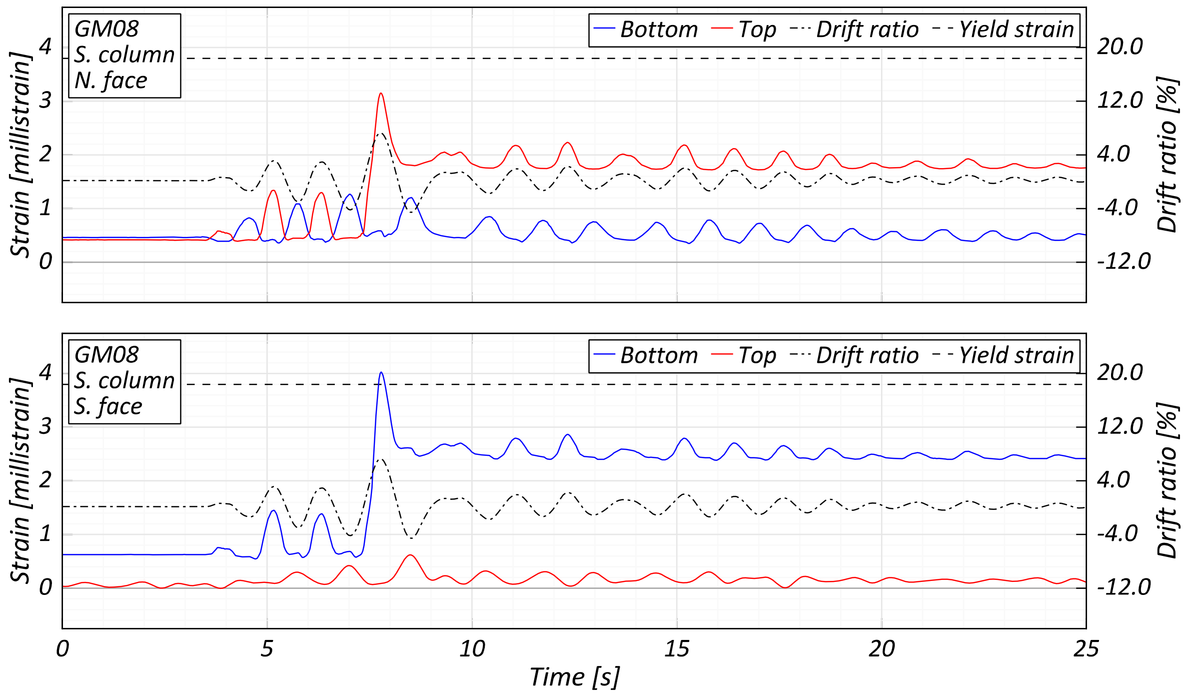

Figure 3.10 Shell strain history, south column, GM08

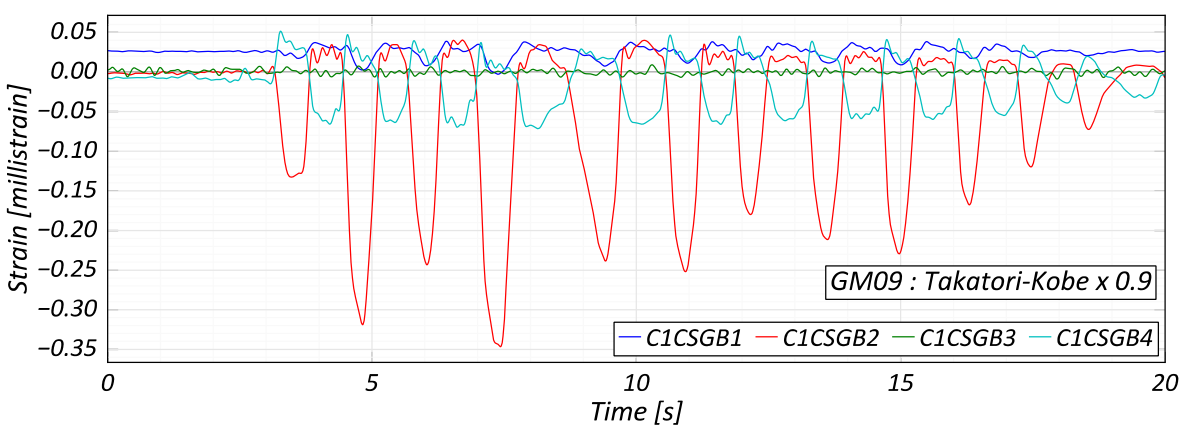

Figure 3.11 Corrugated metal pipe strain history, GM09.

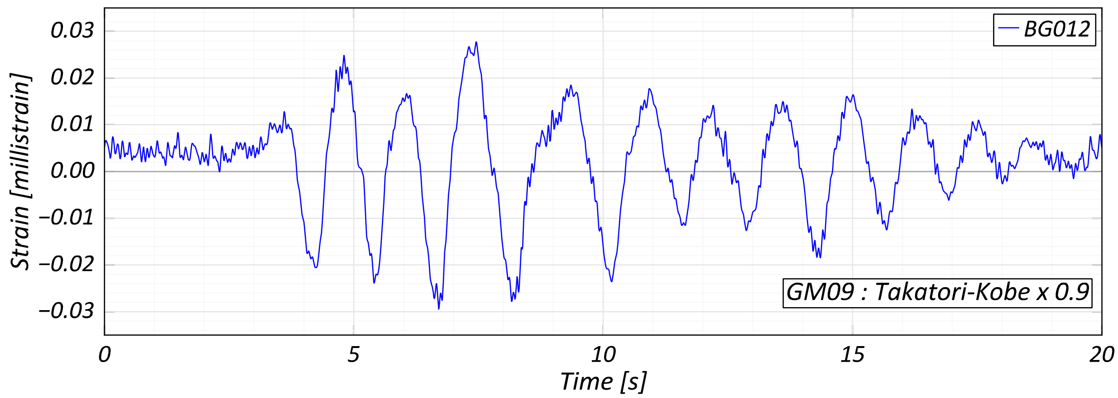

Figure 3.12 **Bent cap hanger reinforcement strain history, GM09.**

3.3 VERTICAL RESPONSE

A plot showing the vertical acceleration, measured positive upwards, versus transverse drift ratio for all the excitations is shown in Figure 5.13 where there is generally no correlation observed between the total vertical force and lateral drift in the system. GM05 and GM07 are the only two excitations that show peaks in vertical acceleration at larger drifts. Their hysteretic response, vertical acceleration versus lateral drift, and the vertical acceleration time histories at the foundation and cap beam are presented in Figure 3.14–Figure 3.17, respectively. The point at the peak vertical acceleration (at large drifts) is marked in all responses for each excitation.

A comparison of the vertical and horizontal responses shows that such a peak in vertical acceleration occurs at the same time as a dip or a “kink” in the base shear–drift response caused by a sudden increase in the axial load and, hence, the P-delta forces in the specimen. The time histories of the vertical acceleration indicate that such a peak is not caused by the peak input acceleration: for GM05, the noted peak occurs at input vertical accelerations that are much smaller than the vertical peak ground acceleration (PGA). It is likely that such peaks occur because of the interplay between the frequency content of the input motion and the modal properties of the specimen.

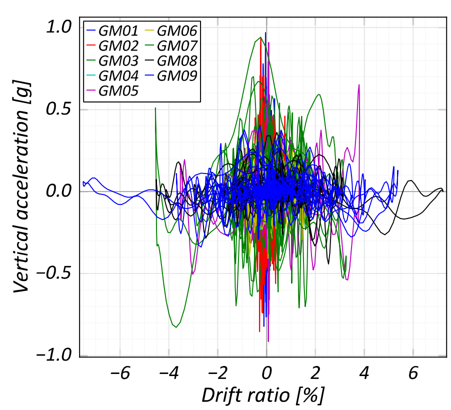

Figure 3.13 **Vertical acceleration versus drift ratio.**

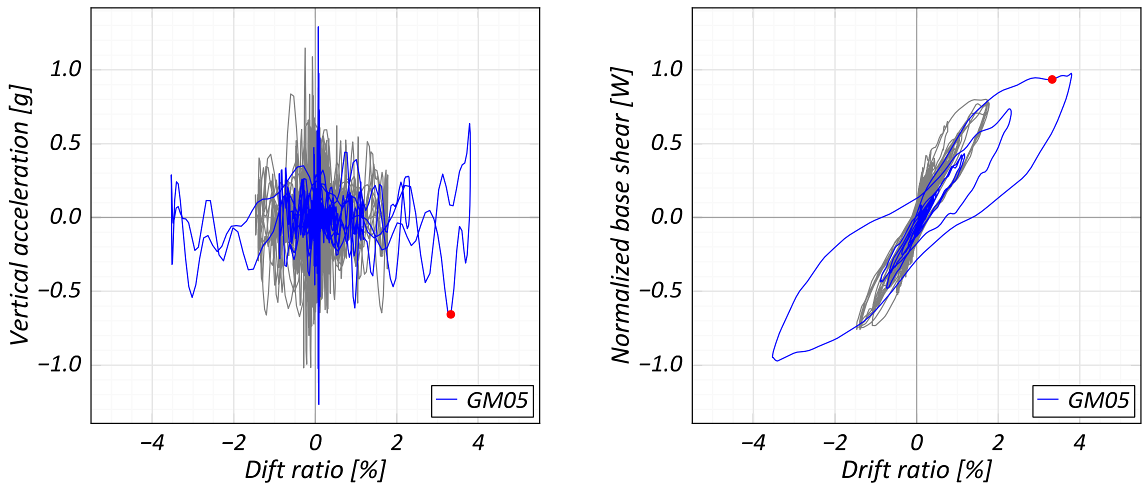

Figure 3.14 GM05 vertical and horizontal response.

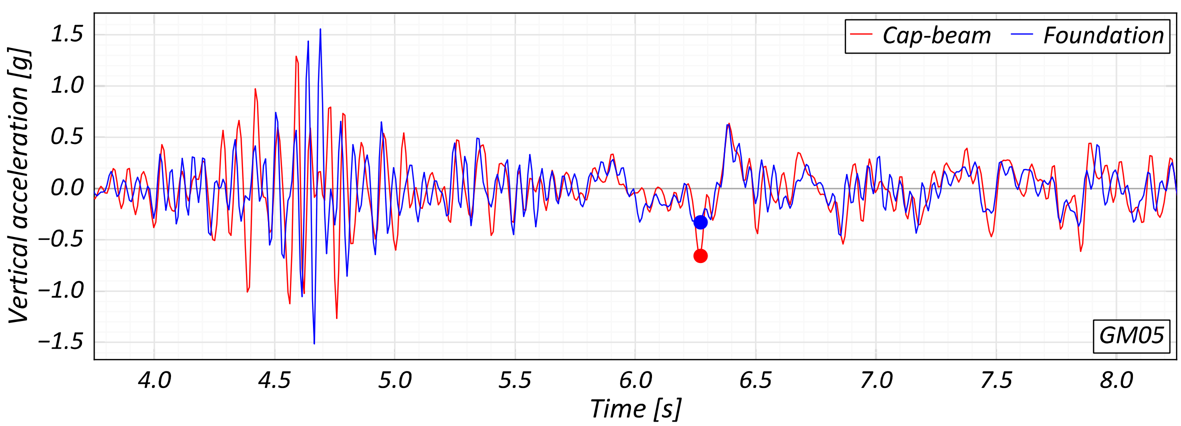

Figure 3.15 GM05 vertical acceleration time history

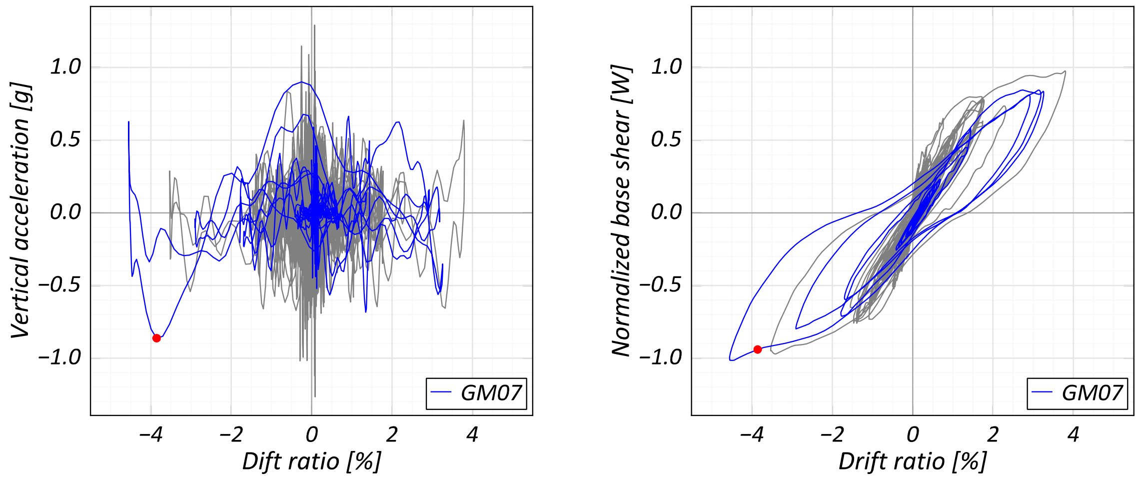

Figure 3.16 GM07 vertical and horizontal response.

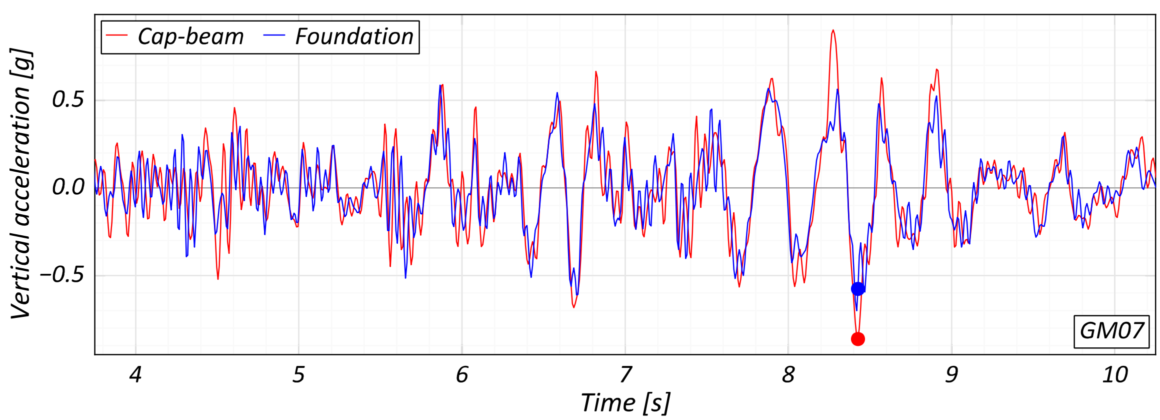

Figure 3.17 GM07 vertical and horizontal response, and vertical acceleration time history.

(a) (b) (c) (d) (e) (f)

Figure 3.18 Specimen response at peak drifts, GM05: Specimen response at peak drifts, GM07: (a) south column interface, north face, Δ=3.28%; (b) south column interface, south face, Δ=-3.5%; (c) south column interface, north face, end of excitation; (d) south column interface, south face, end of excitation; (e) specimen deformation, Δ=3.8%; and (f) specimen deformation, Δ=-3.5%.

(a)

(b)

(c)

(d)

(e)

(f)

Figure 3.19 Specimen response at peak drifts, GM07: (a) south column interface, north face, Δ=3.2%; (b) south column interface, south face, Δ=-4.5%; (c) south column interface, north face, end of excitation; (d) south column interface, south face, end of excitation; (e) specimen deformation, Δ=3.2%; and (f) specimen deformation, Δ=-4.5%.

(a) (b) (c) (d) (e) (f)

Figure 3.20 Specimen response at peak drifts, GM08: (a) south column interface, north face, Δ=7.2%; (b) south column interface, south face, Δ=-4.5%; (c) south column interface, north face, end of excitation; (d) south column interface, south face, end of excitation; (e) specimen deformation, Δ=7.2%; and (f) specimen deformation, Δ=-4.5%.

(a) (b)

(c) (d)

(e) (f)

Figure 3.21 Specimen response at peak drifts, GM09: (a) south column interface, north face, Δ = 5.4%; (b) south column interface, south face, Δ =-7.5%; (c) south column interface, north face, end of excitation; (d) south column interface, south face, end of excitation; (e) specimen deformation, Δ = 5.4%; and (f) Δ = 7.5%.

4 Blind Prediction Contest

4.1 CONTEST DESCRIPTION

The PEER Bridge-Bent Blind Prediction Contest was conducted to identify the uncertainty in predicting important response quantities of the described one-third scale two-column RC bridge bent with enhanced features, subjected to nine consecutive ground motions with one horizontal and one vertical component. The contest was announced nationally and internationally among professional engineers and researchers. Predictions were submitted by 19 teams from different countries. Additional information about their models was sought from contestants in the form of a survey. Although the contestants held either M.S. or Ph.D. degrees, it was not a prerequisite. Two entry categories were formed based on the affiliation of the contestant/team. The contestants/teams that belonged to academic or research groups were designated as *Researchers* (R) and contestants/teams that belonged to structural engineering groups from industry were designated as *Engineering Professionals* (PE). There were 10 teams in the R group and 9 teams in PE group; a winner was chosen from each group.

4.2 INPUT DATA

The contestants of the competition were supplied with all the data required to develop an analytical model and conduct nonlinear time-history analysis. Provided data included the ground motions measured on the table, geometry of the columns, footing, and the cap beam, reinforcement details, material properties obtained from tests of steel and concrete samples, geometry and mass of the weight blocks, post-tension details, and construction drawings.

4.3 PREDICTED QUANTITIES

Contestant teams were asked to predict the maximum response for global response quantities from nine ground motions. Predicted response quantities are listed in Table 4.1 and shown in Figure 4.1. The submittal sheet in Figure 4.2 was used by the contestants to submit their predictions.

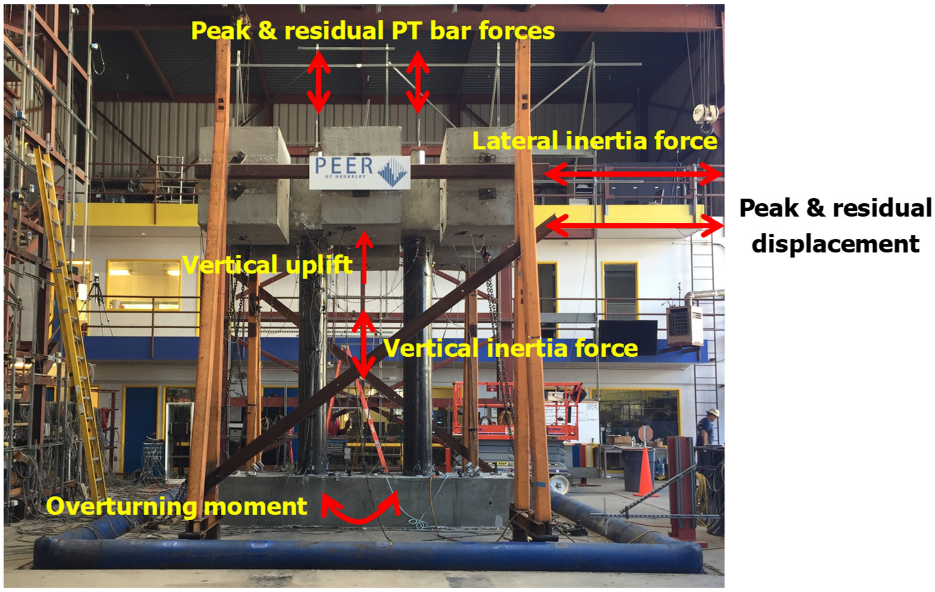

Figure 4.1 Predicted response quantities.

Table 4.1 Table of predicted response quantities.

Response quantity ID	Response quantity
1	Residual post-tension bar force in column 1 (kN)
2	Residual post-tension bar force in column 2 (kN)
3	Largest post-tension bar force in column 1 (kN)
4	Largest post-tension bar force in column 2 (kN)
5	Vertical inertia force (kN)
6	Maximum lateral inertia force (kN)
7	Minimum lateral inertia force (kN)
8	Maximum overturning moment (kNm)
9	Minimum overturning moment (kNm)
10	Maximum horizontal displacement (mm)
11	Minimum horizontal displacement (mm)
12	Vertical uplift with respect to the base of the columns (mm)
13	Residual displacement (mm)

4.4 RULES OF THE CONTEST

The rules of the contest were adopted from Concrete Column Blind Prediction Contest 2010 [Terzic et al. 2015] and were as follows:

1. All information and details regarding the blind prediction contest can be found in the following web site: http://peer.berkeley.edu/prediction_contest/.
2. Contestants may consist of individuals or teams.
3. An individual can only be involved in a single team.
4. If an individual is part of a team, the individual cannot participate in the competition separately as an individual.
5. The individual or team must use the contest submittal spreadsheet and input values as follows:
   - Relative horizontal displacements are to be provided with respect to the base of the footing and are to be provided in millimeter units to one (1) place beyond the decimal point.
   - Overturning moment is to be provided in units of kN-m to one (1) place beyond the decimal point.
   - Shear and axial forces are to be provided in units of kN to (1) place beyond the decimal point.
   - Contestants are expected to submit their predictions in the form of two peak values, one for the maximum of the positive values (indicated with P) and one for the maximum of the absolute of the negative values (indicated with N).
   - Values shall be determined for the 9 applied ground motions (GM1, GM2, GM3, GM4, GM5, GM6, GM7, GM8, and GM9).
6. Structural drawings are provided in U.S. customary units; however, output data is requested in SI units. A translation from US customary to SI units and vice versa can be easily done in the google.com prompt. For example, type in the google.com prompt:
   - 430000 pounds-feet in kN m
   - 4 ft 3 inches in mm
   - 3500 psi in MPa
7. The tested material properties for steel bars, concrete, prestressing bars, steel shell, and grout are provided in U.S. customary units. For grout, a datasheet is provided in addition to the data from the conducted material tests.
8. Description of the construction sequence, supported with photographs, is provided.
9. The recorded data is processed by band-pass filtering with a high-order (5000) FIR digital filter with a 0.25–25 Hz bandwidth. Forces are determined from recorded accelerations and the corresponding masses.

10. Accelerations measured on the table are provided to the contestants in units of *g* without filtering. These accelerations should be used as input to the developed analytical models.

11. The individual or team must declare one of the 2 categories on the Spread Sheet:
    - Researchers (including postdocs and students)
    - Engineering Professional

12. Except for category winners, all submittals will be kept anonymous.

13. Contestants should submit their results before November 27, 2017. Winners in each category will be notified by December 11, 2017.

14. Along with the predictions, contestants should submit a technical report of 5–20 pages electronically as a pdf document in ASCE journal format. Contents of the report may include text, figures, and tables that describe the model, utilized software platform, materials, elements, solution algorithms, assumptions, discussion of the analysis results, and summary of key results beyond those in the spreadsheet. ASCE Journal format can be downloaded from the Submission Format tab.

15. The following system will be used to judge the category winners. Teams or individuals are requested to predict the 10 quantities listed in the provided spreadsheet (Contestantsubmittalspreadsheet.xlsx). Error is defined as the absolute value of the difference between the measured parameter and the values predicted by the contestant.

16. The team with minimum error in a question will receive 8 points
    - The second team will receive 5 points
    - The third team will receive 3 points
    - The fourth team will receive 1 point

    All points will be totaled, and the team with the greatest total will be declared the winner of this category.

    If there are sufficient (based on the judgment of the evaluation committee) participants in each category, there will be one winner for each of the two categories. Otherwise, no distinction will be made between the two categories in announcing the winners. Awards will be given in a special ceremony at the 2018 PEER Annual Meeting.

17. A representative of the category winners will be invited to the 2018 PEER Annual Meeting that will be held in the UC-Berkeley campus, January 18–19, 2018, with a reasonable amount of travel expenses covered. The representative will be asked to make a short presentation on the techniques used (model and analysis) in making the winning predictions.

18. Questions about the blind prediction contest or details of the structure or ground motions can be submitted to peer_center@berkeley.edu until November 1, 2017. Questions and answers will be posted on the web site

http://peer.berkeley.edu/prediction_contest/ under the *Notification* tab and will be updated twice per week.

19. Teams from the UC San Diego or the UC Berkeley experimental research teams are not allowed to participate.

Name of the team representative:	
Entry Category (Researcher or Practicing Engineer):	
Computer platform used:	
Type of element used to model the columns:	
Type of element used to model the cap beam:	
Type of element used to model the footing:	

			Predicted Quantity								
1	Relative horizontal displacement (mm) at z=158":		GM1	GM2	GM3	GM4	GM5	GM6	GM7	GM8	GM9
		P									
		N									
2	Lateral Inertia force above the top of columns (at z =158")		GM1	GM2	GM3	GM4	GM5	GM6	GM7	GM8	GM9
		P									
		N									
3	Overturning moment at the base of the columns (at z=26")		GM1	GM2	GM3	GM4	GM5	GM6	GM7	GM8	GM9
		P									
		N									
4	Vertical Inertia force above the top of columns (at z =158")		GM1	GM2	GM3	GM4	GM5	GM6	GM7	GM8	GM9
		P									
5	Largest Post-tension bar force in Column 1 (kN)		GM1	GM2	GM3	GM4	GM5	GM6	GM7	GM8	GM9
		P									
6	Largest Post-tension bar force in Column 2 (kN)		GM1	GM2	GM3	GM4	GM5	GM6	GM7	GM8	GM9
		P									
7	Relative residual displacement (mm) at z=158":		GM1	GM2	GM3	GM4	GM5	GM6	GM7	GM8	GM9
		P									
8	Peak Vertical Uplift at x=0", z=158" with respect to the base of the columns		GM1	GM2	GM3	GM4	GM5	GM6	GM7	GM8	GM9
		P									
9	Residual Post-tension bar force in Column 1 (kN)		GM1	GM2	GM3	GM4	GM5	GM6	GM7	GM8	GM9
		P									
10	Residual Post-tension bar force in Column 2 (kN)		GM1	GM2	GM3	GM4	GM5	GM6	GM7	GM8	GM9
		P									

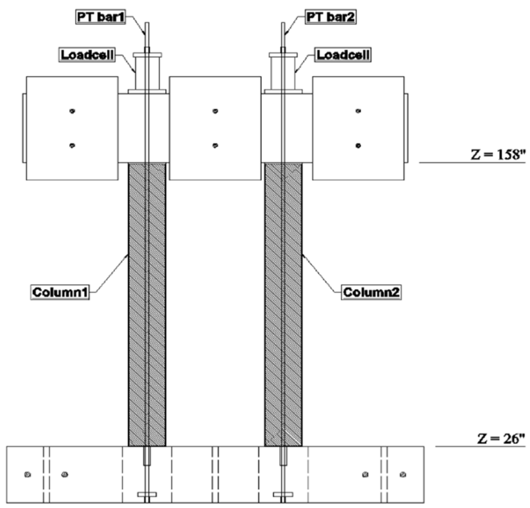

Figure 4.2 Contest submittal spreadsheet.

4.5 RULES FOR SCORING CONTESTANTS

There were a total of 9 ground motions and 13 response quantities to be predicted for each ground motion, which led to a total of 117 quantities. For each quantity, the four closest predictions to the measured responses were awarded 8, 5, 3, and 1 points. The same weight was given to each response quantity. All points were then summed, and the team with the largest total points was declared the winner of its category.

4.6 WINNERS OF THE CONTEST

Overall winners were identified in the Research and Engineering Professional categories.

For the Engineering Professional category, the team of Grigorios Antonellis, Andrew Ma, and Anthony Giammona were ranked first.

- Grigorios Antonellis, Andrew Ma, and Anthony Giammona, of Nabih Youssef Associates, San Francisco, California, U.S., used the program ETABS 2016 Ultimate for their predictions. Fiber Hinge with NL Link for the PT Tendon was used to model the columns. The use of NL springs (Links) was preferred instead of NL truss elements and PMM hinges where possible.

For the Research category, the entry of the team formed by Michele Egidio Bressanelli, Marco Bosio, and Andrea Belleri was identified as the first-place winner.

- Michele Egidio Bressanelli, Marco Bosio and Andrea Belleri, of University of Bergamo, Italy, used the program MidasGEN 2017 in conjunction with fiber elements for their winning entry. A simplified beam model was validated by means of pushover analyses, and the model was further simplified in the time-history analysis.

Response predictions and measured (experimental) response quantities are shown in Figure 4.3–Figure 4.15 for all predicted response quantities. Predictions of the winners from both categories are marked on these plots. The winner from the Research category is designated as "Winner-R," and the winner from the Engineering Professional category is marked as "Winner-PE". Designation Maximum in the figures refers to the peak of the considered response in the positive direction. Designation Minimum refers to the peak in the other direction. The announced winners predicted well most of the column responses; however, some of the predictions were significantly inaccurate as can be observed in Figure 4.3 to Figure 4.15.

As described earlier, the four closest predictions were awarded 8, 5, 3, and 1 points (8 for the best prediction) for each of the 117 entries, all points were then totaled, and the team with the greatest total was declared the winner. The same weight was given to each response quantity. Giving points to only four best predictions and not penalizing poor predictions might have possibly skewed the results.

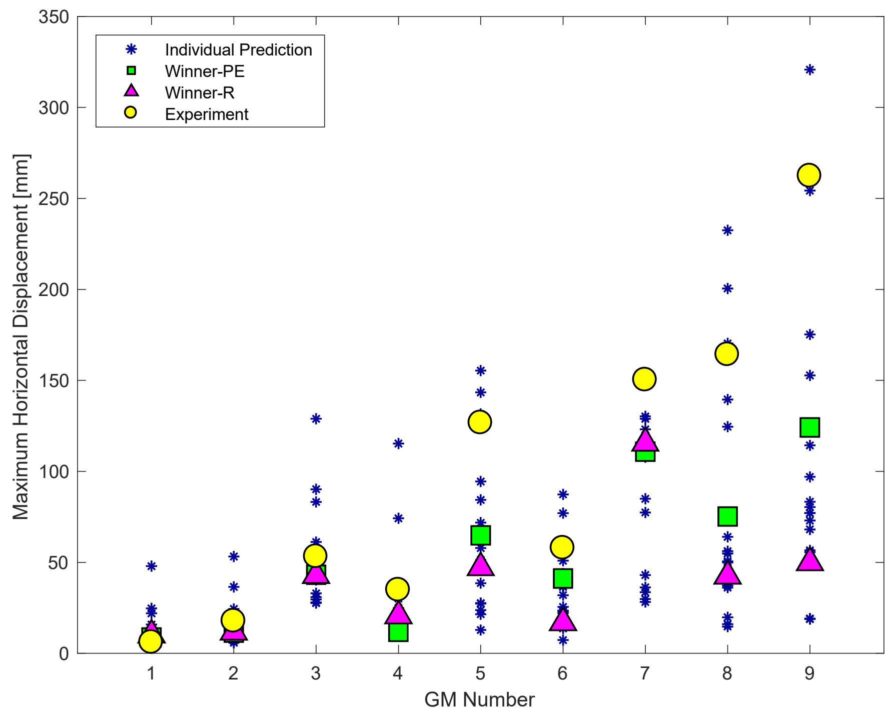

Figure 4.3 **Predictions of maximum horizontal displacement at the top of the columns versus measured response.**

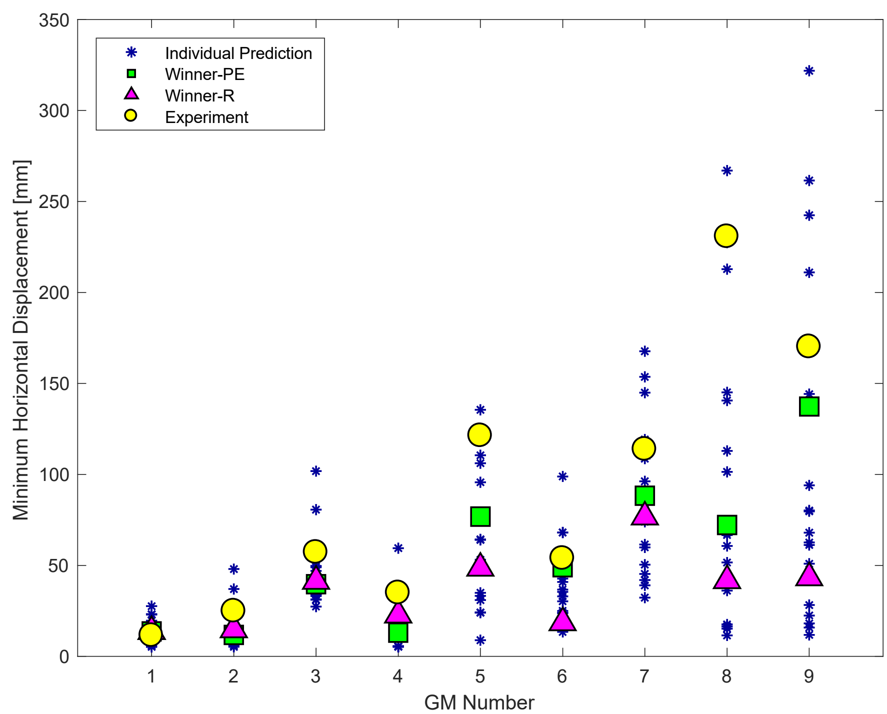

Figure 4.4 **Predictions of minimum horizontal displacement at the top of the columns versus measured response.**

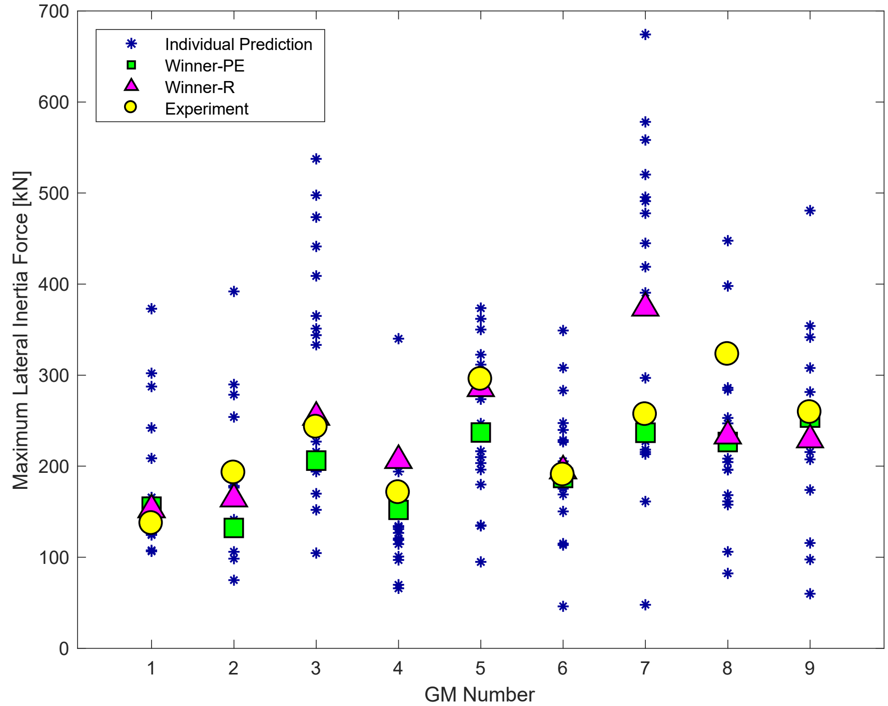

Figure 4.5 **Predictions of maximum lateral inertia force versus measured response.**

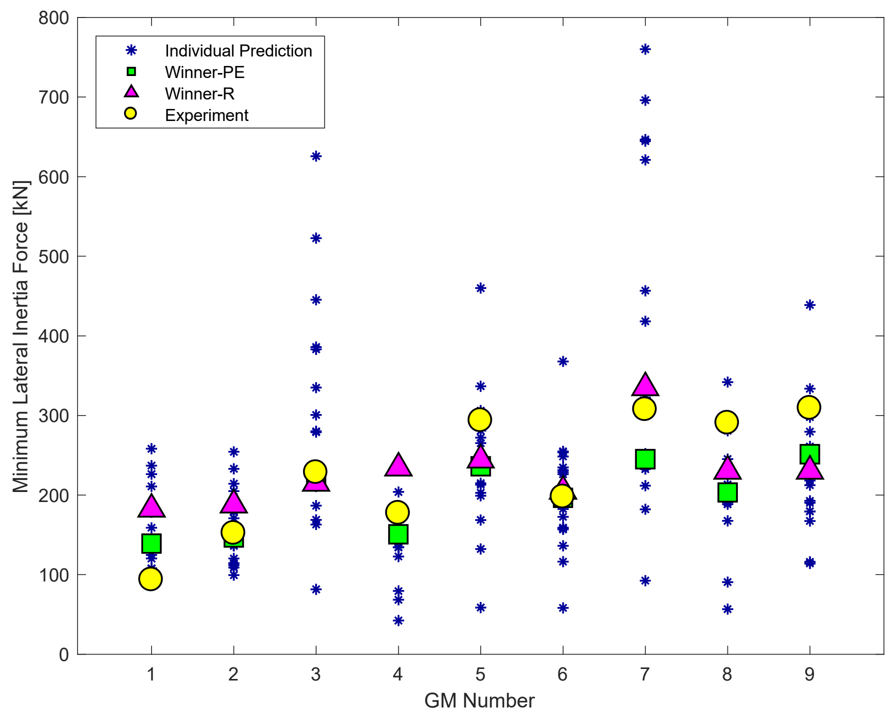

Figure 4.6 **Predictions of minimum lateral inertia force versus measured response.**

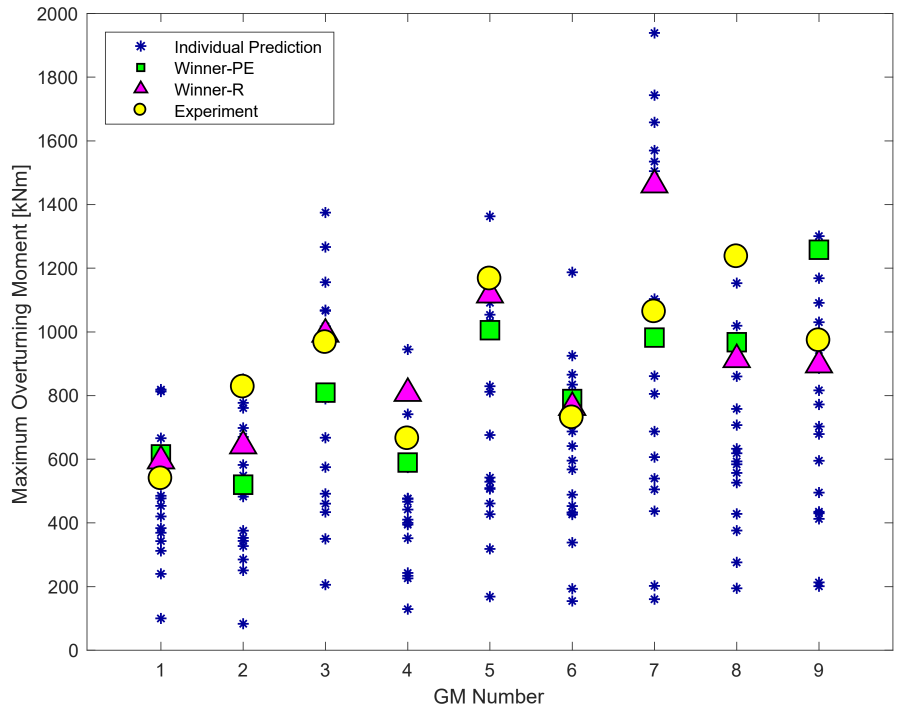

Figure 4.7 **Predictions of maximum overturning moment at the base of the columns versus measured response.**

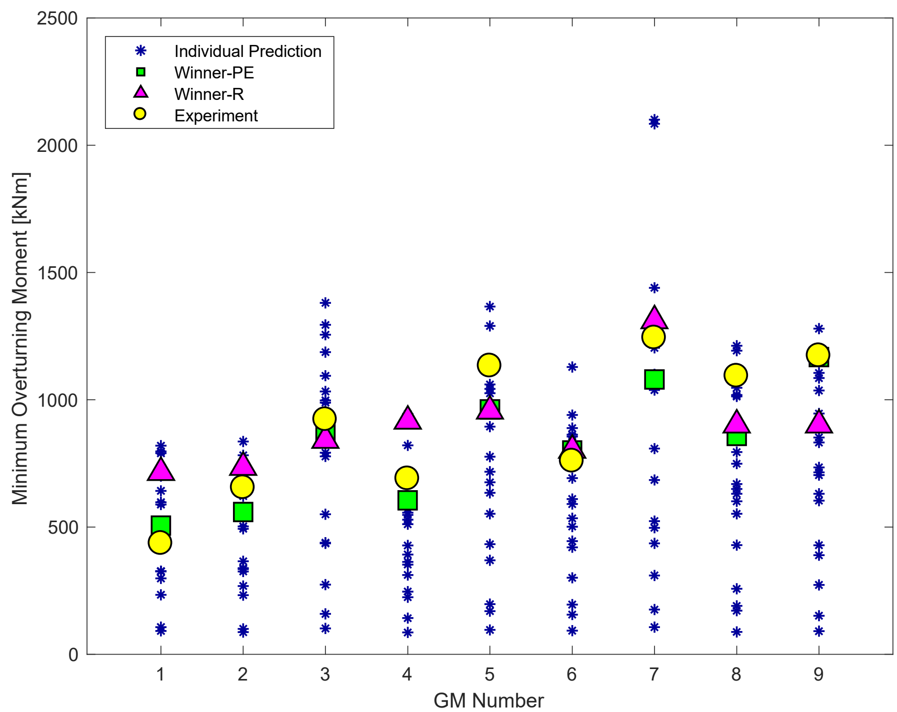

Figure 4.8 **Predictions of minimum overturning moment at the base of the columns versus measured response.**

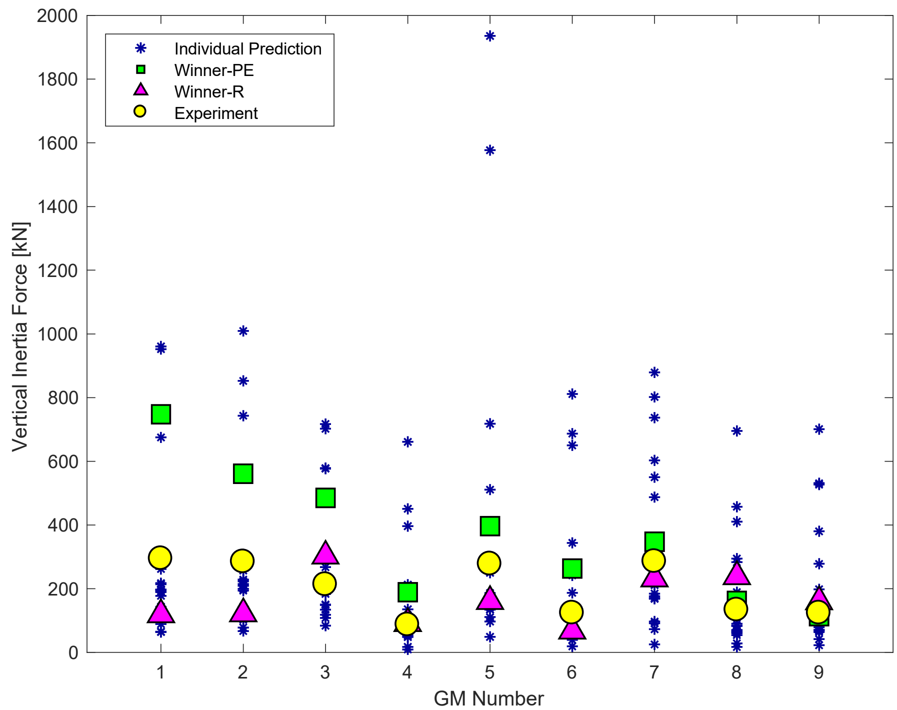

Figure 4.9 **Predictions of vertical inertia force versus measured response.**

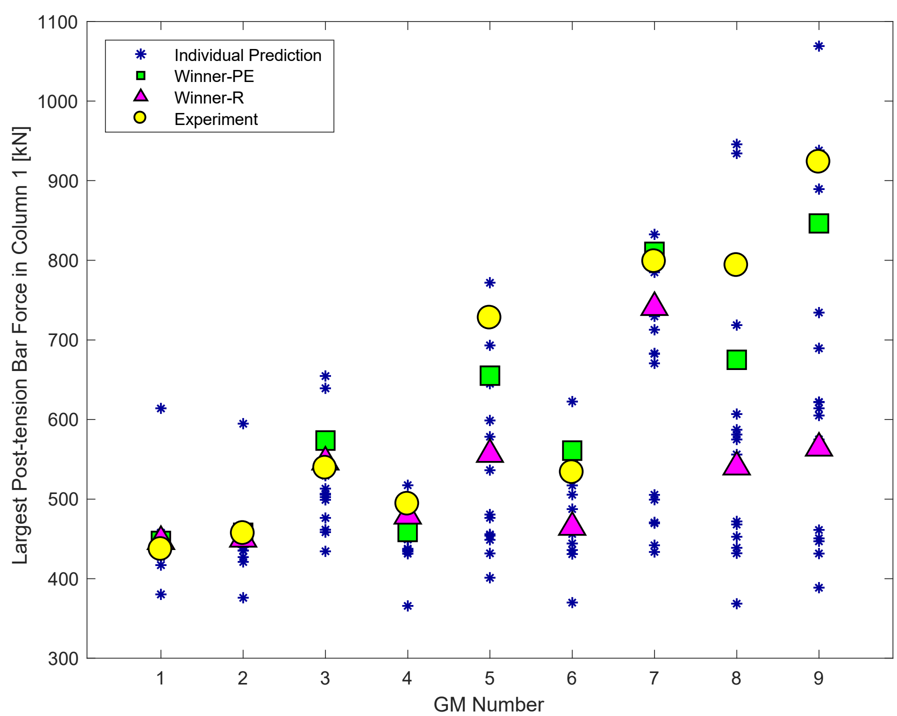

Figure 4.10 **Predictions of largest post-tension bar force in Column 1 versus measured response.**

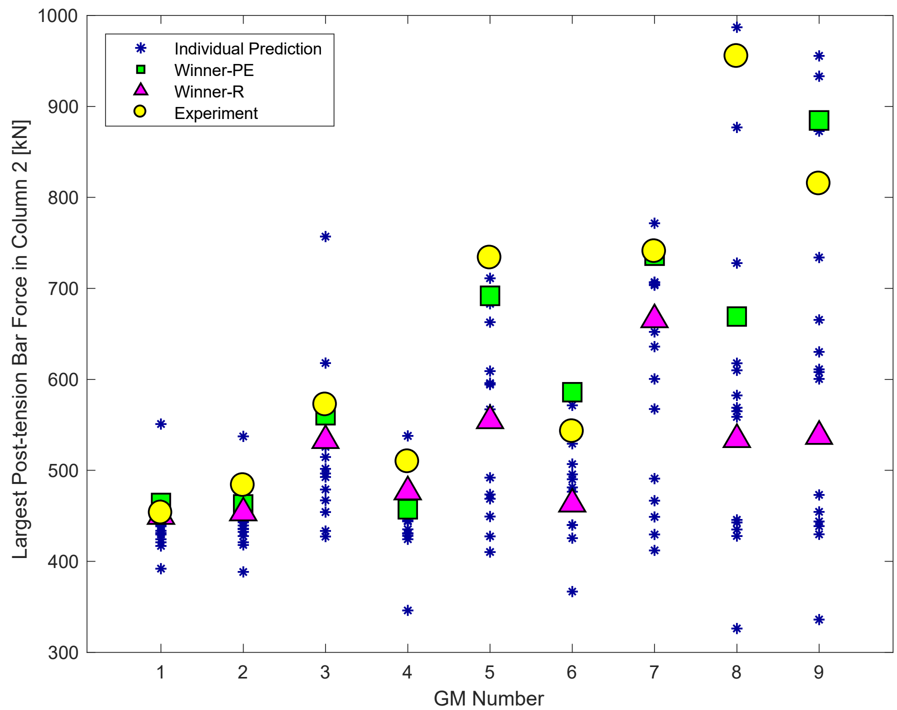

Figure 4.11 Predictions of largest post-tension bar force in Column 2 versus measured response.

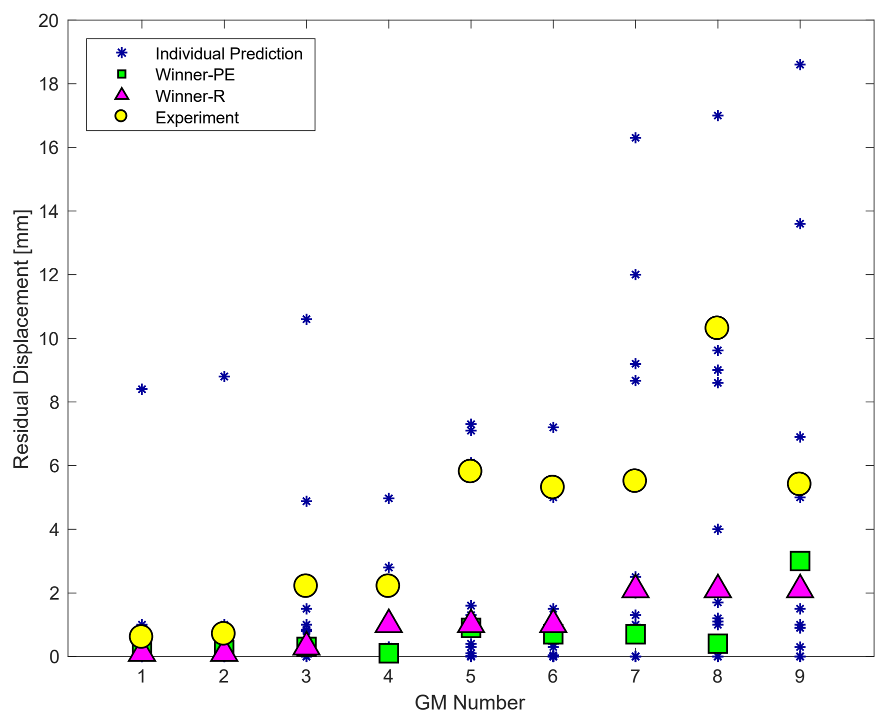

Figure 4.12 Predictions of residual displacement at the top of the columns versus measured response.

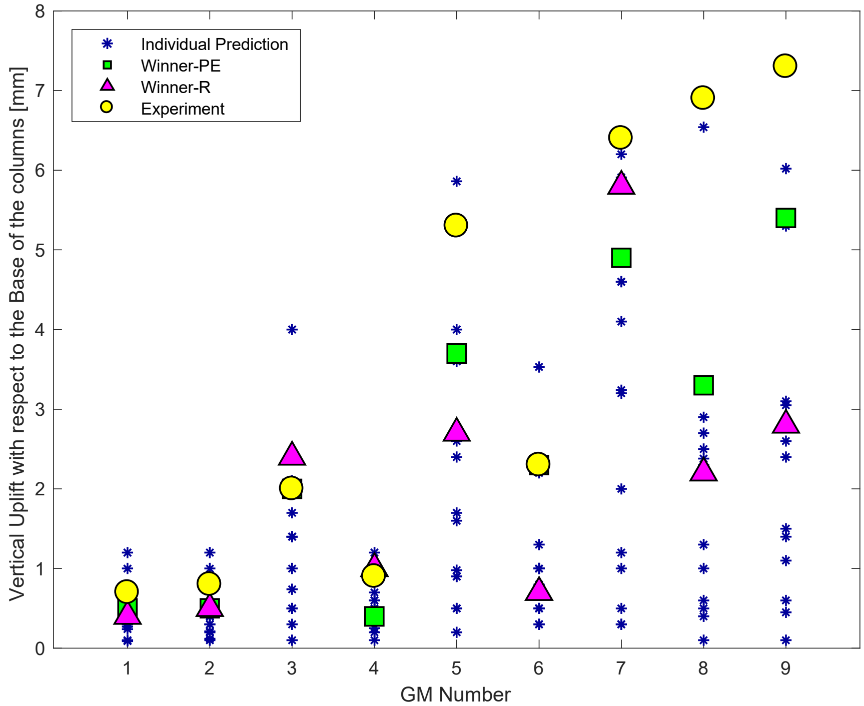

Figure 4.13 **Predictions of vertical uplift with respect to the base of the columns versus measured response.**

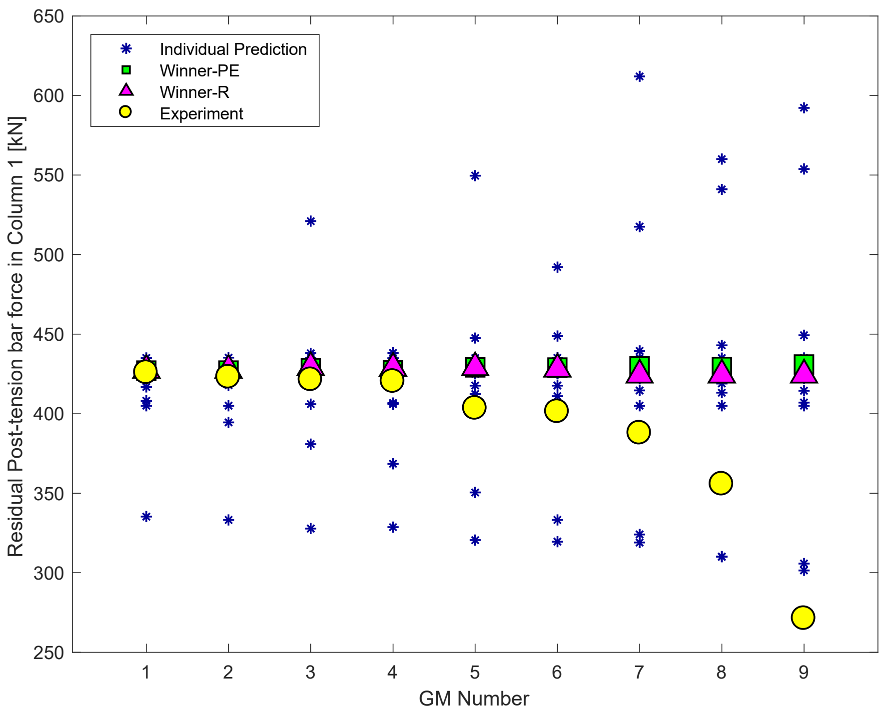

Figure 4.14 **Predictions of residual post-tension bar force in Column 1 versus measured response.**

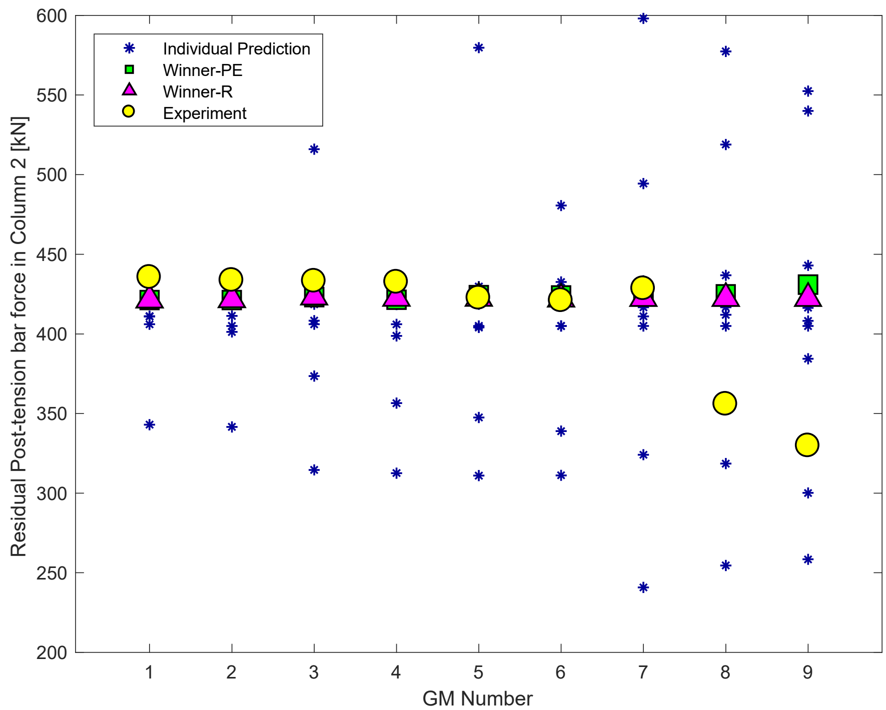

Figure 4.15 Predictions of residual post-tension bar force in Column 2 versus measured response.

4.7 SURVEY STATISTICS

Contestants were asked to provide information about their models via survey forms. The questions on the survey were seeking information on

- Nonlinear analysis program used;
- Column modeling;
- Cap beam modeling;
- Footing modeling;
- Post-Tension bar modeling;
- Mass block formulation;
- Rotational mass;
- Damping model;
- Damping ratio;
- Integration scheme;
- Integration time-step;
- Second-order effects; and
- 80% confidence estimations.

The information acquired from the survey is summarized in Figure 4.16–Figure 4.23. A total of 11 different analysis software programs were used to numerically model and analyze the bridge column; see Figure 4.16. The largest number of contestants (6, 31.6%) used OpenSees. ANSR, LS-DYNA, and ETABS were each used by two contestants (10.5%), and SeismoStruct, SAP2000, Perform 3D, Midas Gen, GiD+OpenSees, Extreme Loading for Structures and Canny were each used by one contestant (5.3%). Force-based beam–column was used by eight contestants to model the columns, while three teams used beams with springs and a variety of other element types were used by other teams; see Figure 4.17. Truss and Corotational Truss were used by six and five teams respectively for post-tension bar modeling with a variety of element types used by other teams; see Figure 4.18. Rayleigh damping with mass and initial damping was employed by nine teams, while Rayleigh damping with mass and tangent stiffness was used by seven teams; see Figure 4.19. Five percent (5%), 3%, 2%, 4% and <1% damping was utilized by five, five, three, two, and four teams, respectively; see Figure 4.20.

As expected, the Implicit Newmark algorithm was the most widely used integration algorithm (by 11 teams), while the Hilber-Hughes-Taylor (HHT), Explicit Newmark and finite difference were used by three, four, and one teams, respectively; see Figure 4.21. Most of the teams (14) used the time step of the provided motions (0.005 sec) as the integration time step; see Figure 4.22. Ten, six, and three teams indicated that they used large displacement theory, approximate P-Delta effects, and small displacement theory, respectively; see Figure 4.23. The effect of the modeling parameters on the results is elaborated in Chapter 6.

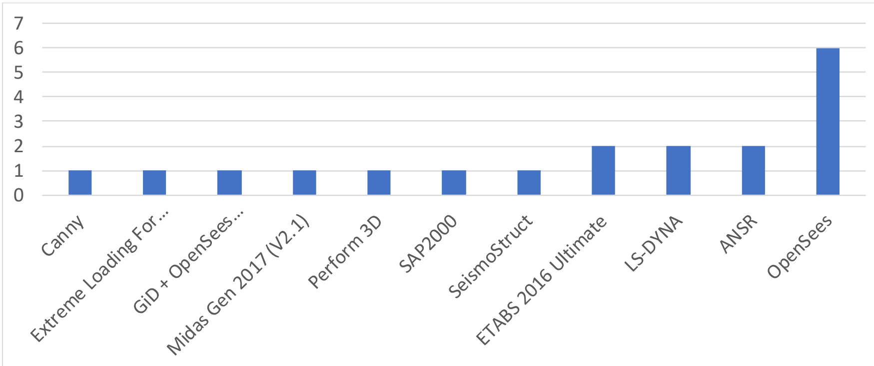

Figure 4.16 Survey statistics: nonlinear analysis program.

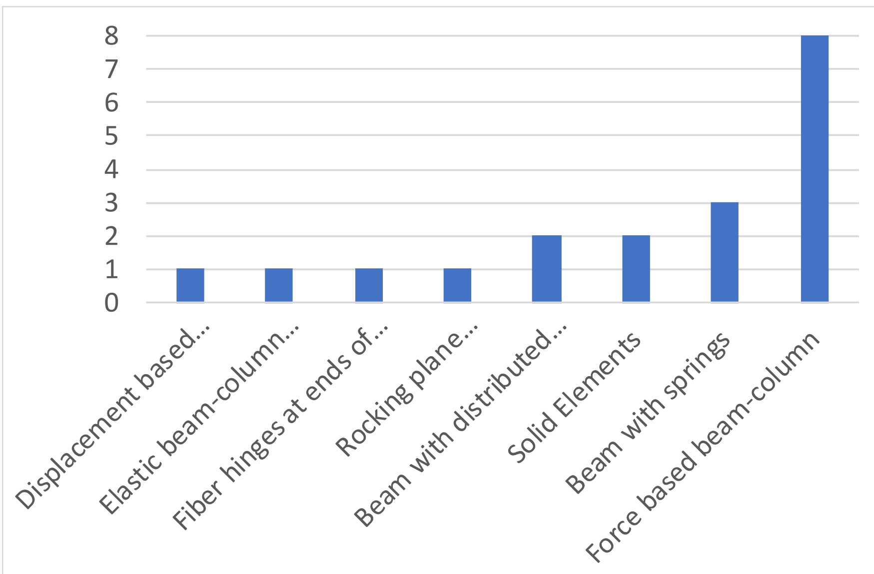

Figure 4.17 Survey statistics: element used for column modeling.

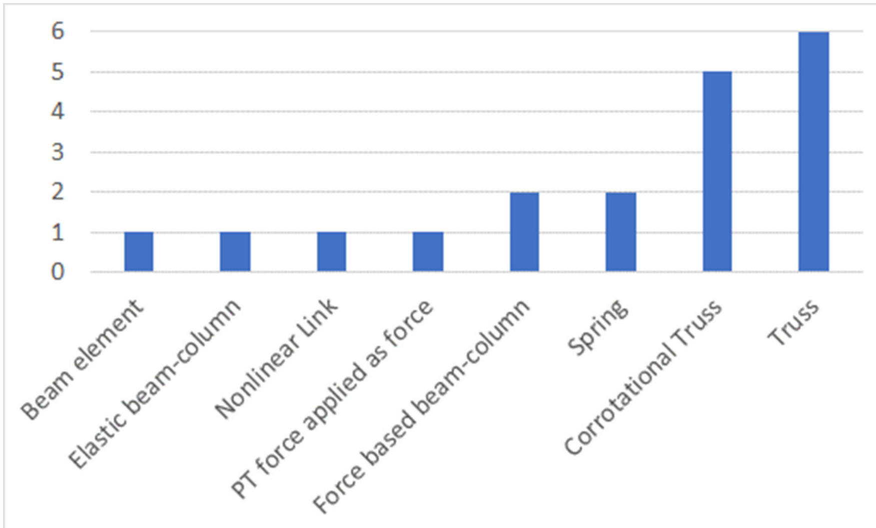

Figure 4.18 Survey statistics: element used for the post-tensioning (PT) bar.

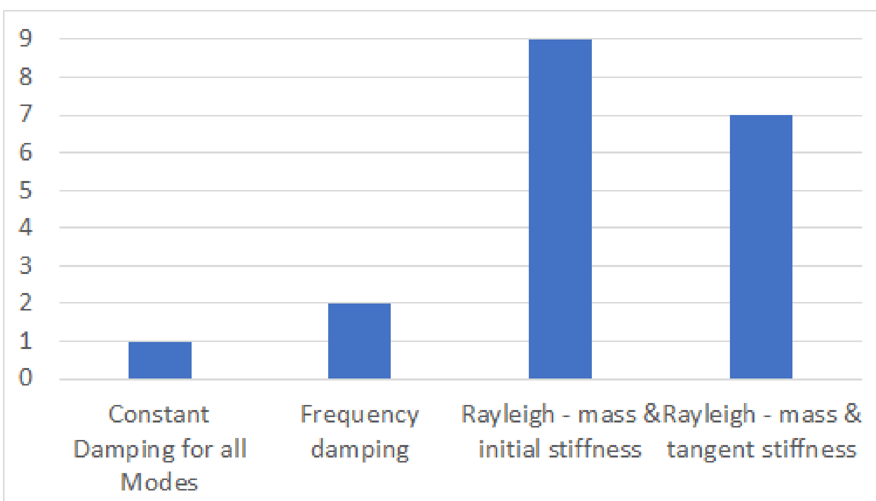

Figure 4.19 Survey statistics: damping model.

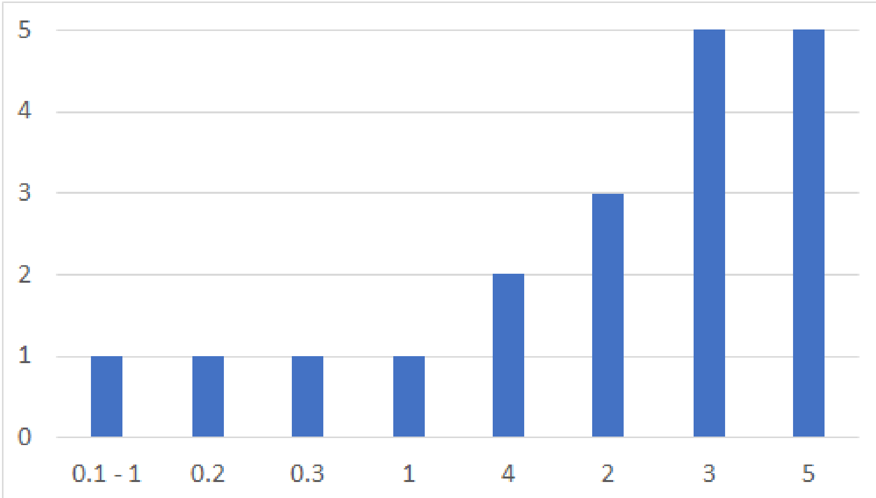

Figure 4.20 Survey statistics: damping ratio (%).

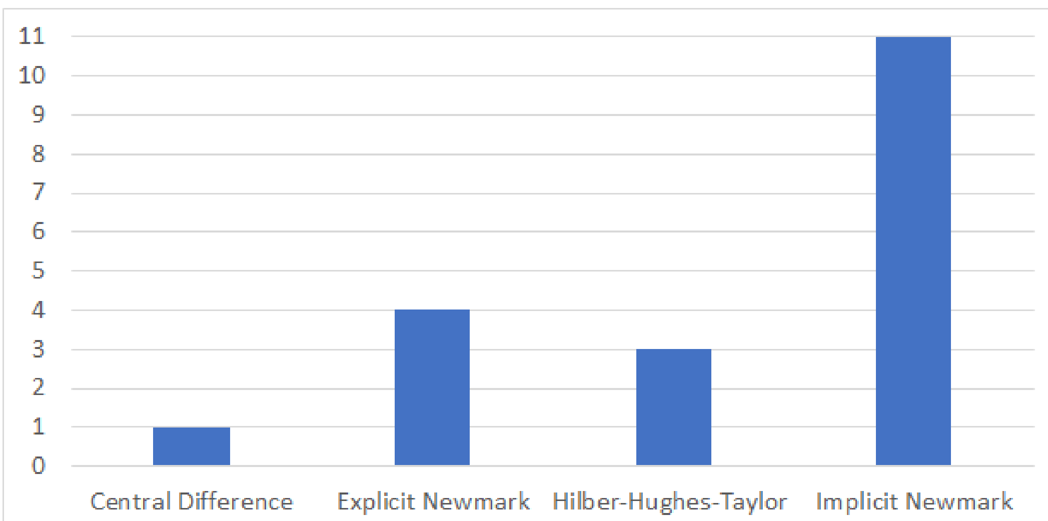

Figure 4.21 Survey statistics: integration method.

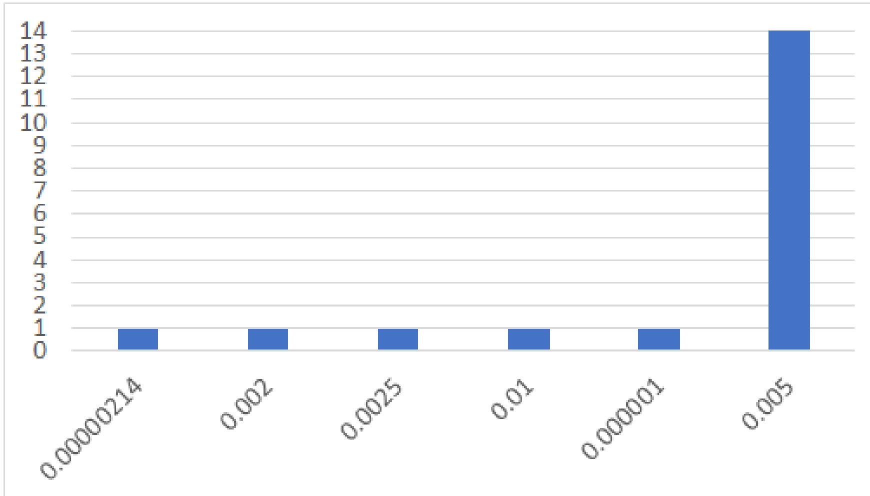

Figure 4.22 Survey statistics: integration time step (sec).

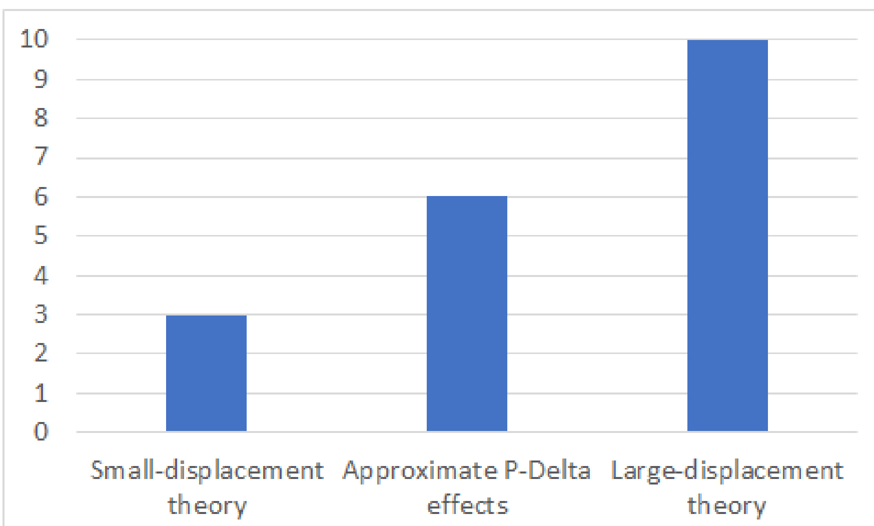

Figure 4.23 Survey statistics: second-order effects.

5 Statistical Analysis of Data

Predictions of the thirteen response quantities by the contestants are statistically analyzed in this chapter. The following sections summarize the results of these analyses, including: (1) mean and median error; (2) coefficient of variation (COV); (3) bias; and (4) histograms of average error for all predicted quantities over the nine ground motions, and histograms that show the increasing error of predicted displacement and acceleration quantities as the test sequence progressed. The following sections also evaluate (1) the performance of the single versus the combined models, and (2) the predicted error bounds.

5.1 MEAN AND MEDIAN ERROR AND COEFFICIENT OF VARIATIONS FOR CONSIDERED RESPONSE QUANTITIES

The predicted data were statistically analyzed to quantify their variation from the measured responses and show the dispersion of predicted responses. Figure 5.2–Figure 5.14 show the predictions, test results, mean and median error, and COV for each predicted quantity and each ground motion. Error is defined using Equation (5.1) as the absolute value of the difference between the prediction (R_a) and the measured response ($R_{\exp}$) normalized by the measured response. The COV is defined as the standard deviation of the predictions of the teams normalized by the mean of the predictions. The designation "Maximum" in the figures refers to the absolute maximum of the considered response in the positive direction. The designation "Minimum" refers to the absolute maximum in the opposite direction of "Maximum". Since "Maximum" and 'Minimum" are absolute maximums in the two directions, positive error in the figures indicates that the predictions are larger than measured.

Table 5.1 lists average COV and error over all considered earthquakes for different response quantities. Note that the predictions that deviated unreasonably from the measured responses were excluded from the statistical analysis.

$$Error = \left(R_a - R_{\exp}\right) / R_{\exp} \tag{5.1}$$

Accuracy of the predictions is evaluated using the Average Error column in Table 5.1 as Error indicates the difference between the prediction and measurement. Although the COV shows the dispersion in the predictions of different teams, it is not necessarily indicative of the accuracy as it does not involve the measured responses. As shown in Figure 5.1, however, there is a good correlation between the Average Error and Average COV.

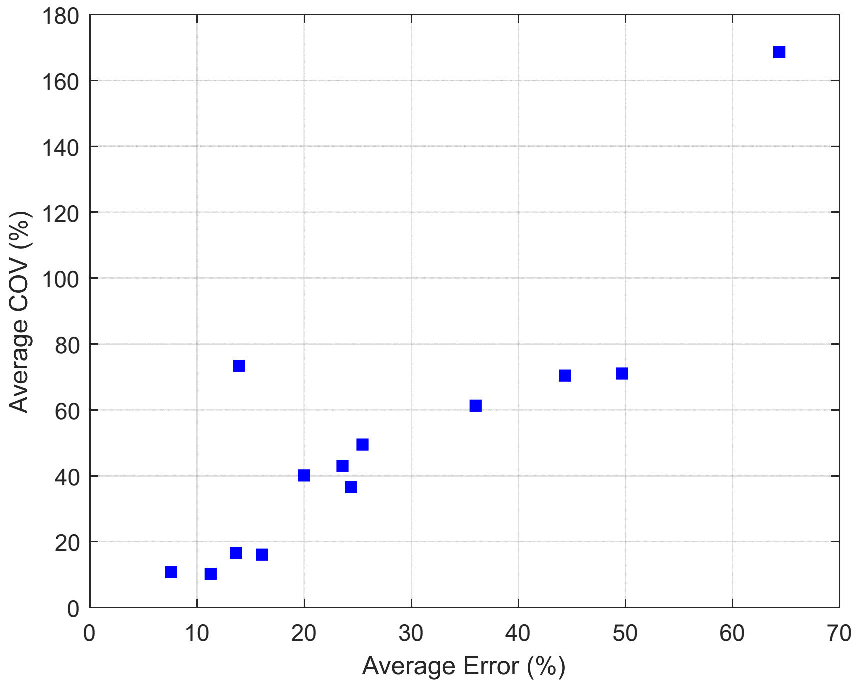

Figure 5.1 Average Error versus Average COV for the considered response quantities.

As shown in Table 5.1, forces were predicted better than displacements. The post-tension bar forces were predicted with the best accuracy. This is followed by the vertical inertia force, the maximum lateral inertia forces, and the overturning moments. Note that the vertical inertia force had a substantially larger COV compared to other quantities with a small Error (less than 16.6% versus 73.4%). The peak and residual displacements were predicted with the least accuracy. These results indicate that the accelerations and forces were predicted better than the displacements. The inaccuracy of the displacement predictions is a concern for the performance-based evaluation of this type of resilient systems as the displacement is a good indicator of the column response and damage. As a potential future study, loss curves can be determined with the analytical models developed by different teams, and these loss curves can be compared against a reference model that is tuned well to match the experimental results.

Table 5.1 demonstrates that COV of some of the predicted quantities were larger than 50%, including the vertical inertia force, maximum horizontal displacement, vertical uplift, and the residual displacement; however, in general, it can be stated that the scatter in the predictions of different teams was not significantly large.

Table 5.1 Average coefficient of variation (COV) for different response quantities.

Response quantity	Average COV (%)	Average error (%)	# of outliers	# of data
Residual post-tension bar force in Column 1 (kN)	10.2	11.3	2	17
Residual post-tension bar force in Column 2 (kN)	10.7	7.6	2	17
Largest post-tension bar force in Column 1 (kN)	16.6	13.6	2	17
Largest post-tension bar force in Column 2 (kN)	16.0	16.0	2	17
Vertical inertia force (kN)	73.4	13.9	3	16
Maximum lateral inertia force (kN)	40.1	20.0	0	19
Minimum lateral inertia force (kN)	36.5	24.4	1	18
Maximum overturning moment (kNm)	43.0	23.6	0	19
Minimum overturning moment (kNm)	49.5	25.4	0	19
Maximum horizontal displacement (mm)	70.4	44.4	0	19
Minimum horizontal displacement (mm)	61.3	36.0	0	19
Vertical uplift with respect to the base of the columns (mm)	71.0	49.7	4	15
Residual displacement (mm)	168.6	64.4	5	14

5.1.1 Residual and Largest Post-Tension Bar Forces

Residual post-tension bar force was predicted with the best accuracy among all the response quantities. Although the accuracy was quite good, the predictions were not successful in terms of predicting the trends. As shown in Figure 5.2, the residual post-tension bar force in Column 1 decreased with increasing GM#; however, only two teams predicted this trend. Figure 5.2 shows that Error and COV increased with increasing ground-motion intensity, as expected. Note that errors in GMs 8 and 9 are significantly larger than the errors in all other motions. As discussed in Chapter 3, both post-tension bars were observed to yield in these ground motions, and some of the teams did not predict this yielding. Similar observations can be made for the largest post-tension forces; most of the predictions were smaller than the measured values.

5.1.2 Inertia Forces and Overturning Moments

The COV of both horizontal and vertical inertia forces do not show an obvious trend as a function of the GM. They are mostly constant over all GMs. The COV of vertical inertia force is much larger than that of the horizontal inertia force. Errors also do not show a clear trend. GM1 with elastic response had a larger error than some of the larger intensity motions. This is also an expected outcome because the elastic response mainly depends on the period and damping ratio, and any small change in these quantities can result in a large error.

Response spectra of the vertical component of GM02 are plotted in Figure 5.15 for different damping ratios in the vertical period range of the bridge bent. The vertical period of the bridge bent is identified to be in the range of 0.06 and 0.08 using the transfer function of accelerations, which is computed as the FFT amplitude of the average of the two vertical accelerations in the center of the cap beam divided by the FFT of the accelerations measured on the table in the vertical direction. To match the vertical response accelerations analytically in GM2, the damping ratio in the vertical direction is determined to be 11%. Note that the specimen remained elastic in GM2; therefore, the identified period and damping ratios correspond to the elastic response. The response spectra shown in Figure 5.15 demonstrates that the spectral acceleration at 0.08 sec for damping of 11% is less than half of the spectral acceleration at 0.06 sec for 5% damping; therefore, any big error in the predictions can be caused by a small difference in the period and a wrong choice of damping.

To identify the source of errors in a more systematic way in future blind predictions, it is recommended to add the natural periods to the list of predicted quantities. Also, providing the contestants with the damping ratios in the elastic range should be considered.

The error of the horizontal inertia force is the smallest for GM9 with the largest intensity, indicating that the teams were able to predict the base-shear capacity of the bridge bent with better accuracy.

Although the overturning moment is proportional to the inertia force, there are some differences between the error of both quantities. As observed in Figure 5.10 and Figure 5.11, the overturning moment is predicted to be lower than the measured, which is not observed for the inertia force. A potential reason for this phenomenon could be the underestimation of the moments at the base of the columns.

5.1.3 Maximum and Residual Displacements

Errors of predicted displacements were larger than those in the predicted forces. For the maximum displacement, the error was the largest in GM1, which was again due to the inaccurate prediction of the period and damping. As indicated and demonstrated in the previous section, in the case of elastic response, even small changes in the dynamic characteristics (like a small difference between the period from the analytical model and the period from the tests) can lead to large errors (depending on the shape of the response spectrum) as the damping is small. In the case of inelastic response, the energy dissipated in inelastic response can be considered as equivalent damping. Accordingly, the inelastic response would lead to larger equivalent damping values, and the modeling issues that result in differences in dynamic characteristics can be interpreted to lead to fewer errors for larger damping. As an example, the response spectrum with 11% damping in Figure 5.15 shows less variation between different periods compared to the response spectrum with 5% damping.

Predicted maximum displacements were smaller than the measured displacements for all ground motions except the first one. Predicted residual displacements and uplift were also smaller than the measured values, and the errors and COV were largest for these quantities among all predicted quantities.

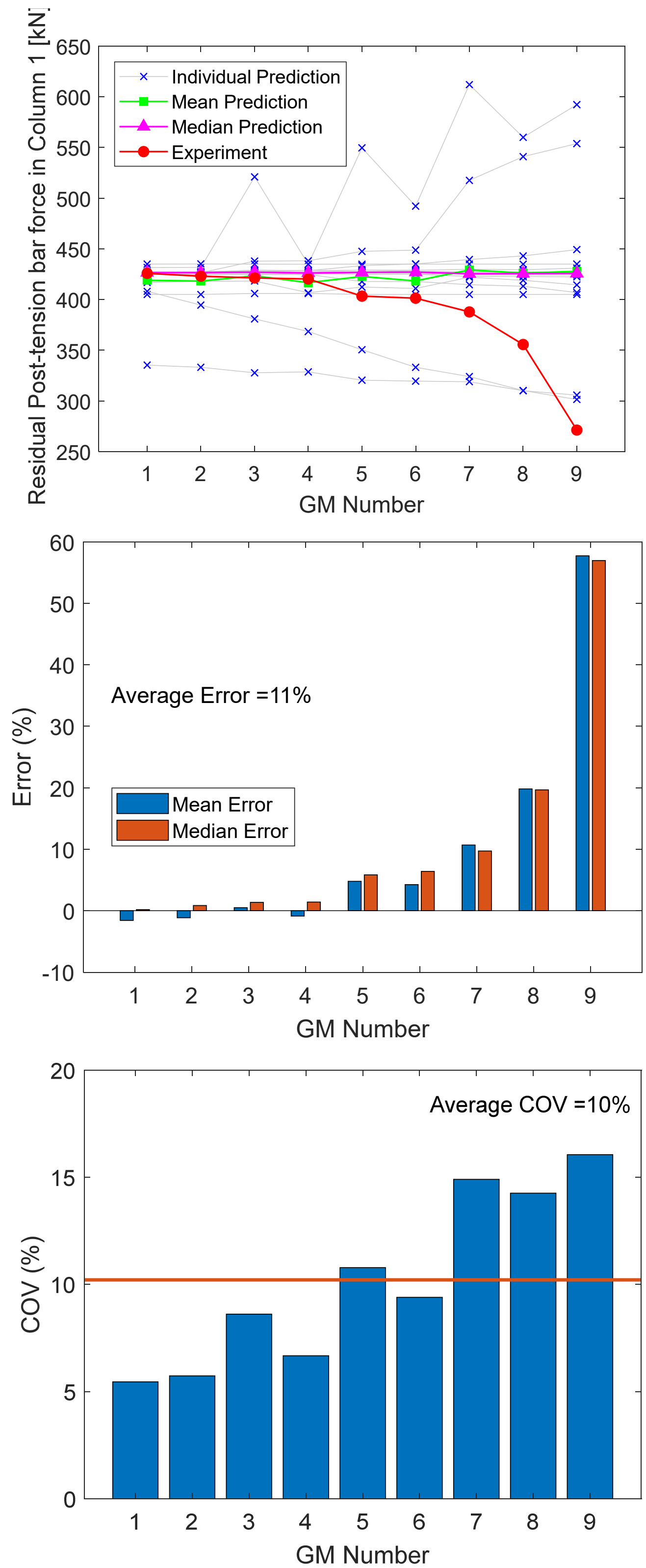

Figure 5.2 **Statistical analysis of the residual post-tension bar force in Column 1.**

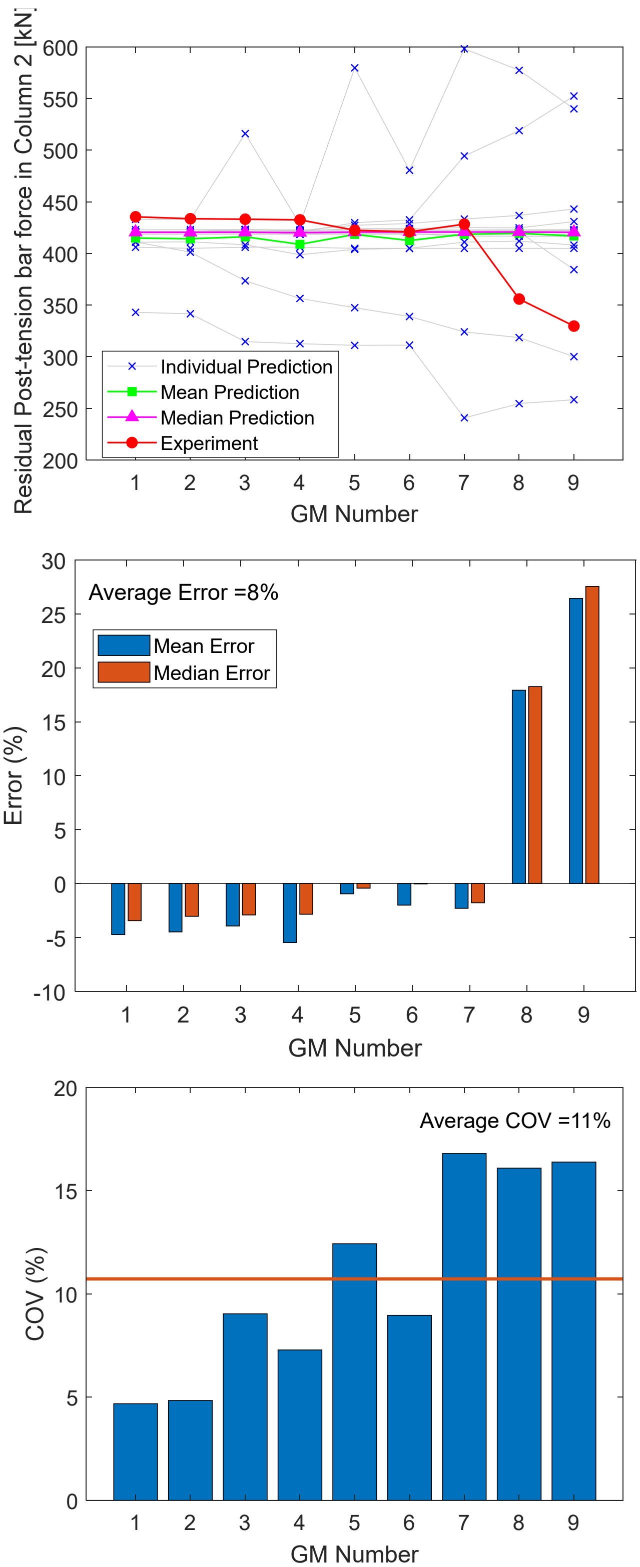

Figure 5.3 Statistical analysis of the residual post-tension bar force in Column 2.

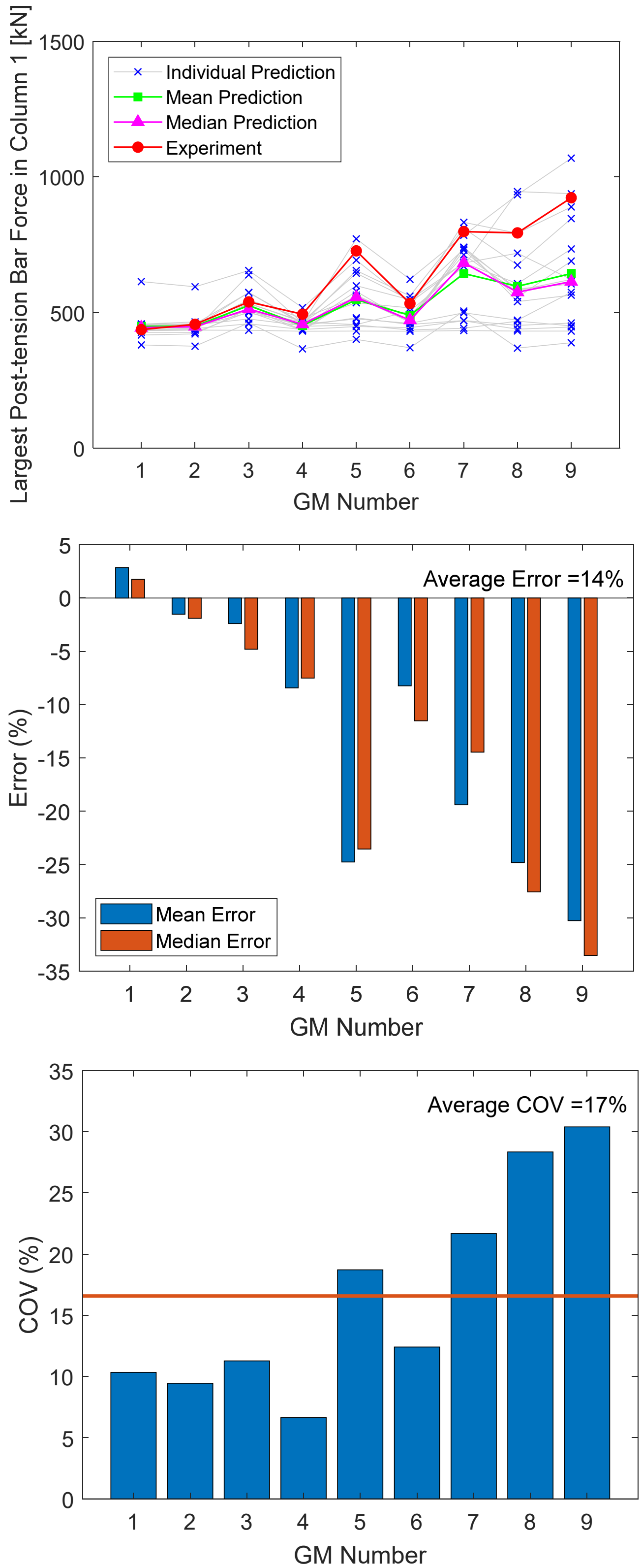

Figure 5.4 Statistical analysis of the largest post-tension bar force in Column 1.

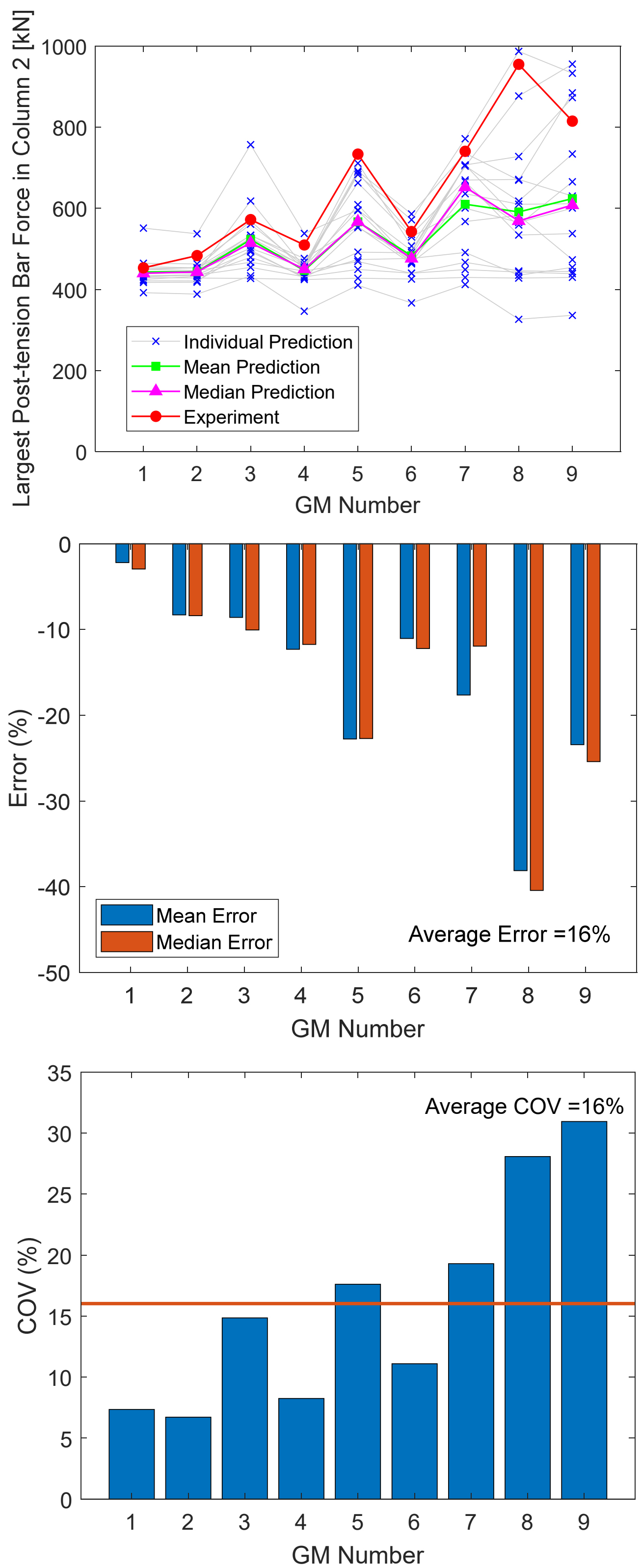

Figure 5.5 **Statistical analysis of the largest post-tension bar force in Column 2.**

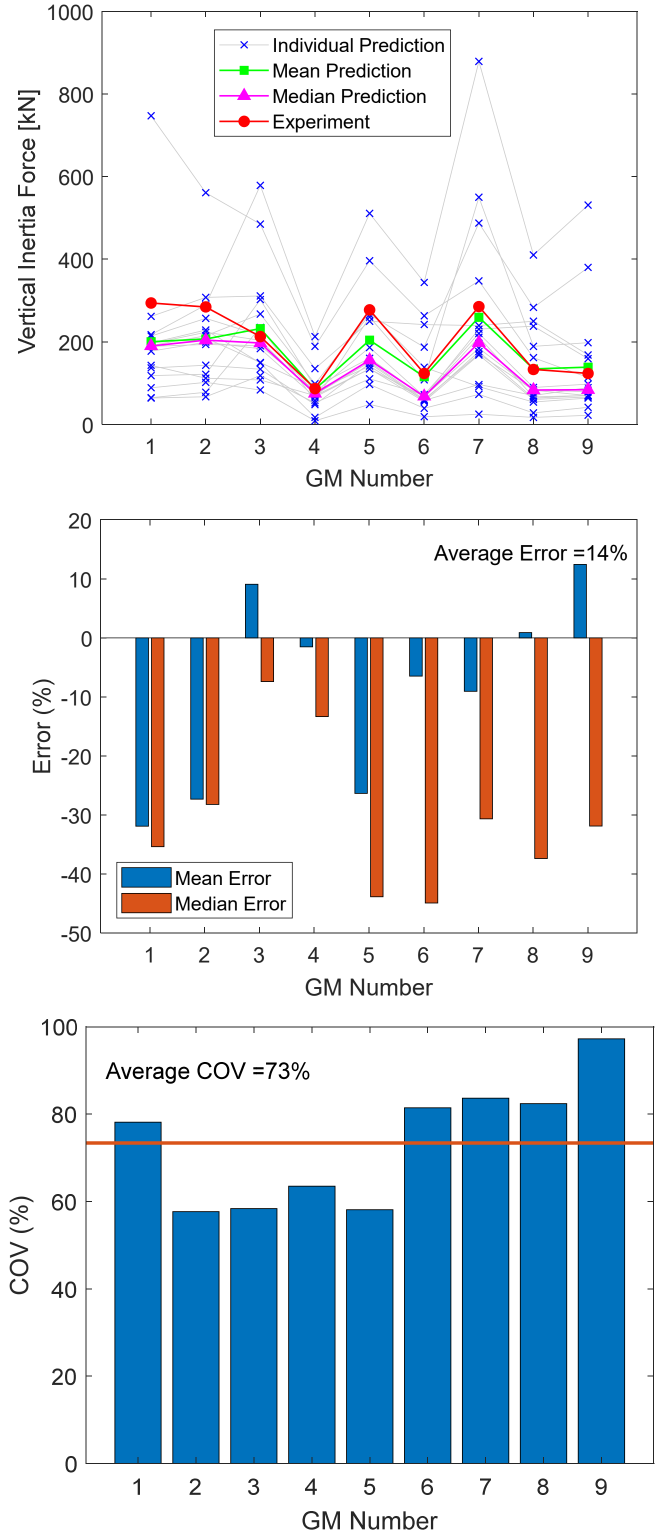

Figure 5.6 Statistical analysis of the vertical inertia force.

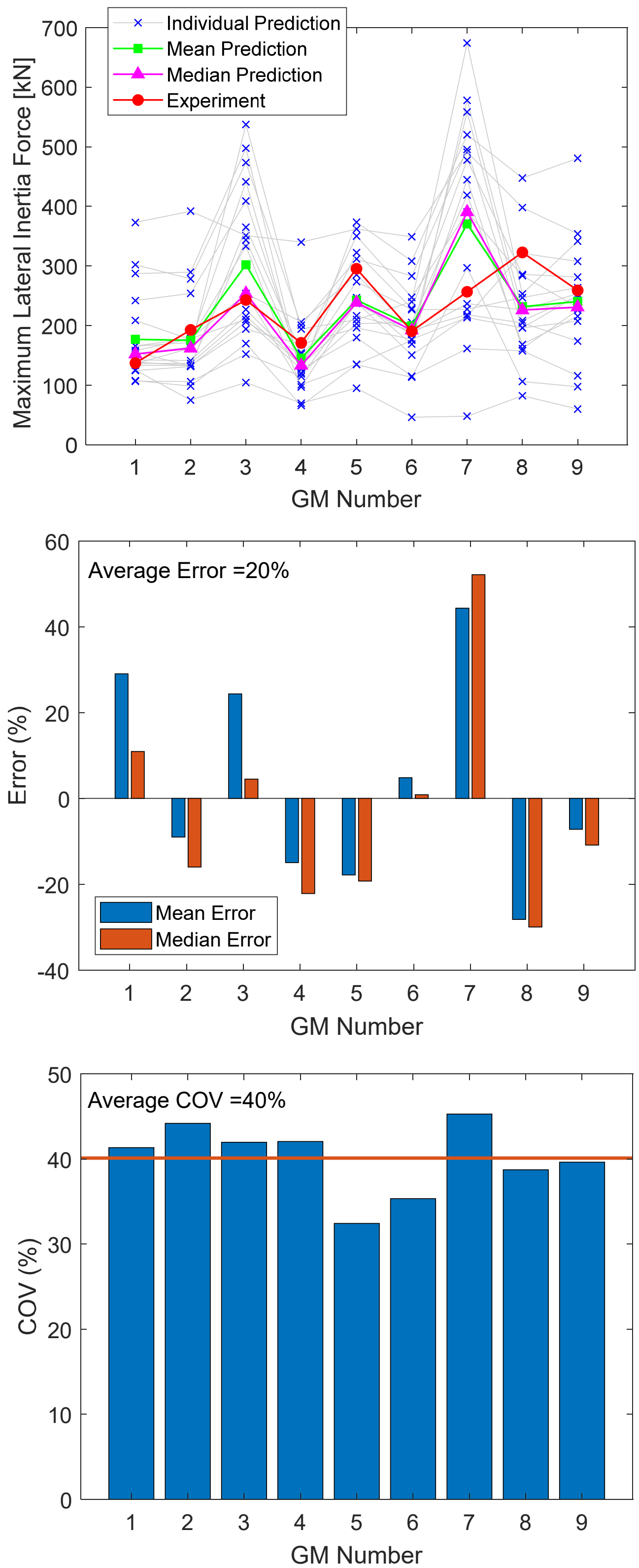

Figure 5.7 **Statistical analysis of the maximum lateral inertia force.**

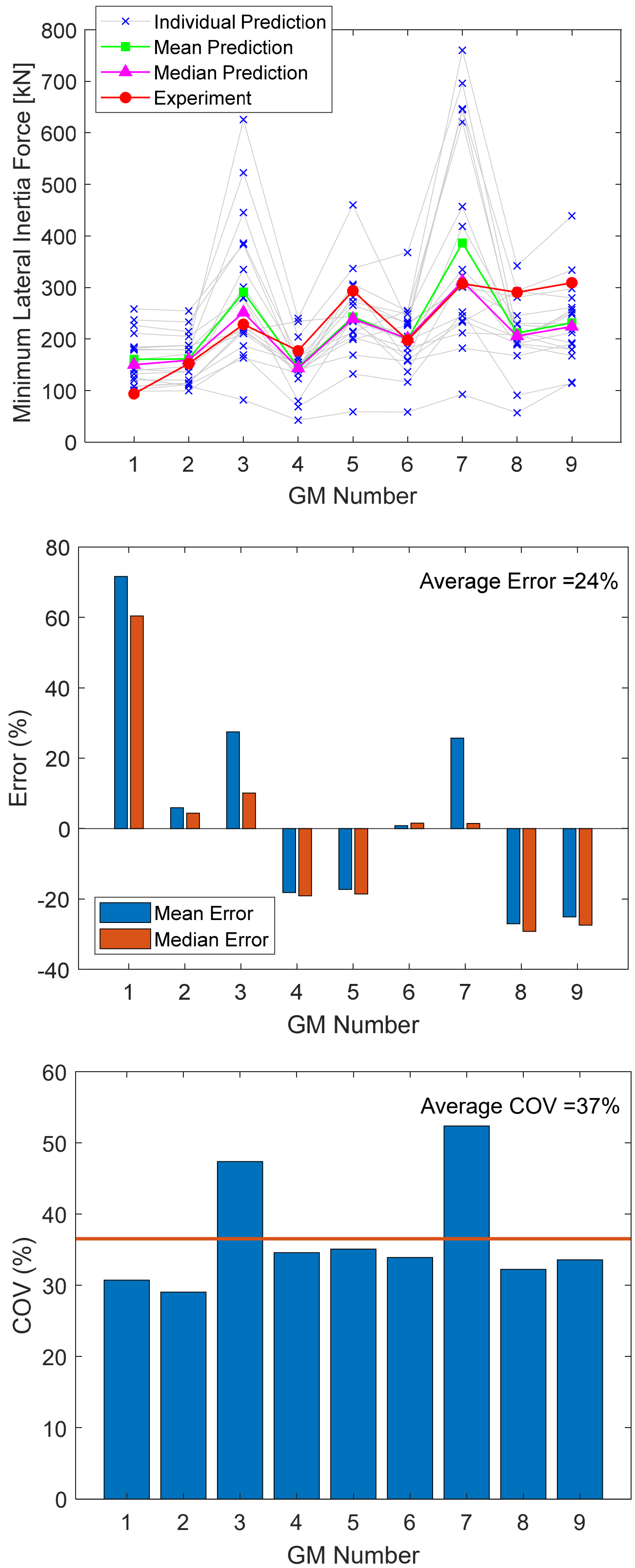

Figure 5.8 Statistical analysis of the minimum lateral inertia force.

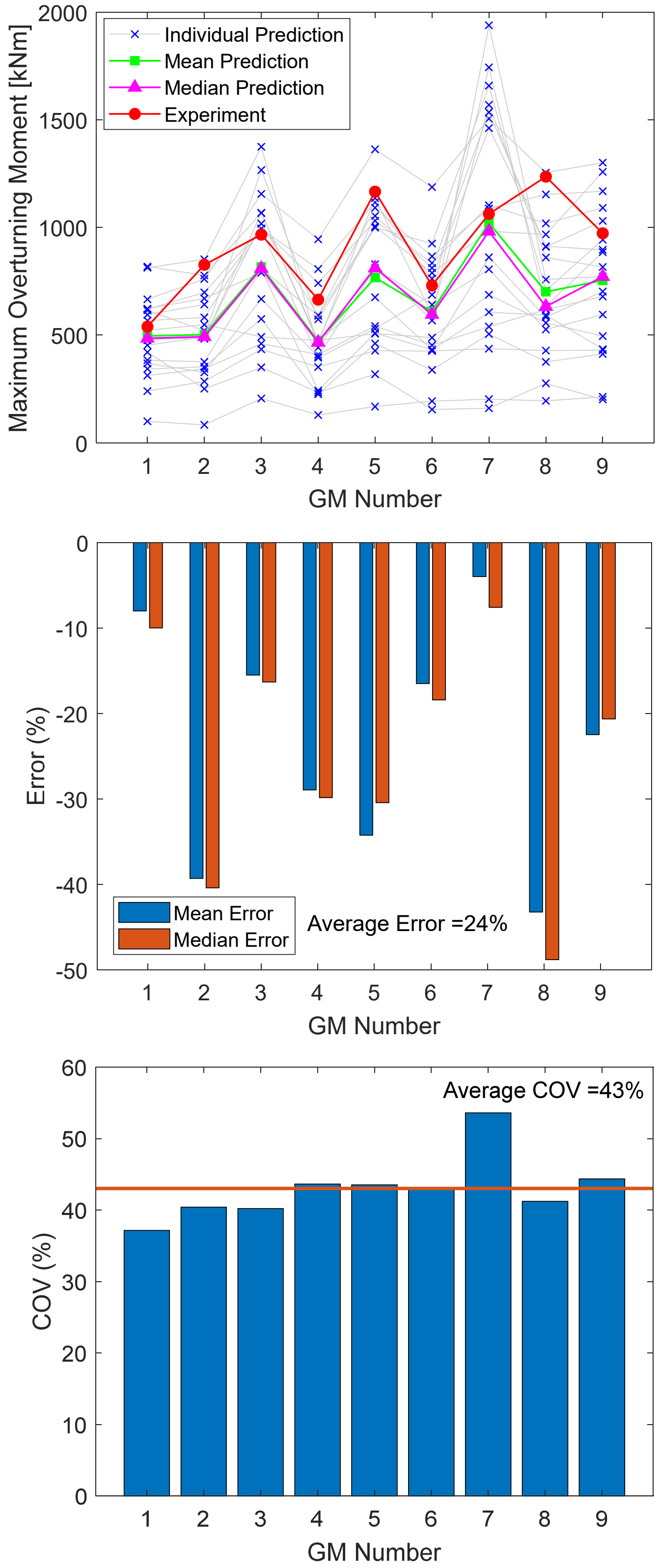

Figure 5.9 Statistical analysis of the maximum overturning moment.

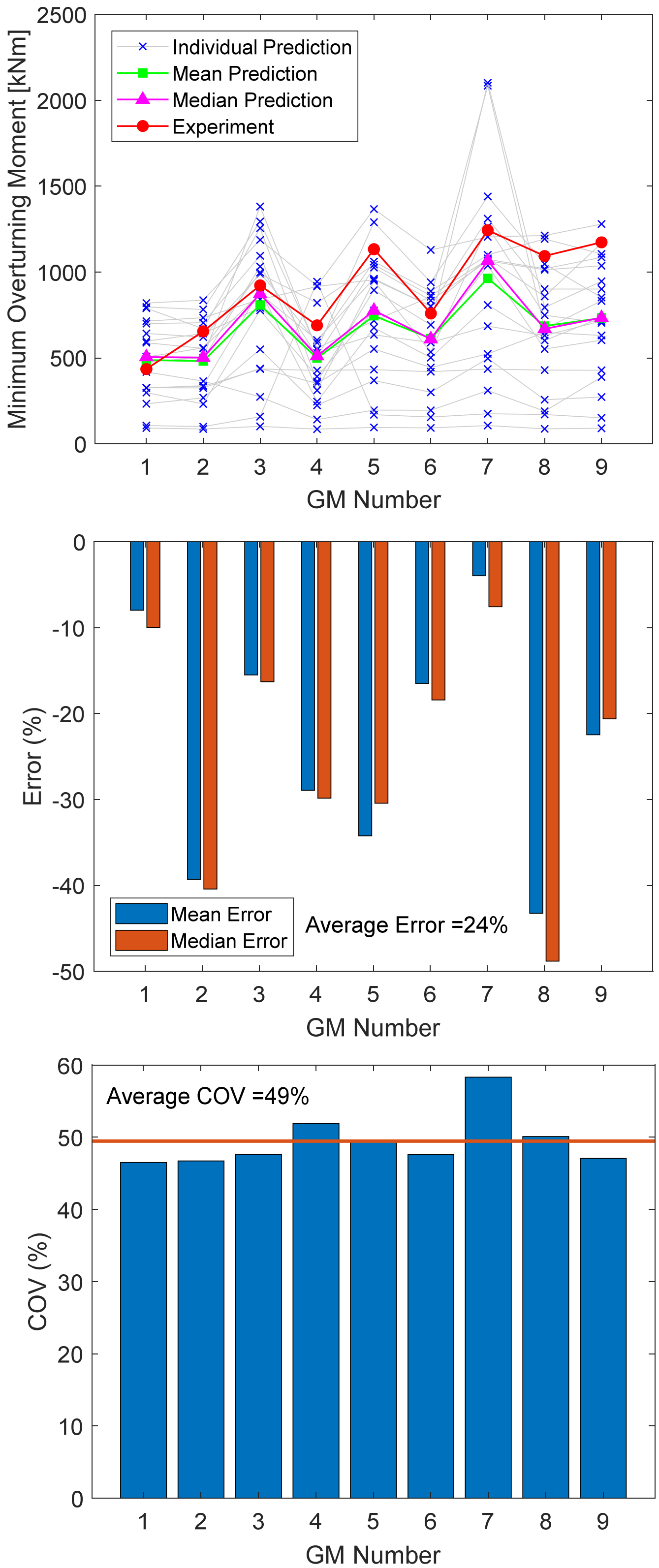

Figure 5.10 **Statistical analysis of the minimum overturning moment.**

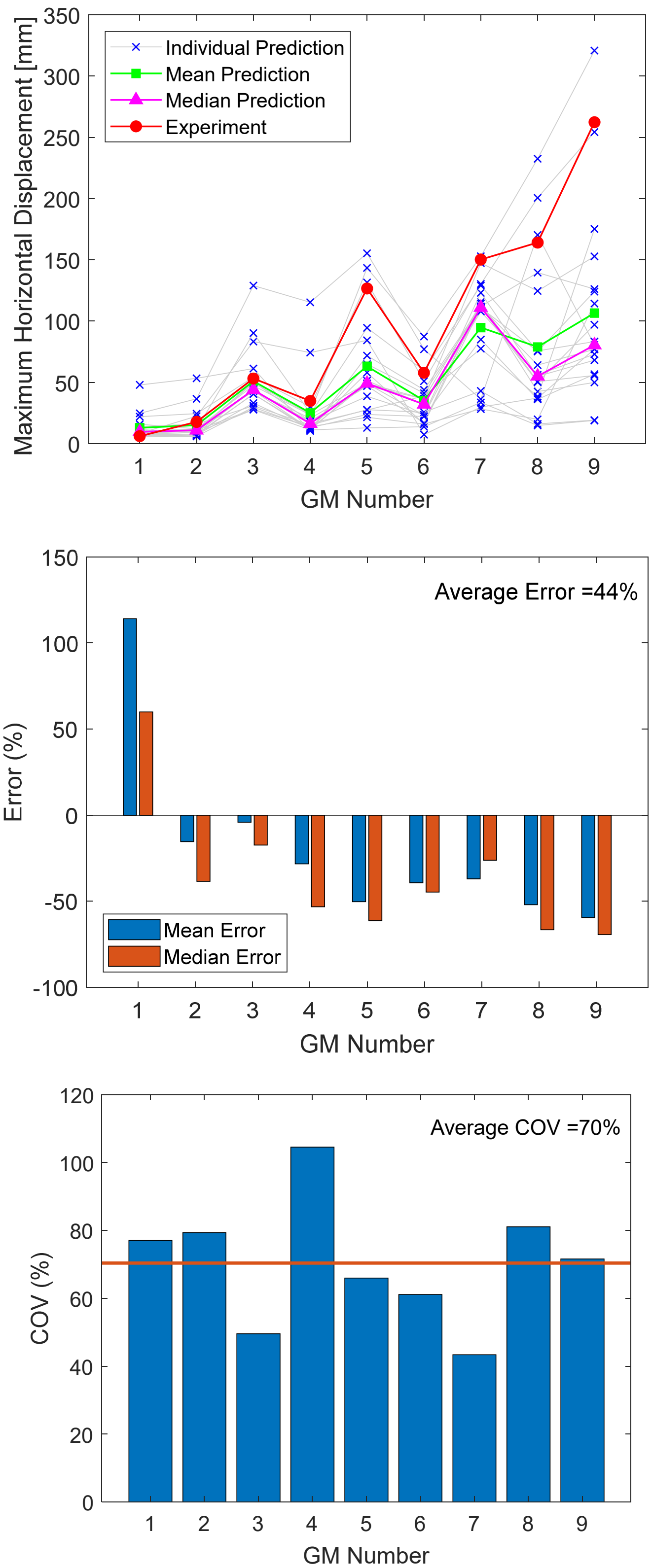

Figure 5.11 Statistical analysis of the maximum horizontal displacement.

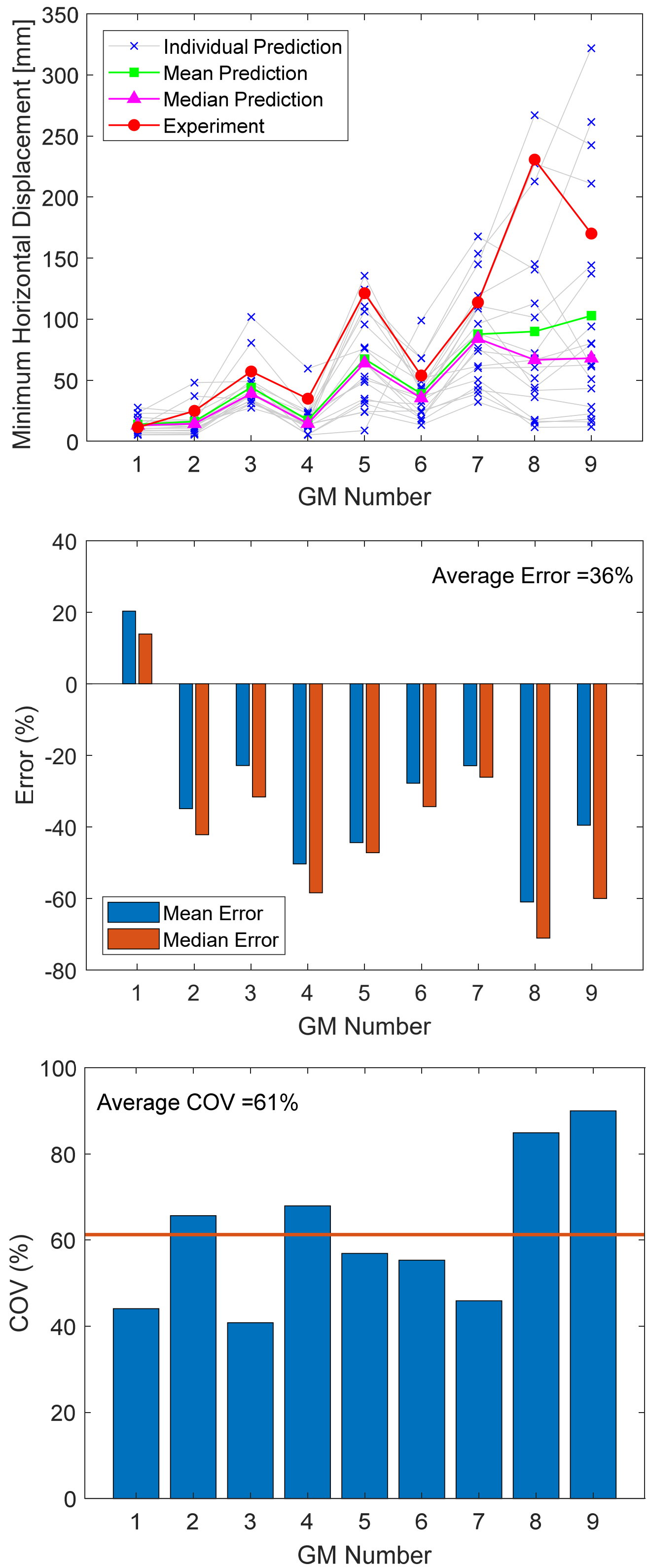

Figure 5.12 Statistical analysis of the minimum horizontal displacement.

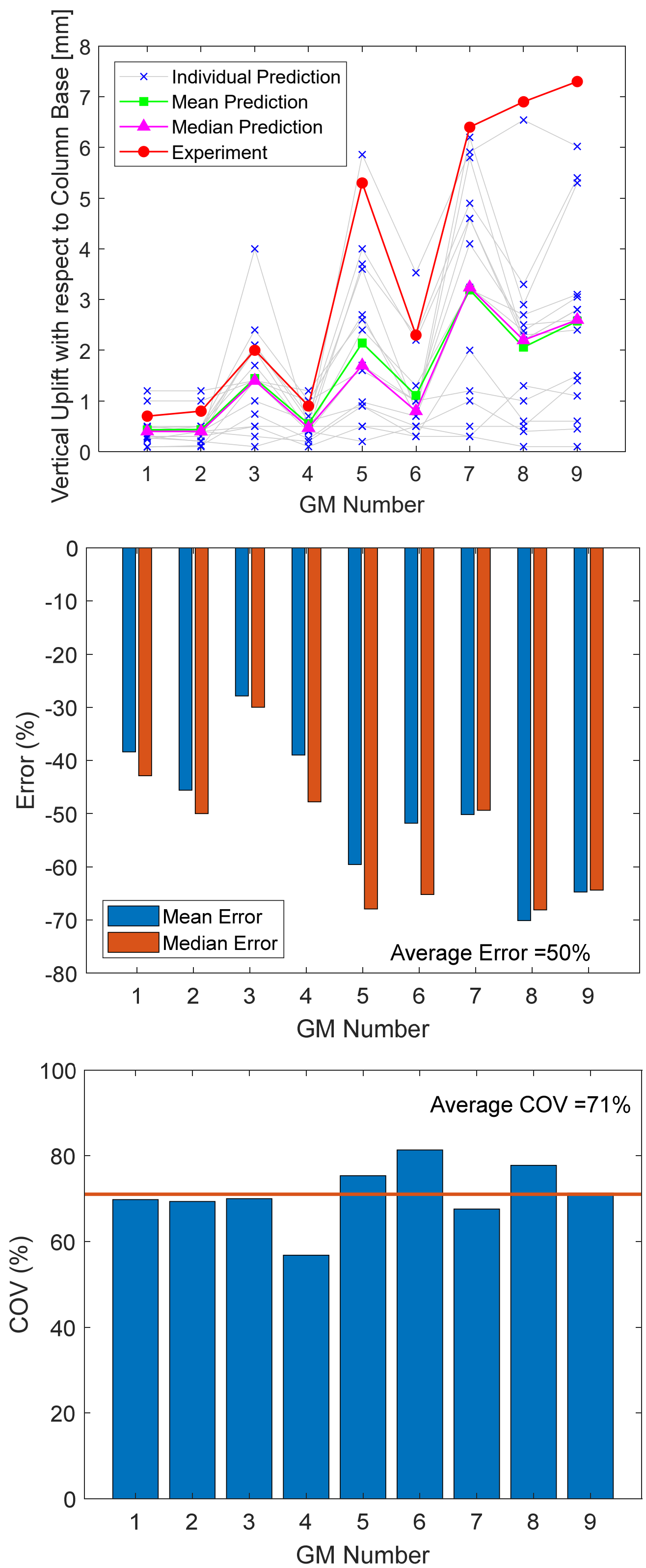

Figure 5.13 Statistical analysis of the vertical uplift with respect to the base of the columns.

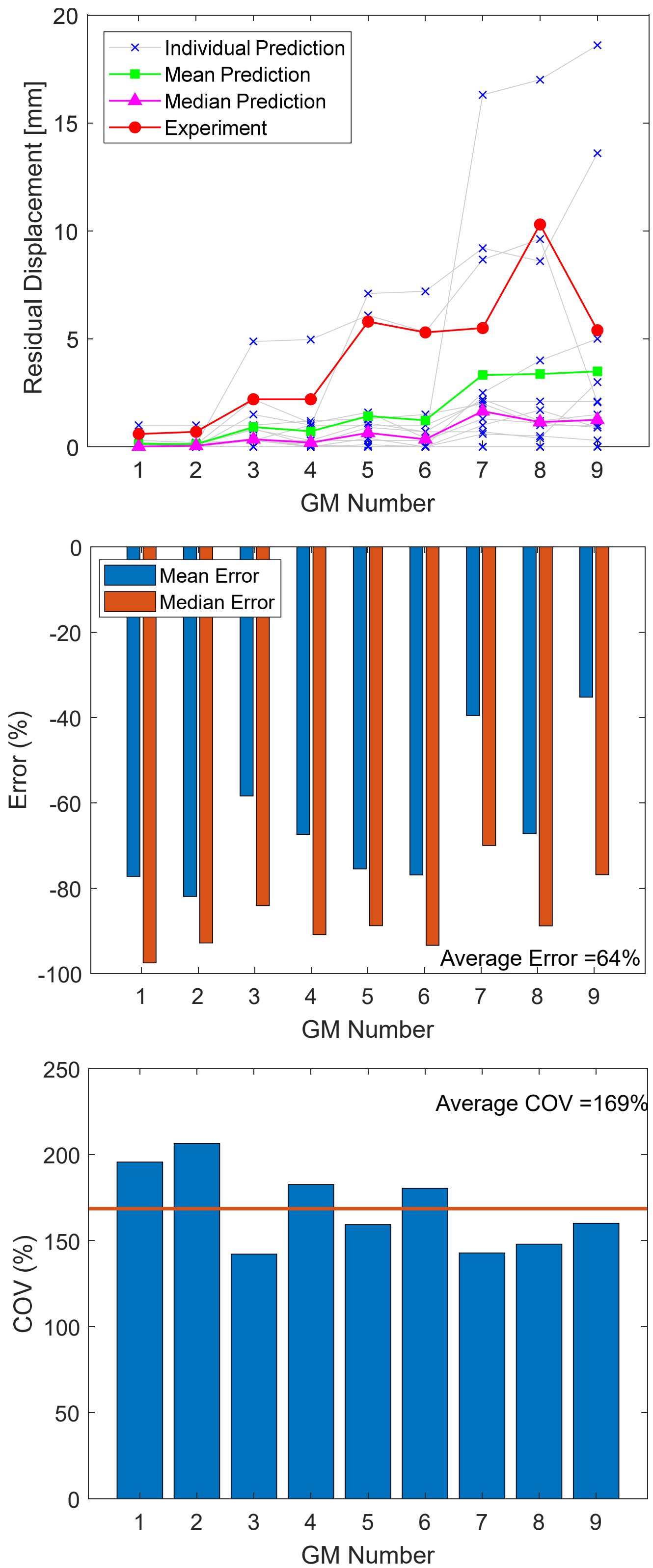

Figure 5.14 Statistical analysis of the residual displacement.

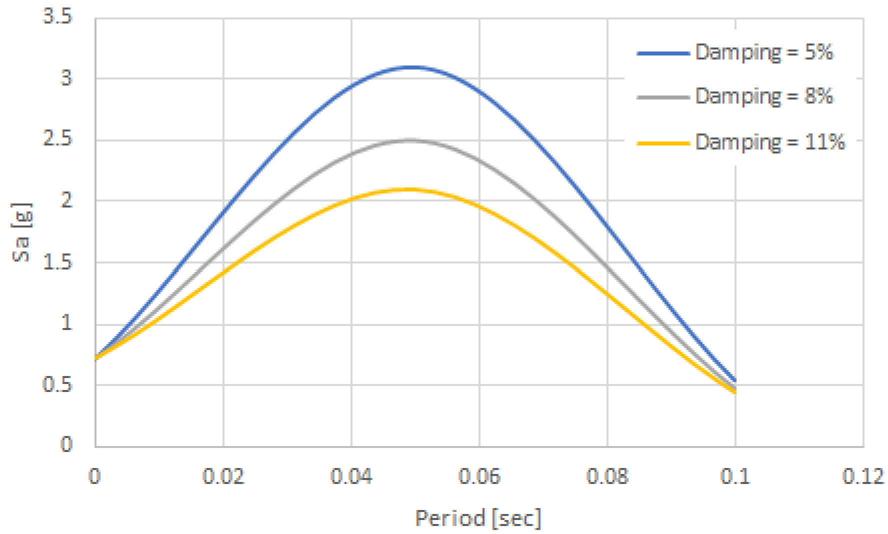

Figure 5.15 **Response spectra of GM2 input vertical acceleration over the vertical period range.**

5.2 DISTRIBUTIONS OF AVERAGE ERROR

Figure 5.16–Figure 5.28 show the lognormal distribution of error in predicting different quantities. The lognormal distribution is obtained by finding the maximum likelihood estimates of the lognormal distribution parameters to fit the data. In these figures, the solid curve shows the fitted lognormal distribution, while the markers represent the data. Note that the data is spread with equal intervals along the *y*-axis. The error is quantified by an average error of a predicted response quantity over a set of ground motions and is calculated as follows:

$$AvgErrRC = \frac{1}{j}\sum_{i=1}^{j} abs\left[\left(R_a - R_{\exp}\right)/R_{\exp}\right] \tag{5.2}$$

where j is the number of ground motions for one predicted response quantity, R_a is analytically predicted response, and $R_{\exp}$ is a response measured from the experiment. To present the results in percentages, the average error calculated by Equation (5.2) is multiplied by 100.

The median and the standard deviation (β, referred to as dispersion) of the natural logarithm of the average error are listed in Table 5.2. Table 5.2 and Figure 5.16–Figure 5.28 lead to observations similar to those discussed above: Forces were predicted better than displacements. For example, the average error that corresponds to a probability of non-exceedance of 1 is around 120% for the maximum horizontal displacement, while it is around 80% for the maximum lateral force. The post-tension bar forces were predicted with the best accuracy. This is followed by the maximum lateral inertia forces, overturning moments, and the vertical inertia force. The peak and residual displacements were predicted with the least accuracy.

Table 5.2 **Median and dispersion (β) of the average error for different response quantities.**

Response quantity	Median (%)	Dispersion (β)
Residual post-tension bar force in Column 1	11.5	0.068
Residual post-tension bar force in Column 2	6.9	0.068
Largest post-tension bar force in Column 1	14.4	0.078
Largest post-tension bar force in Column 2	16.5	0.085
Maximum lateral inertia force	32.2	0.176
Minimum lateral inertia force	34.0	0.184
Maximum overturning moment	34.9	0.189
Minimum overturning moment	34.8	0.222
Vertical inertia force	44.7	0.300
Maximum horizontal displacement	52.8	0.239
Minimum horizontal displacement	48.7	0.138
Vertical uplift with respect to column base	53.5	0.177
Residual displacement	84.1	0.143

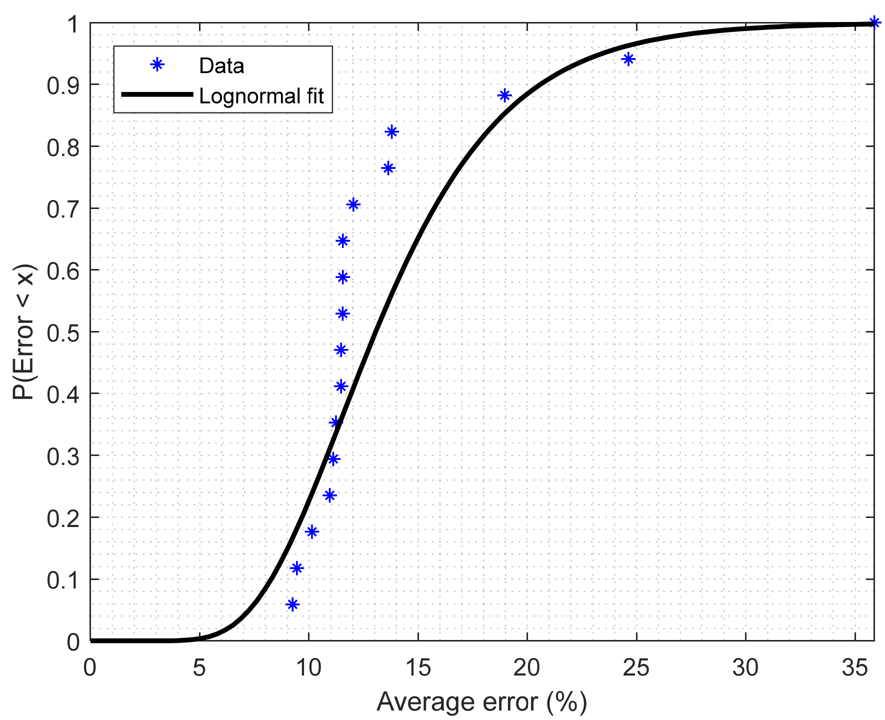

Figure 5.16 Lognormal distribution of average error for the residual post-tension bar force in Column 1.

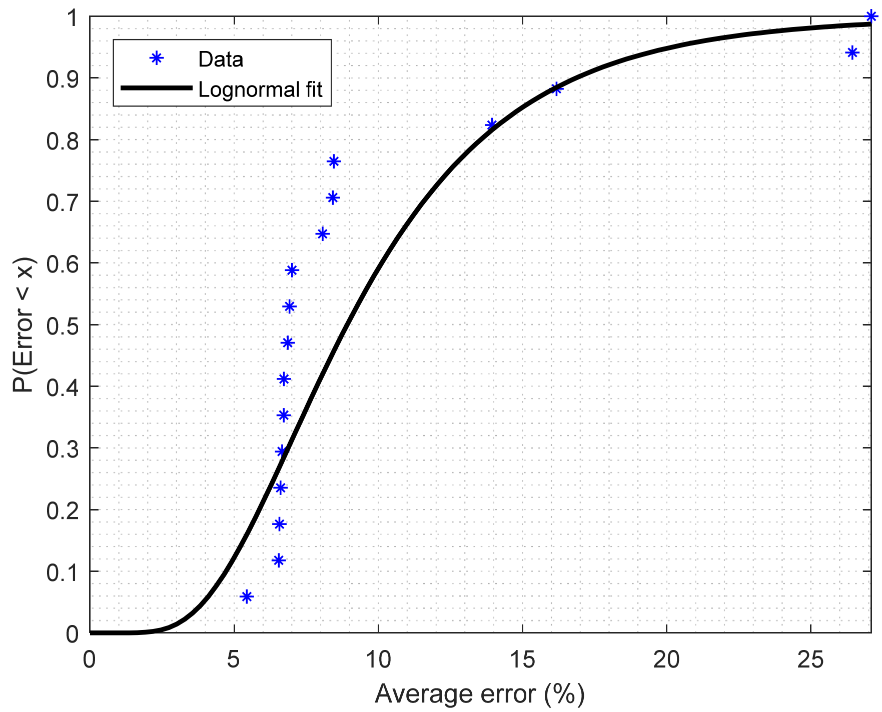

Figure 5.17 **Lognormal distribution of average error for the residual post-tension bar force in Column 2.**

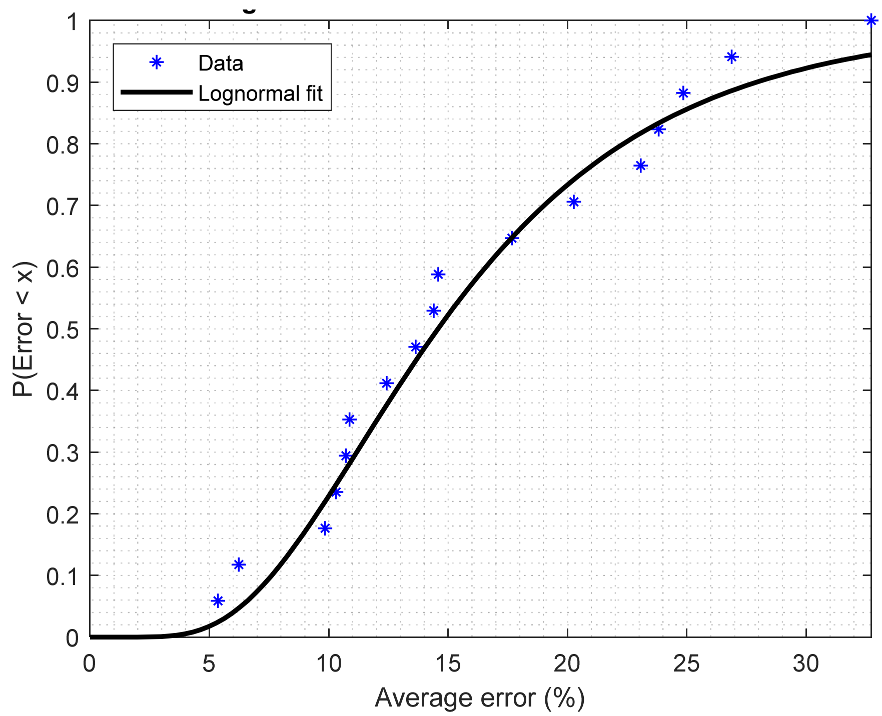

Figure 5.18 **Lognormal distribution of average error for the largest post-tension bar force in Column 1.**

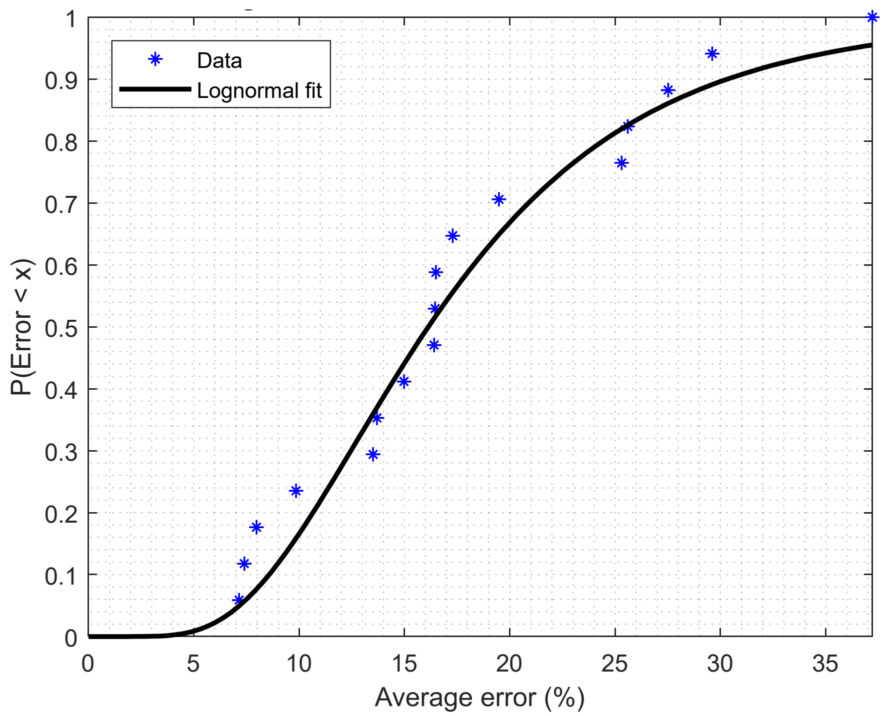

Figure 5.19 Lognormal distribution of average error for the largest post-tension bar force in Column 2.

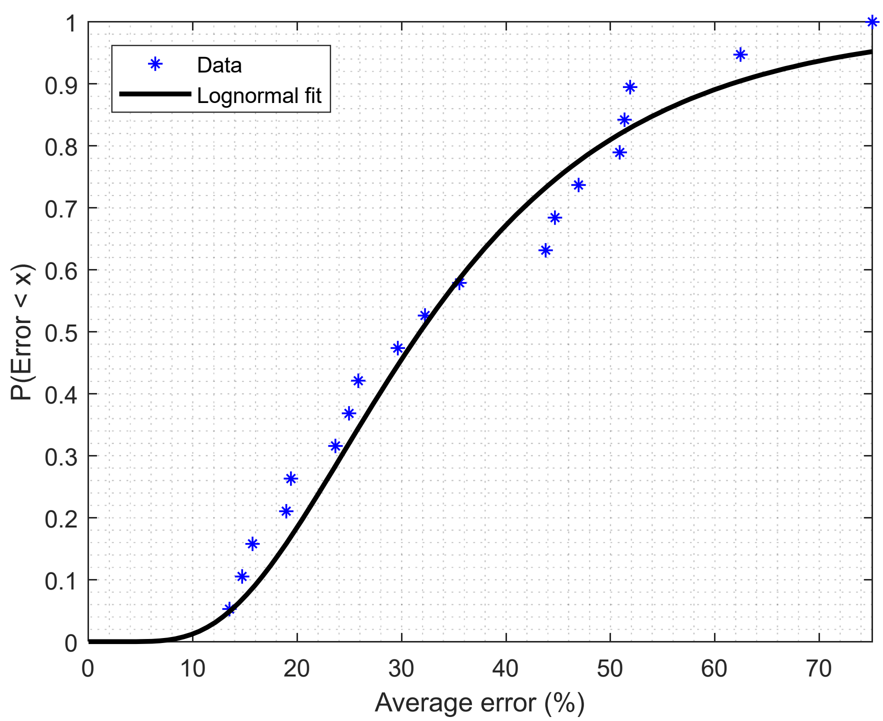

Figure 5.20 Lognormal distribution of average error for the maximum lateral inertia force.

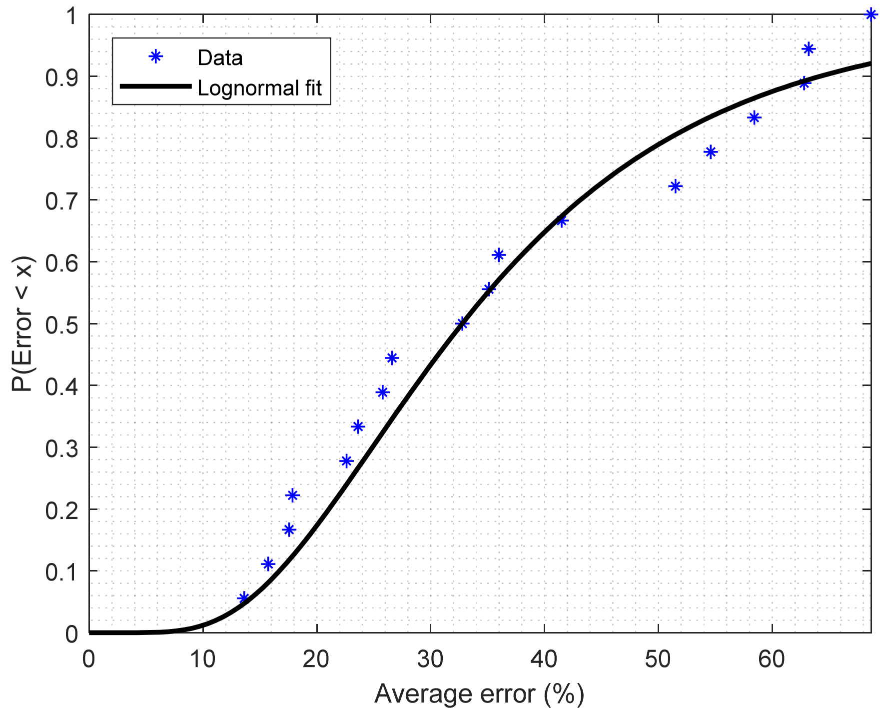

Figure 5.21 Lognormal distribution of average error for the minimum lateral inertia force.

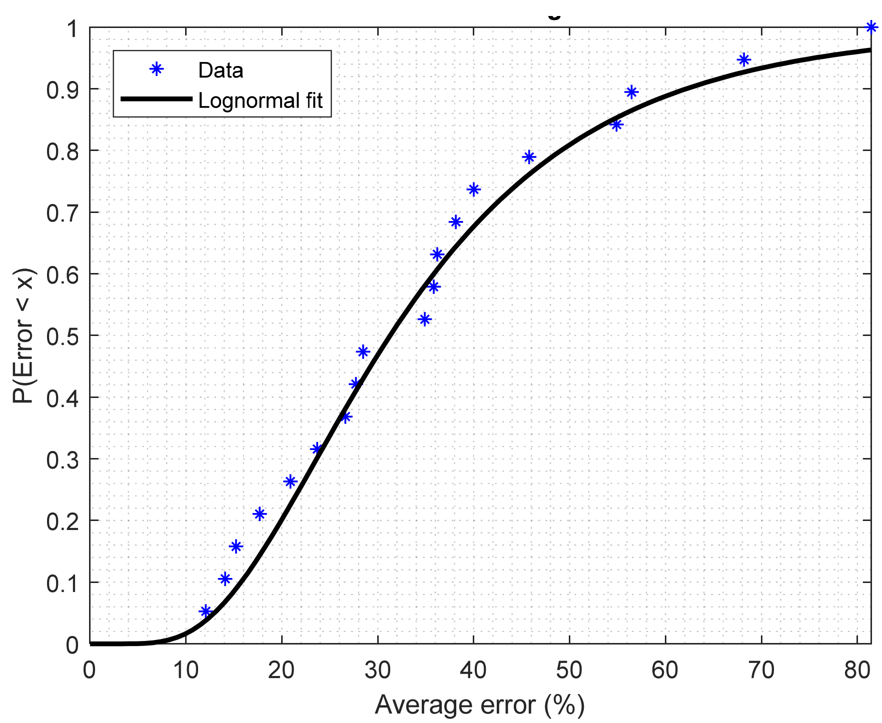

Figure 5.22 Lognormal distribution of average error for the maximum overturning moment.

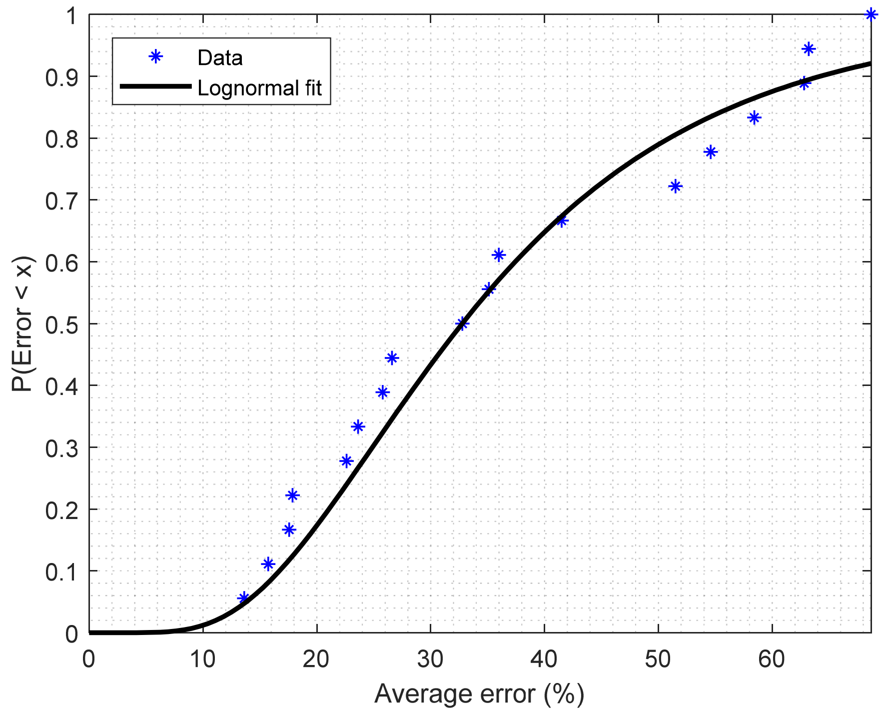

Figure 5.23 Lognormal distribution of average error for the minimum overturning moment.

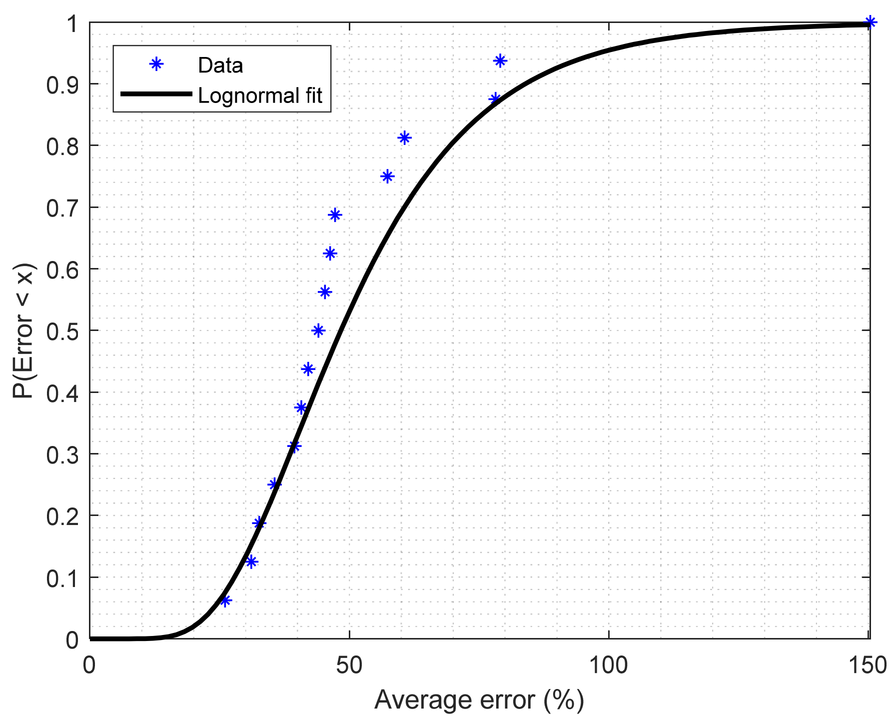

Figure 5.24 Lognormal distribution of average error for the vertical inertia force.

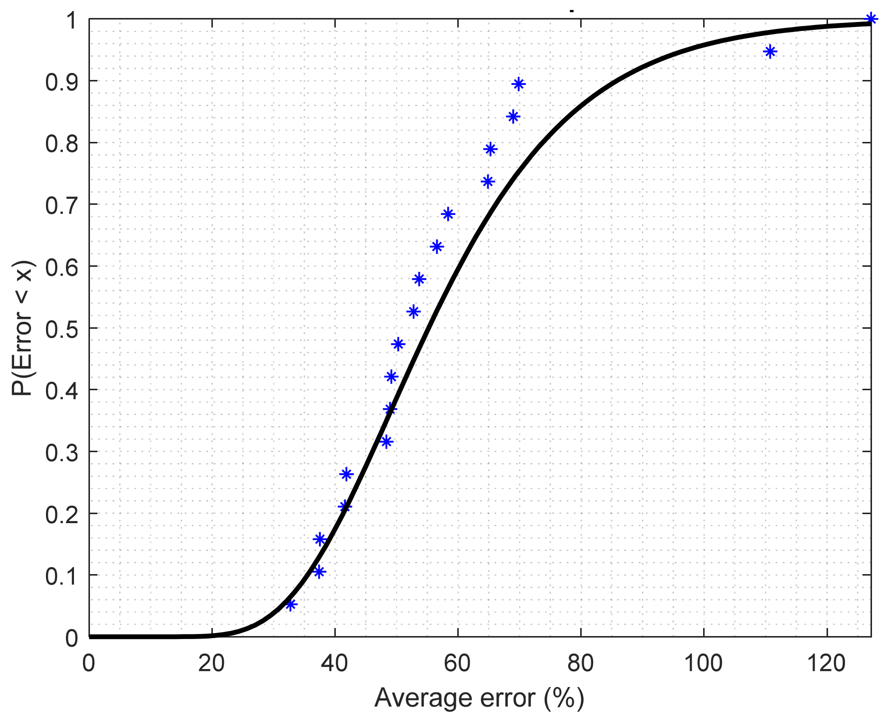

Figure 5.25 Lognormal distribution of average error for the maximum horizontal displacement.

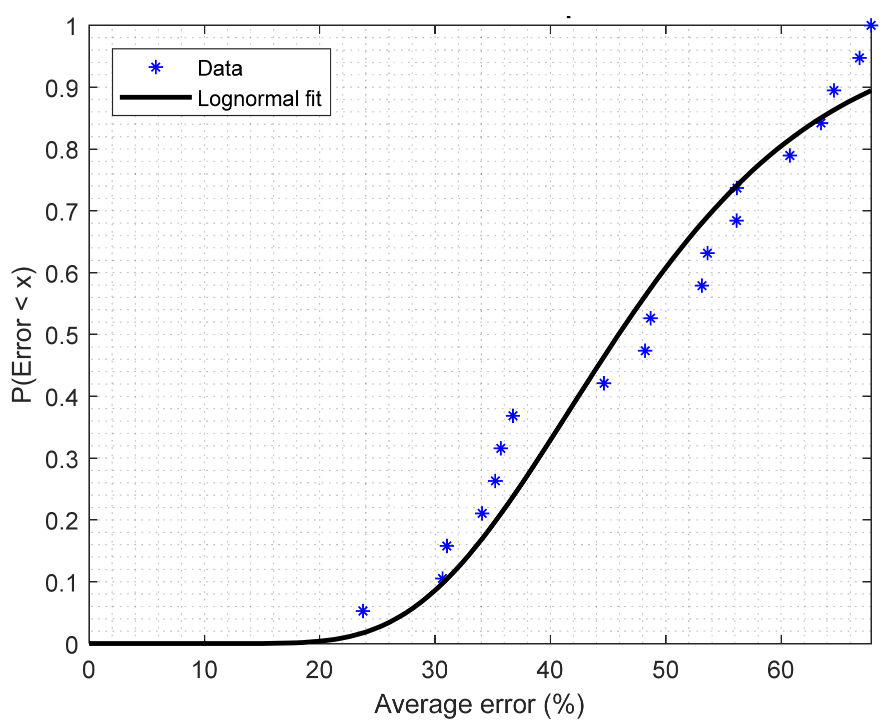

Figure 5.26 Lognormal distribution of average error for the minimum horizontal displacement.

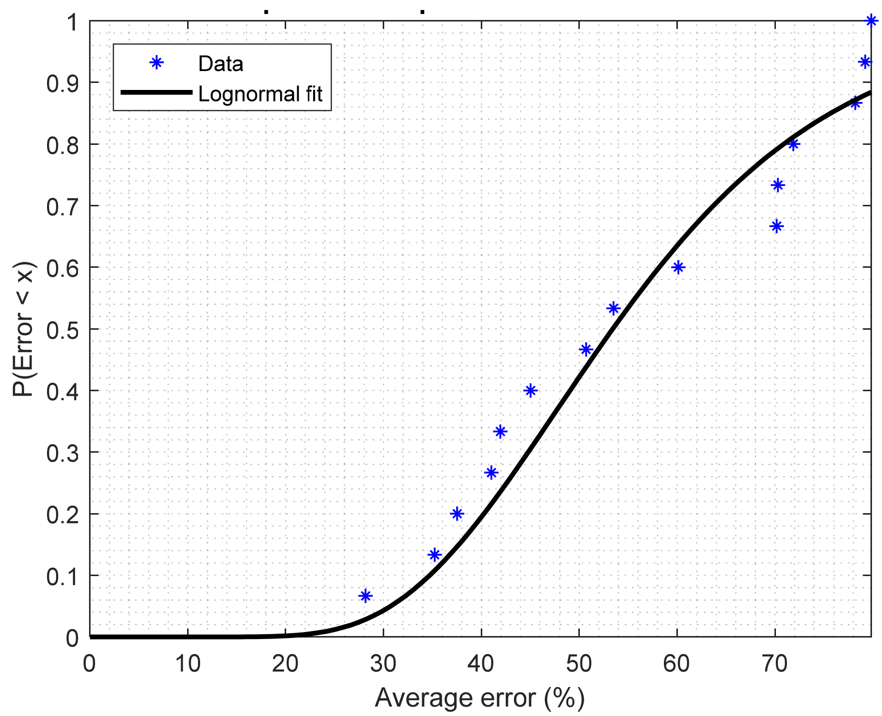

Figure 5.27 **Lognormal distribution of average error for the vertical uplift with respect to column base.**

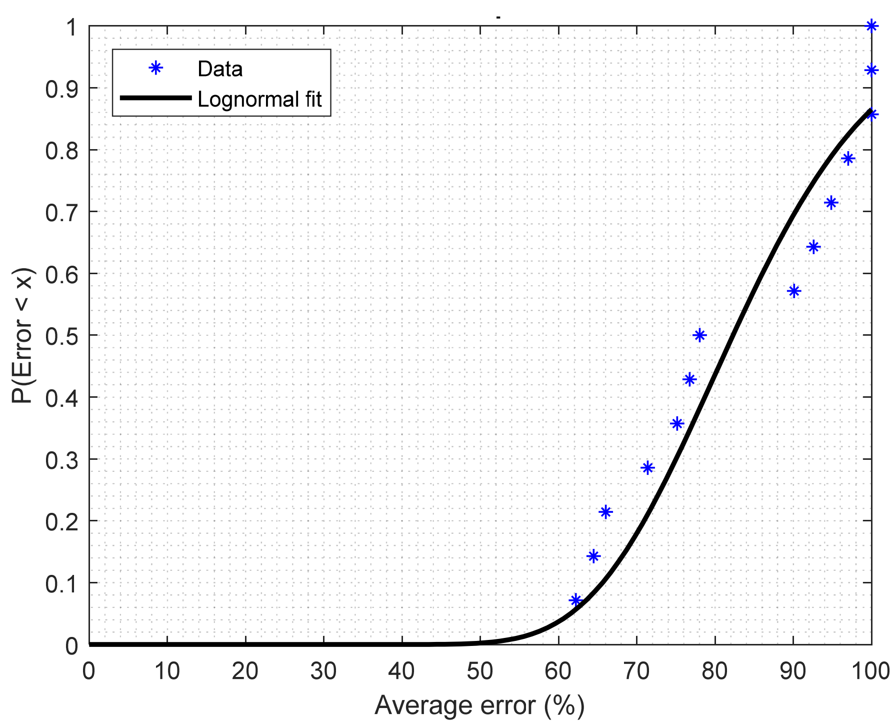

Figure 5.28 **Lognormal distribution of average error for the residual displacement.**

5.3 ERROR AS A FUNCTION OF DAMAGE STATE

Currently, lateral displacements and accelerations are the most used engineering demand parameters (EDPs) in the framework of performance-based earthquake engineering (PBEE). Therefore, it is important to identify the distribution of error in predicting these response quantities over a range of earthquakes and for different damage states. The damage observed after each ground motion is described in Chapter 3.

The distribution of error in predicting a response quantity is presented in two formats: as cumulative error and as average error over a set of ground motions. In both types of plots (Figure 5.29–Figure 5.32), the error was disaggregated to show the contribution of each set of ground motions to the cumulative or average error. Cumulative error and average error were calculated using Equations (5.3 and (5.4), respectively:

$$CumErr = \sum_{i=1}^{n} abs\left[\left(R_a - R_{\exp}\right)/R_{\exp}\right] \tag{5.3}$$

$$AvgErrRC = \frac{1}{n}\sum_{i=1}^{n} abs\left[\left(R_a - R_{\exp}\right)/R_{\exp}\right] \tag{5.4}$$

where n is the number of ground motions considered, R_a is the analytically predicted response, and $R_{\exp}$ is a measured response.

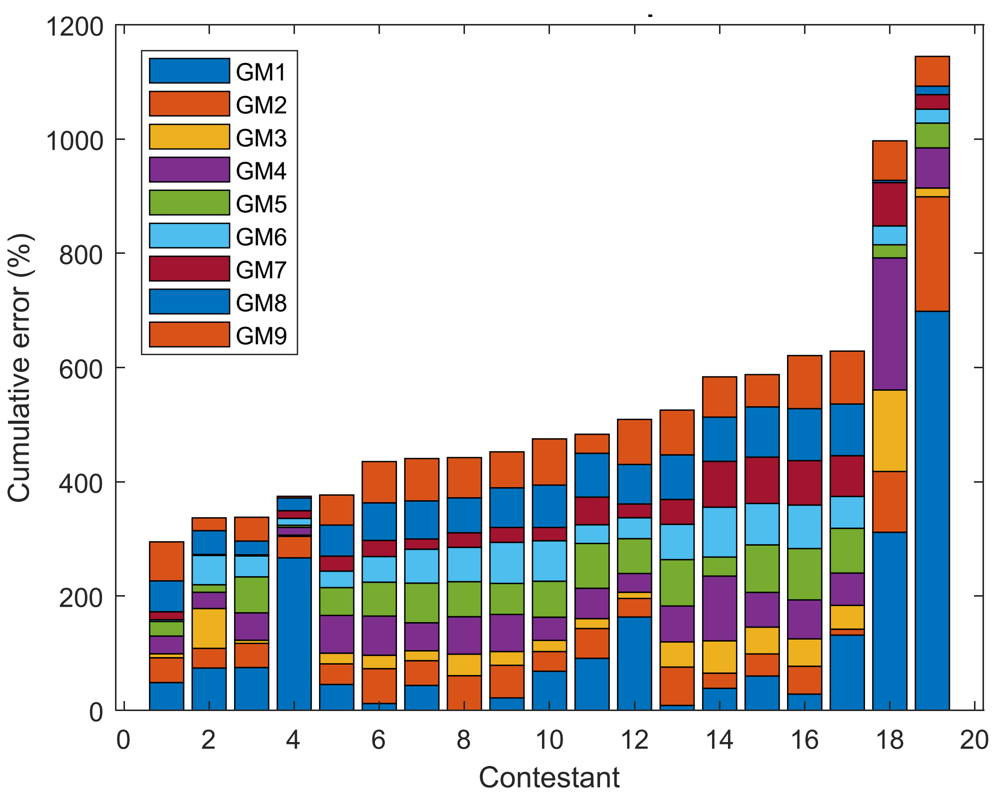

Figure 5.29 Cumulative error over the ground motions in predicting maximum horizontal displacement.

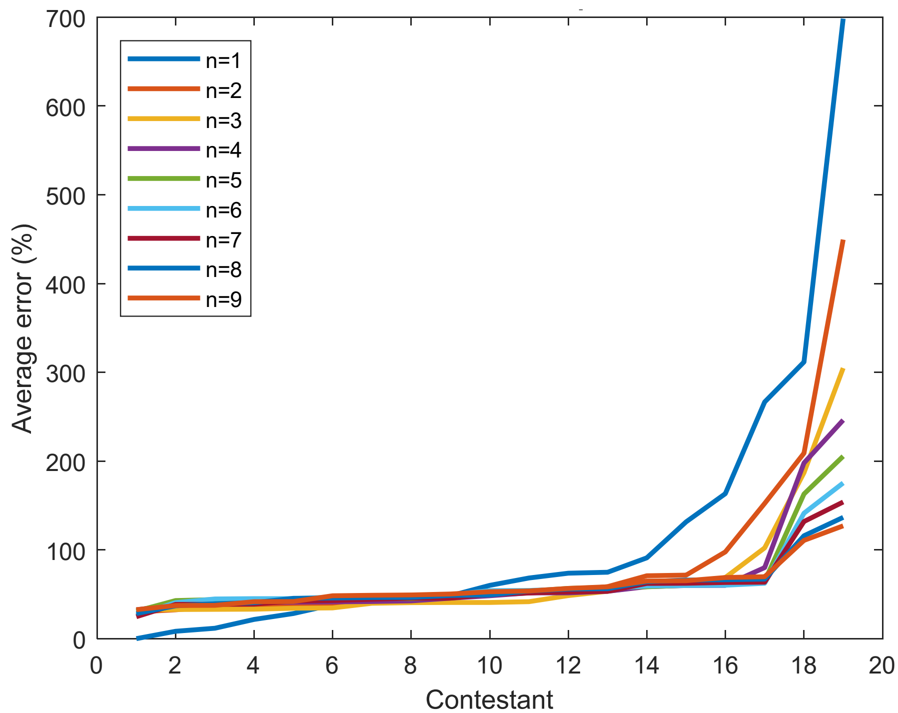

Figure 5.30 **Average error in predicting maximum horizontal displacement considering different numbers of ground motions ("*n*" represents number of considered ground motions).**

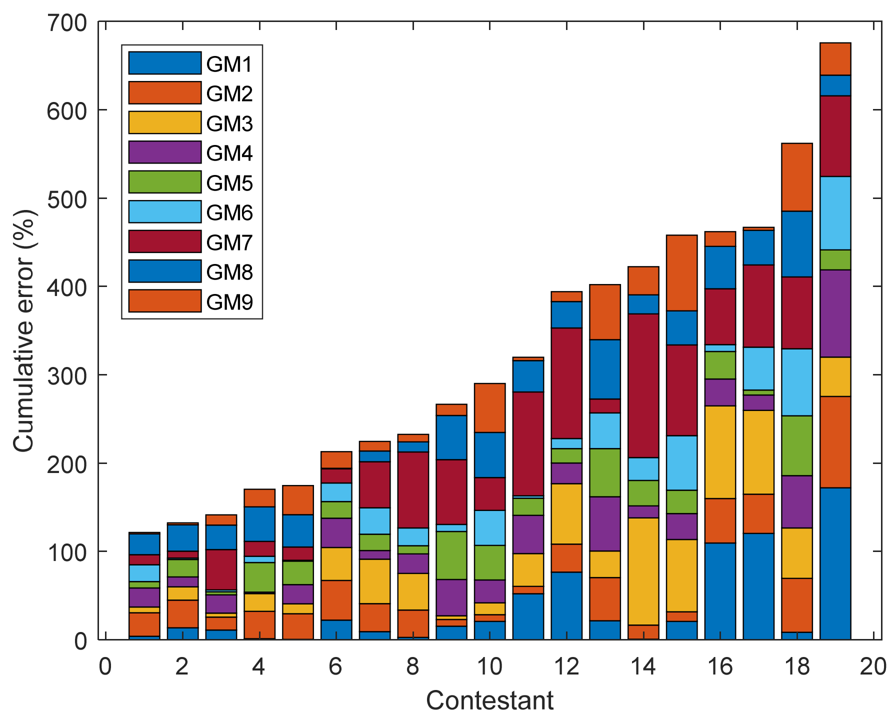

Figure 5.31 **Cumulative error over the ground motions in predicting maximum lateral inertia force.**

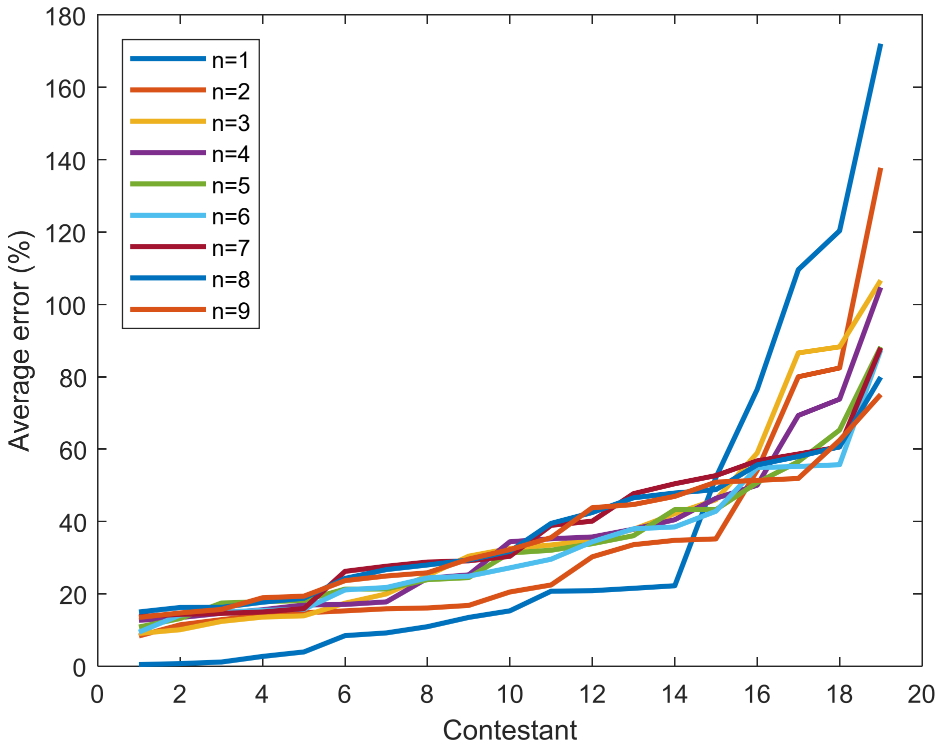

Figure 5.32 **Average error in predicting maximum lateral inertia force considering different numbers of ground motions ("n" represents number of considered ground motions).**

These figures show that GM1 was the largest contributor to the displacement error for most of the teams, while GM7 was the largest contributor to the force (hence the acceleration) error. The reason for the large contribution of GM1 to the displacement error is the elastic response in GM1 and the errors due to the incorrect estimation of the period and damping ratio; the contribution of GM7 to the force error can be explained by the errors in the estimation of the base-shear capacity.

5.4 BIAS IN PREDICTED RESPONSE

This section explores the bias (i.e., systematic error) in predictions. Bias is important because earthquake engineers typically consider model uncertainty using a zero-mean random error term that follows a normal or lognormal distribution. Using a zero-mean error term assumes that through many simulations, the errors are randomly distributed around the real answer, and the average of predictions has a negligible error. In other words, predictions are expected to be unbiased.

Meaningful evaluation of bias requires multiple samples. The blind prediction data from this contest provides samples from each team for multiple response quantities in multiple experiments. Since each team had its own approach to modeling, structural response predictions were available from a suite of models. Each experiment provided a sample of error between simulated and real structural responses for each model. The assumption of independence among these error samples does not strictly hold because the experiments were performed sequentially on the same specimen. However, since the inelastic response was limited in all but the last three experiments, we can omit the last two results and get approximately independent samples. Furthermore, measurement problems in the first experiment (see Section 3.1 for details) make it difficult to observe model uncertainty in those results. Hence, it was decided to remove the first experiment from the samples in this section where bias is evaluated.

The above decisions leave six error samples for each of the 13 response quantities for each of the 19 models (teams). Some of the models produced obvious outliers and were removed earlier; see Table 5.1. As shown below, general observations made with this sample set are similar to those that could be made with the complete pool of samples.

5.4.1 Bias in the Predictions of Individual Models

An illustrative example is used below to introduce the error measure and define the bias in predictions. Figure 5.33(a) compares the predictions of one team to the experimental results for the positive peak horizontal displacement response quantity, and Figure 5.33(b) shows the relative error and bias in those predictions. The predictions are evaluated in logarithmic space, and the relative error (ε) is defined as the log-relative difference between the analysis (R_a) and the experiment (R_{exp}):

$$\varepsilon = \log R_a - \log R_{exp} = \log \frac{R_a}{R_{exp}} \tag{5.5}$$

The percentage values in the vertical axis of Figure 5.33(b) describe the distance of predictions from the test value. Note that the same ε magnitude is assigned to predictions that are x and $1/x$ of the reference value (e.g., 50% and 200%) as it is considered that those errors lead to consequences of similar severity.

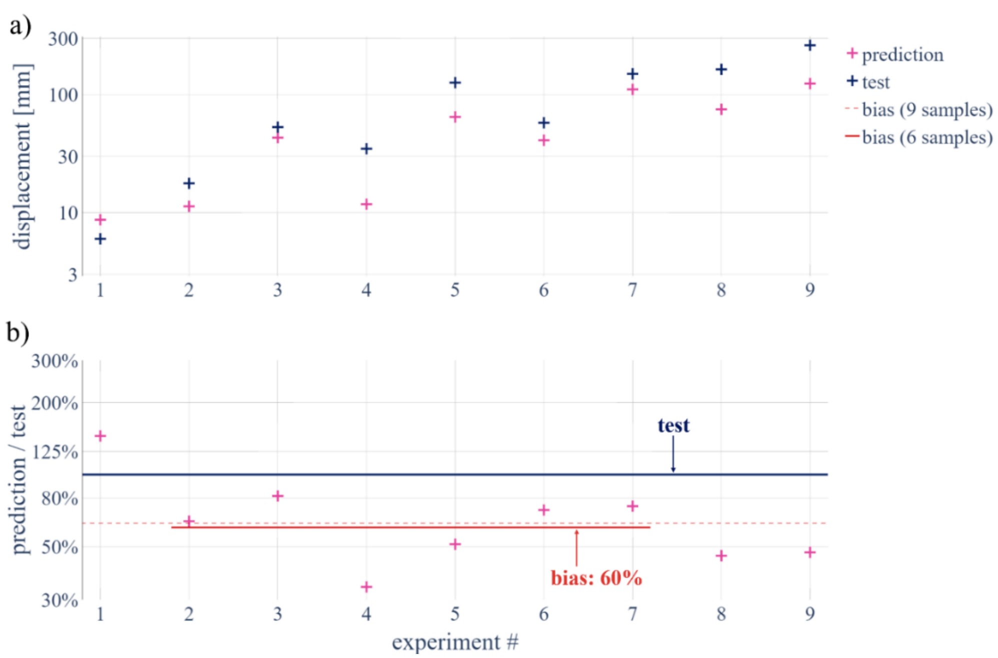

Figure 5.33 Illustrative example of the calculation of relative error and bias.

Bias (μ_ε) is defined as the mean relative error over n samples:

$$\mu_\varepsilon = \frac{1}{n}\sum_{i=1}^{n}\varepsilon \tag{5.6}$$

The dashed red line in Figure 5.33 shows the bias over all samples. The continuous red line illustrates how the bias changes considering only Samples 2–7, following the argument presented earlier. The results in this example suggest that this model systematically underpredicted the peak displacement of the specimen. The calculated bias is equivalent to a prediction-to-test ratio of 60%. About half of the predictions are expected to be even farther away from the test results.

The approach described above was used to evaluate the bias in the predictions of every model in every response quantity. Figure 5.4 shows the calculated biases corresponding to three different sample sizes to demonstrate the results for the following cases:

- all nine experiments considered;
- the first experiment discarded; and
- the first and the last two experiments discarded.

Each column displays the bias in the predictions of one model. The numbers identifying the models are shown on the horizontal axis. The vertical axis breaks down the results into various response quantities. Response quantities are grouped by type: force, acceleration, and displacement-like measures are identified by an F, A, and D after their description, respectively. Red-colored cells mark systematic overpredictions, while blue colored ones mark systematic underpredictions. White cells suggest that the corresponding response quantities were estimated without considerable bias (±5% average error). Predictions that were earlier identified as outliers and omitted are marked in yellow.

The three figures show similar patterns and confirm that the bias in predictions is not controlled by the last two experiments. The residual post-tension bar force estimates are the only exception. As emphasized in Section 5.1.1, these response quantities only changed substantially in the last two tests because of the yielding of post-tension bars, and none of the teams were able to capture those changes well. Hence, the last two experiments introduce significant new information by highlighting this deficiency of the models, which is especially apparent when the second rows of the plots in Figure 5.34 are compared. Nevertheless, forces were predicted with the smallest bias; the majority of models were able to capture these quantities with less than 20% error on average.

The bias in acceleration-like quantities is often beyond 20% for most models. Predictions on the peak vertical inertia force have the worst performance in this group: three sets were considered outliers and none of the teams were able to predict this quantity with less than 5% bias. Unlike the peak post-tension bar force and the displacement-like quantities discussed below, both over- and underpredictions are observed in the acceleration-like quantities. The advantages of this pattern are discussed in the next subsection.

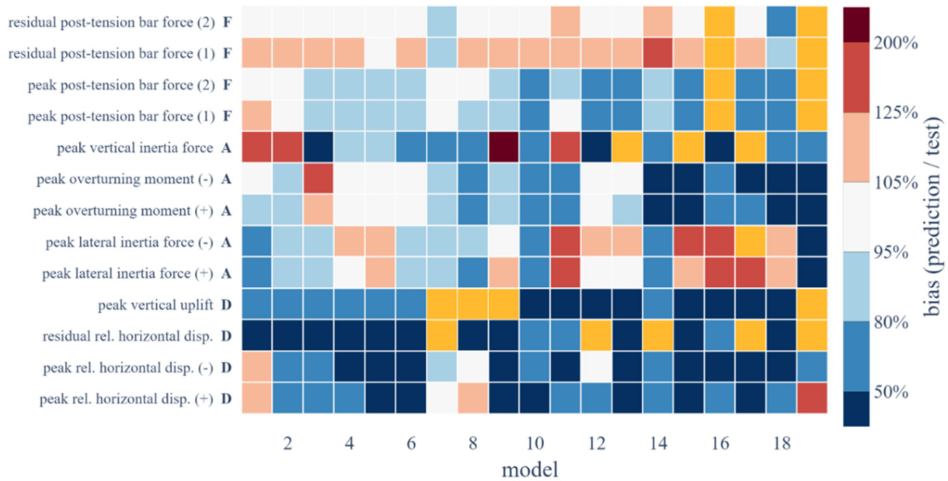

(a)

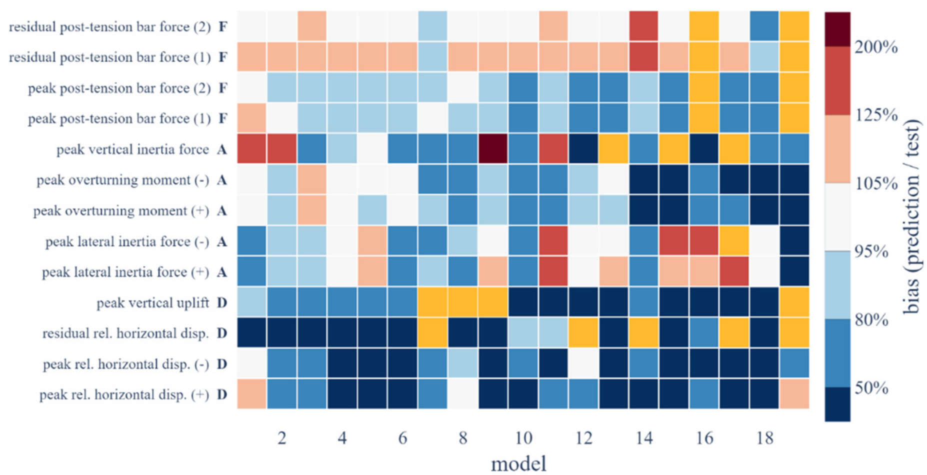

(b)

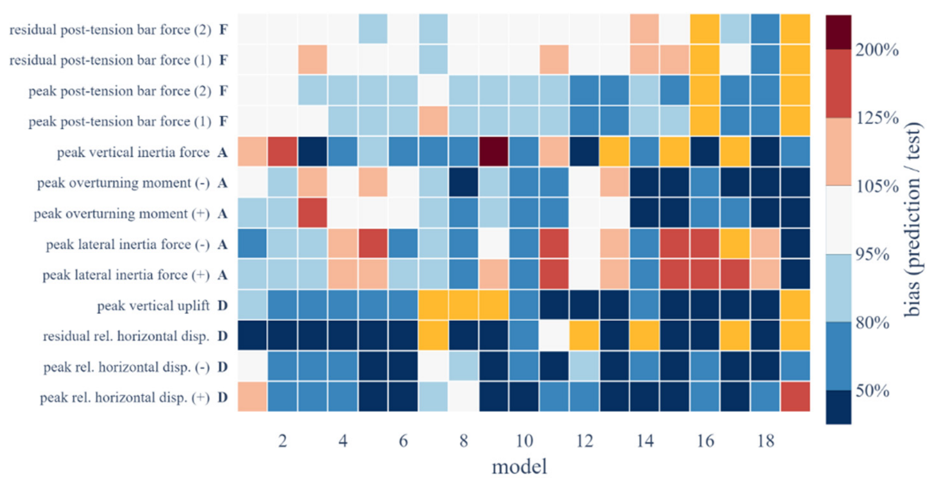

(c)

Figure 5.34 Bias in response estimates by model and response quantity based on (a) all experiments; (b) Experiments 2–9; and (c) Experiments 2–7. Omitted predictions are marked in yellow.

The last four response quantities in Figure 5.34 describe displacements. Displacements are an important type of structural response for performance-based design and assessment of structures because the damage in structural components is often controlled by drift ratios. These were the most challenging to predict: the systematic underprediction often exceeded 50%. Two of these quantities had the highest number of outliers: the predictions of Models 4 and 5 were discarded. The systematic underprediction of displacements suggests that there is a general problem either in the assumptions made or the models used in the engineering community to simulate the response of this type of rocking bridge column. The large bias in horizontal displacements and peak vertical uplift is especially concerning.

The first ranked model performed significantly better than any other in the contest in predicting displacement-based quantities. (Model 7 and 8 were also better than average, but their performance was not as consistent as that of the first model.) It is believed that the community would benefit from understanding the rationale behind that model, as well as the factors that caused the other models to fail to produce similarly good results.

The bias in residual displacements is the highest among all response quantities. The tested specimen belongs to a group of structures known for their good self-centering capability. The experiments demonstrated that the residual displacements in this specimen were negligible even after it had gone through significant inelastic behavior. The largest residual displacement was measured after the penultimate test: 10.3 mm, which is equivalent to 0.3% drift (Table 3.1 and Figure 4.12); therefore, any small differences in the predictions can lead to large bias because of the small nature of the reference.

A large number of teams predicted zero—or close to zero—residual displacements for all experiments. These predictions correspond to relatively large errors when compared to the few millimeters measured in the tests. However, from a practical point of view, those predictions are sufficiently accurate. These observations suggest that, in order to evaluate structural response estimates by how they affect engineering decisions, they need to be considered using non-symmetric error functions, and it must be recognized that predictions within a finite range around a test result can be considered free of errors.

5.4.2 Evaluation of Model Performance

Engineers often consider answers from multiple models to reduce error and bias in their predictions. In the next subsection, the accuracy of predictions from multiple models is explored. Here, a method is presented to evaluate the performance of individual models. This is used to quantify the robustness of each model and helps choose the best models for the combinations in the next subsection.

Because minimizing the bias in structural response estimates is of interest, the performance of individual models is described using the bias in their predictions. The pink crosses in Figure 5.34 indicate the absolute value of bias ($|\mu_\varepsilon|$) in predictions of relative horizontal displacement for the 19 models. The labels on the horizontal axis show the absolute error in percentages (i.e., the absolute difference between the prediction and the test result normalized by the test result). The histogram illustrates the distribution of biases among the 19 models. This is a typical result; a large number of models tends to cluster in the middle between the best and worst predictors.

The aim is to identify the models that perform significantly better than other models. Therefore, we measure the performance of a model by comparing its bias to the average bias of all models. Red vertical lines show the average bias and ±1 standard deviation distance from it in Figure 5.34. The performance of a model is measured as follows:

$$p_m = \frac{\mu_{\varepsilon,m} - E\left[\left|\mu_\varepsilon\right|\right]}{\sqrt{\mathrm{Var}\left[\left|\mu_\varepsilon\right|\right]}} \tag{5.7}$$

where the index m identifies the model, $E[|\mu_\varepsilon|]$ is the average bias, and $\mathrm{Var}[(|\mu_\varepsilon|)]$ is the variance of biases. The above expression measures the distance of the model's marker in Figure 5.34 from the average bias line in units of standard deviation. A good model will receive a negative score because its bias is less than the average. Because this performance measure is unitless, it can be determined for each response quantity, and an average p value across response quantities can be computed for each model. This process is shown in Figure 5.35.

Each cell in the figure describes the performance of one model in predicting one response quantity. Models that perform well have more blue cells, while poorly performing models have more red cells in their column. Every row has a variety of blue and red cells because this performance measure describes the relative performance of the models and not the accuracy of their predictions. Residual displacement predictions are omitted in this evaluation.

The bottom part of the figure shows the aggregate score of each model. When calculating the aggregate value, uniform weights were used for the response quantities to support models that are well-balanced and provide accurate predictions for all quantities. The models are ordered by this aggregate score in every figure in this section.

The distribution of aggregate scores is not symmetric. Models demonstrating poor performance are further from the average than those that perform well. This is partially explained by those models producing several outliers (even though those scores were replaced with the worst score among the acceptable models). Most of the acceptable predictions of the worst models are worse than average, while all predictions of the top four models are close to or better than average. This suggests that the higher-ranked models are consistently better than the others and are considered good candidates for use in the combined prediction approach.

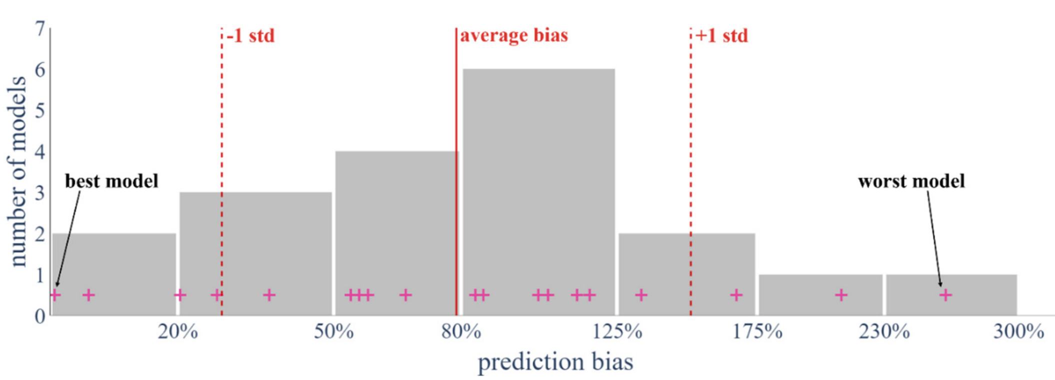

Figure 5.34 Illustrative example of the evaluation of model performance.

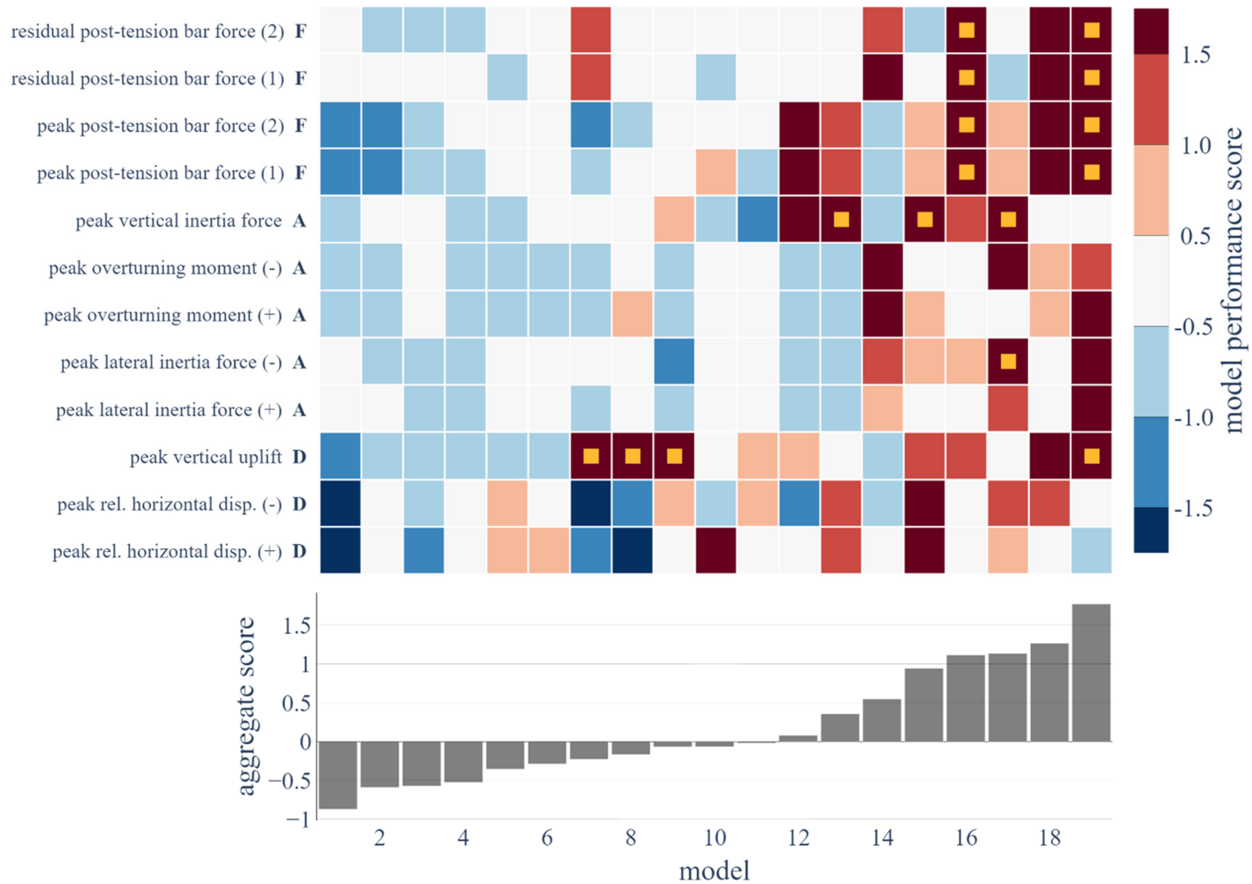

Figure 5.35 **Quantified performance of each model by response quantity (top); and aggregate performance measure for each model (bottom). The scores measure how far the bias of the given model is from the average of all models in units of standard deviation. Omitted predictions are marked in yellow.**

5.4.3 Bias in the Predictions of a Combination of Models

If the various models used by engineers are characterized by a zero-mean random bias, then it can be expected that a combination of predictions from a set of models will provide more reliable estimates than an average individual model. This technique is often used for the design or assessment of highly important structures. Either multiple teams of engineers perform the same task independently, or the work of one engineer team is checked by an independent peer-review panel. In both cases, the predictions of a set of teams are expected to identify the domain of plausible outcomes. In this subsection, the predictions of teams are combined to determine if it is possible to improve estimates of response quantities.

In Figure 5.36, the combination of results from the four highest-performing models from Figure 5.35 is used to estimate peak horizontal displacement in the nine experiments. The same test results were estimated in Figure 5.33 by a single model. Combined predictions were obtained by calculating their geometric mean (i.e., the exponential of their mean in logarithmic space). For most experiments, an individual prediction (pink crosses) that is more accurate than the combined prediction (green crosses) can be found. However, the superior individual predictions are from various models over the nine experiments, and the bias of any individual model is typically worse than the bias of a combined model.

The bias in combined predictions depends on the number of models used for the combination. Figure 5.37 shows how increasing the number of models (horizontal axis) initially reduces the bias; but after four or five, the predictions gradually worsen. This behavior is explained by the reduction in model quality after the fourth model, as shown in the aggregate scores at the bottom of Figure 5.35. The combination of the full set of models is not unbiased: their bias is shown in Figure 5.37 in the rightmost column. The results in Figure 5.37 confirm that combining the better models can reduce the bias in force- and acceleration-based response quantities.

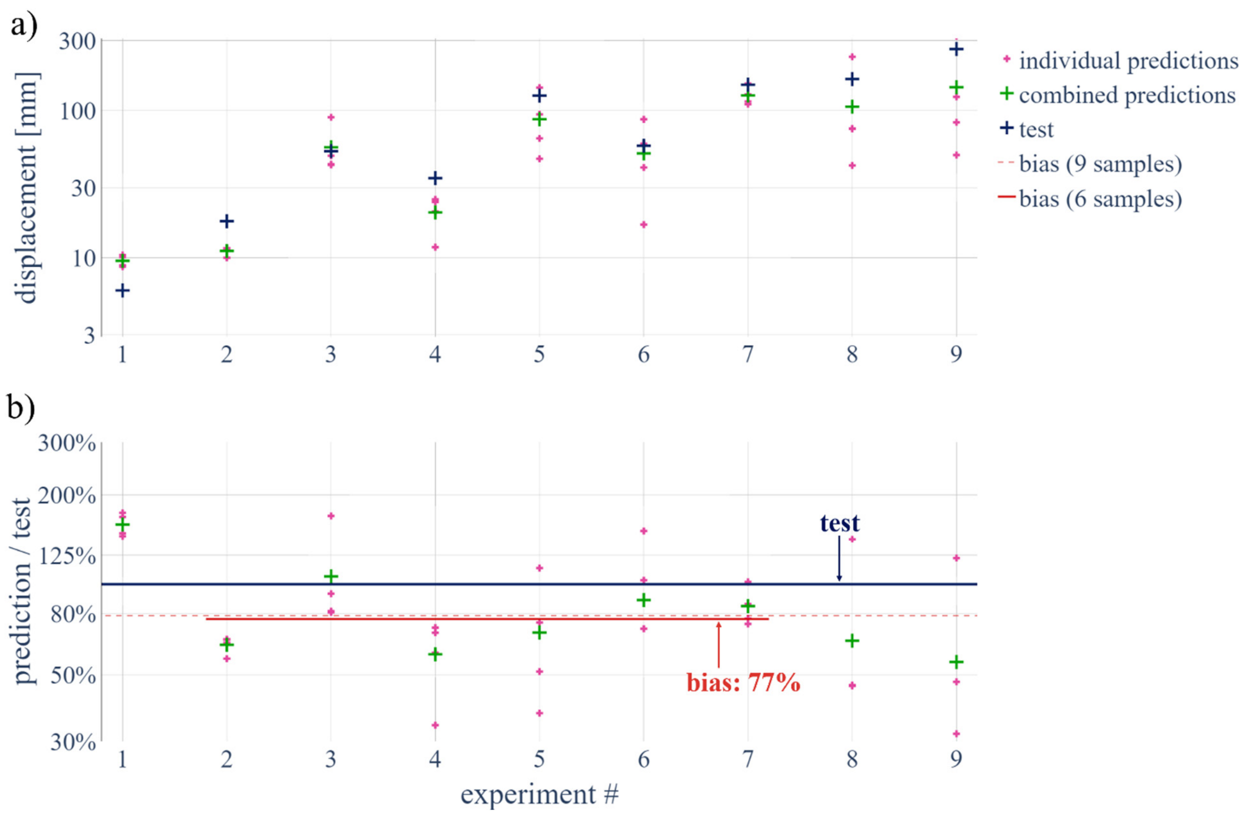

!

Figure 5.36 Illustrative example of the combination of predictions.

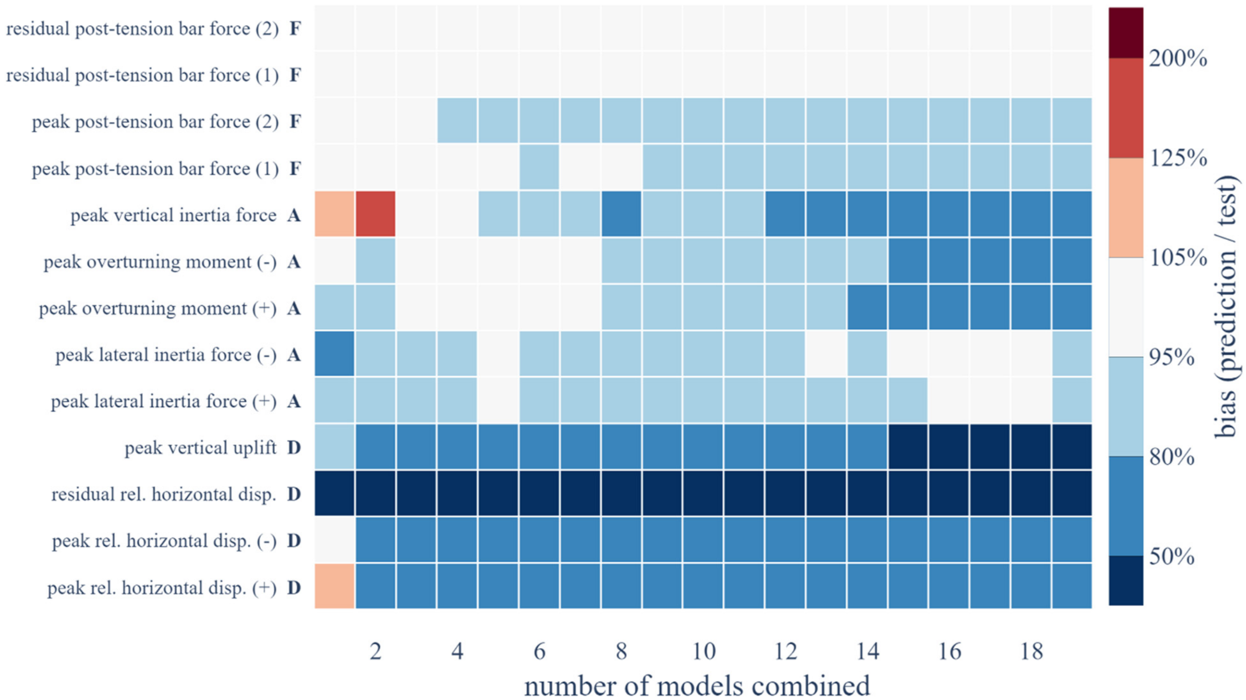

!

Figure 5.37 Bias in response estimates by combinations of models. The horizontal axis shows various set sizes; models for each set chosen based on their relative performance; see Figure 5.35.

The results for displacement-based response quantities show a different pattern. Since almost every team underestimated displacement responses (see Figure 5.34), the combination of those models will not bring the predictions closer to the true value. This suggests that even if multiple groups of engineers are tasked to perform independent predictions, their results will not capture the epistemic uncertainty in the models and will not provide accurate information about the magnitude of potential displacements. A more detailed investigation of the modeling approaches and identification of problems with the models would be an important step forward to understand the reasons behind this systematic bias.

5.5 ESTIMATES OF ERROR IN PREDICTIONS

In this contest, teams had the opportunity to specify 10% and 90% confidence bounds for their estimates, which will be referred to as lower and upper bounds, respectively, in the following discussion. Every team provided such data, but it is important to point out that their score was not influenced by the prescribed bounds. Such data was collected to investigate if teams were aware of the errors in their response estimates.

First, the estimated error (i.e., the size of the confidence region for each response quantity) is evaluated. Figure 5.38 shows the estimated error normalized by the predicted value for every team and response quantity. The majority of estimates are in line with the typical assumptions in earthquake engineering literature: 10–30% error is expected. Several teams submitted the same range for all response quantities. It is believed that this was due to a lack of incentives to invest in more sophisticated error modeling or a lack of resources for engineers to calibrate their error estimates. Those who differentiated between response quantities always predicted larger errors in displacements (e.g., Teams 4, 5, and 12), demonstrating that engineers are aware of the difficulties in estimating displacement-based response quantities. Residual displacements were an exception; it is assumed that some engineers were certain about negligible residuals, hence the small error estimates in that row in Figure 5.38 (e.g., Teams 2, 6, and 13).

The approach to evaluating error estimates is illustrated through the four examples shown in Figure 5.39. Each prediction is marked by a pink cross that extends in both vertical directions to show the upper and lower bounds assigned to the predicted value. Example Models A, B, and C underpredict the test response, while Model D overpredicts it. When evaluating the error estimates, the bounds, which are the upper bounds for A, B, C and the lower bound for D, are compared with the test value. If the test result is within the confidence bound, it is concluded that the team overestimated the error (B, C); otherwise, it is concluded that they have underestimated it (A, C).

The results of the above evaluation depend on the confidence of the team as well as on their accuracy. For example, Model C illustrates a team that is less confident than A (the upper confidence bound is 225% of the predicted value for C versus 115% for A), but their prediction is less accurate. Even though they assigned a significantly wider confidence region, they still underestimated the error in their predictions.

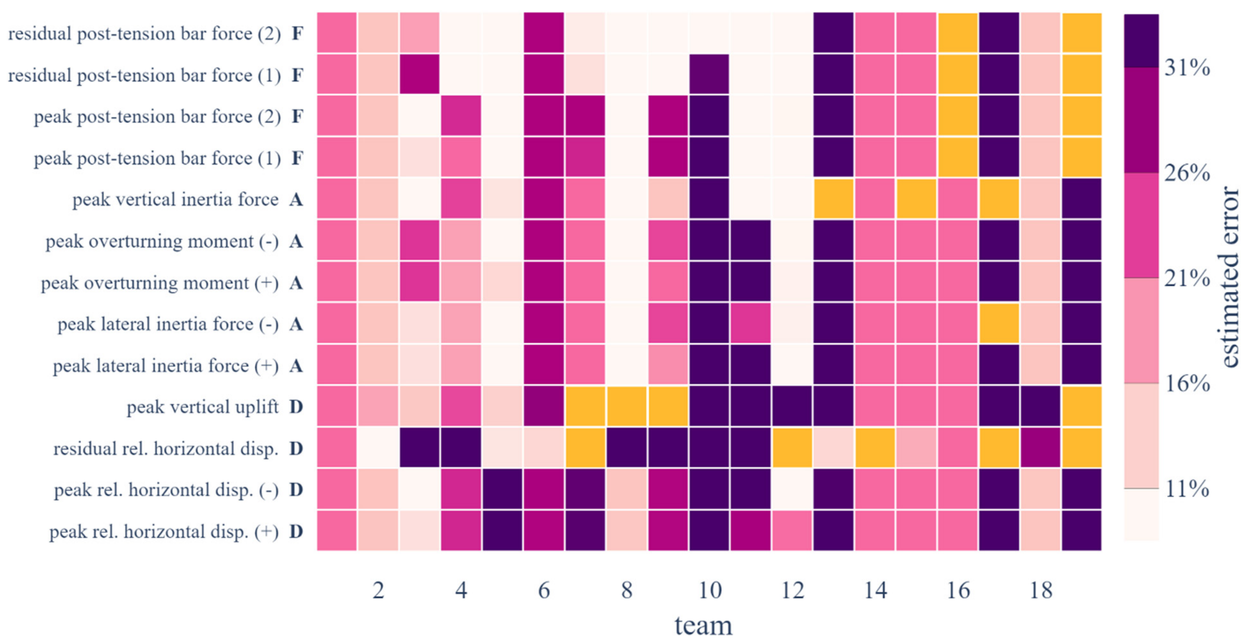

Figure 5.38 **Estimated error in predictions by team and response quantity. Each error estimate was normalized by the corresponding prediction to get the relative error value.**

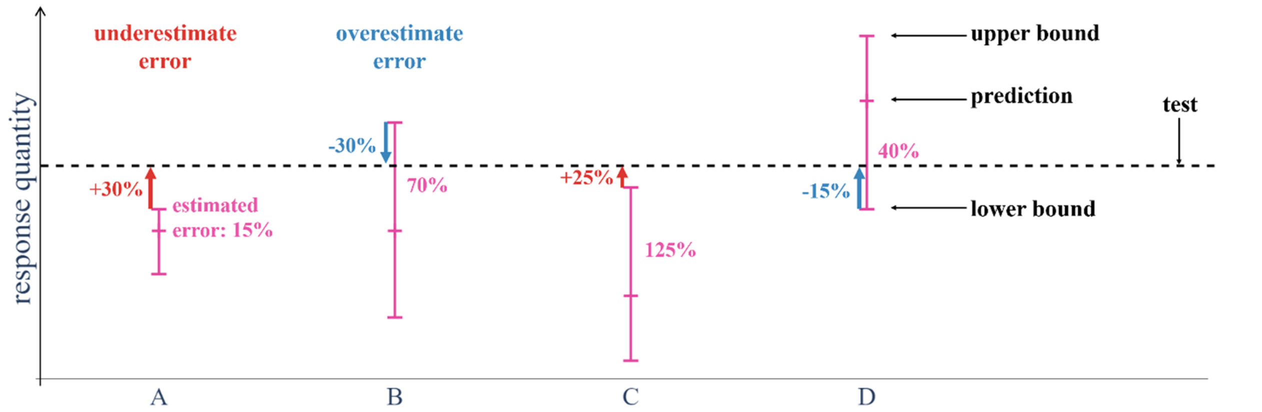

Figure 5.39 Evaluation of error estimates for four illustrative examples.

Accuracy of error estimates is quantified by measuring how much they would need to be adjusted to get a confidence bound that matches the test value. In the case of the Example Model A, the team would have had to assign an upper bound at 145% of the predicted value, which corresponds to adding 30% error to their 115% estimate. Model C would need an upper bound at 150%, which is 25% more than their 125% estimate. Accuracy measures always refer to the location of the confidence bound relative to both the test result and the prediction. Note that both B and D overestimated the error.

Accuracy of error estimates of each team for each response quantity in each experiment is evaluated using the approach presented above and displayed the average of results over Experiments 2–7 in Figure 5.40. Teams are ordered in the figure from left to right by their relative performance with respect to overall bias; see Figure 5.35. Most teams performed well in force-based quantities, and the highest-ranked teams also estimated their error in acceleration-based quantities accurately. The errors in peak vertical inertia force were an exception. These errors were larger, and only Team 4 anticipated this by adjusting their confidence bounds.

Previous figures that show error estimates and biases suggest that the good results in Figure 5.40 are better explained by the accuracy of predictions (Figure 5.34) than by the estimated size of error; see Figure 5.38. Lower-ranked teams were often more conservative when they assigned confidence bounds, but their predictions were significantly less accurate and their conservative error estimates proved to be too small.

Errors in displacement-based quantities were underestimated by almost every team; this stems from the poor performance of the models in addition to unconservative error estimates by most teams. Similar to the other quantities, the few good results here also coincide with the more accurate predictions (e.g., Teams 1, 7, and 8).

The results in Figure 5.40 show overconfidence in displacement-based response estimates. In addition to earlier suggestions on improving models and reducing their bias, it is also suggested collecting information about confidence bounds in future blind prediction contests. Such data is expected to help develop a better understanding of engineers' perception of model error and recognize those areas not sufficiently conservative in practice. Note: these results are limited to the scope of this experimental work, and it would be quite valuable to explore if similar patterns emerge for other types of structural systems.

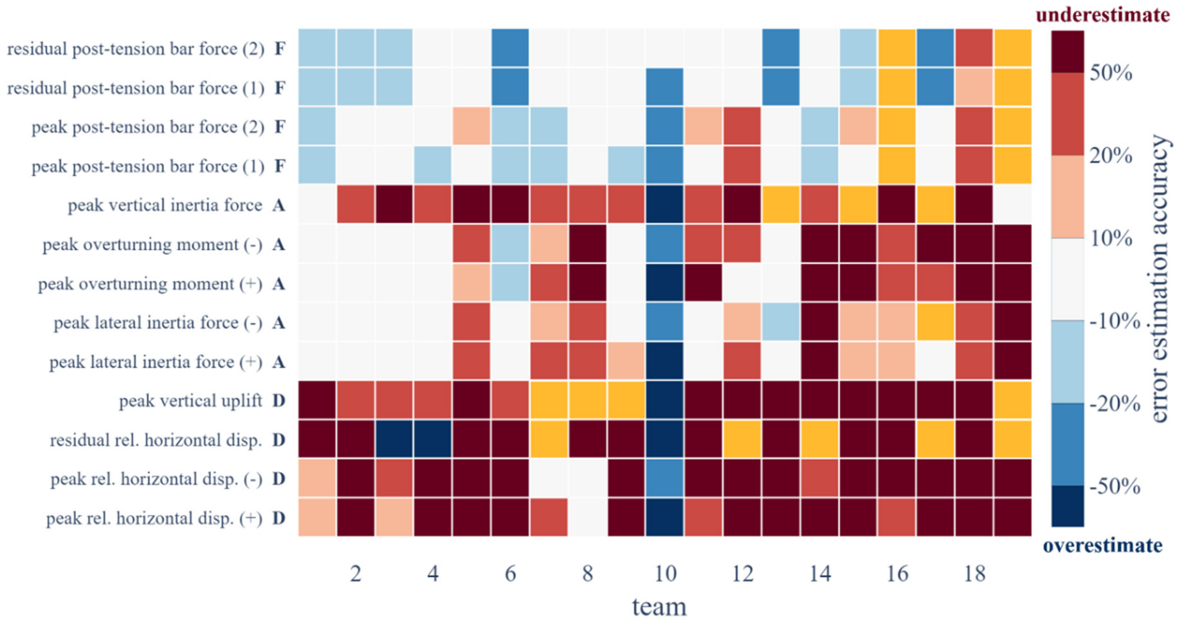

Figure 5.40 **Accuracy of error estimates by team and response quantity. Each cell shows the average of results from Experiments 2–7. Accuracy is measured by the required adjustment to the confidence bounds so that they match the test results.**

6 Effect of Modeling Parameters on the Predictions

To enhance understanding of different modeling parameters on the accuracy of predictions, a questionnaire was sent to all participants. The questionnaire contained questions related to the following: software used for numerical simulations, model description (e.g., type of element used to model the columns or the post-tension bars, material models, and number of elements), mass and damping formulations, damping ratio, and the integration scheme. Using the information provided by the contestants in the questionnaire, the effects of different modeling parameters on the predictions are investigated in the following sections using the error definition in Equation (6.1).

$$AvgErrRC = \frac{1}{n}\sum_{i=1}^{n} abs\left[\left(R_a - R_{\exp}\right)/R_{\exp}\right] \tag{6.1}$$

where n = 9, which is the number of ground motions considered, R_a is the analytically predicted response, and $R_{\exp}$ is the measured response.

6.1 POST TENSION BAR MODELING

To study the accuracy of different models as a function of the element type used for modeling the post-tension bars, the questionnaire was divided into five groups. These five groups are labeled as follows:

- truss;
- co-rotational truss
- spring or NL link;
- beam–column; and
- applied force.

The first four sections represent the element types used for post-tension bar modeling. In the fifth section, post-tension is applied directly as an external compression force to the columns. Figure 6.1–Figure 6.4 show the average error of largest and residual bar forces over all ground motions [calculated using Equation (6.1)].

The average errors are marked with different colors for each group. It is observed that the teams that used springs or NL link (nonlinear link) elements had the smallest error for largest and residual post-tension bar forces. Teams that used truss elements had the biggest errors for the largest forces, and teams that used co-rotational truss elements had the biggest errors for the residual forces. Teams that used beam–column elements had good predictions for the residual forces but bigger errors for the largest forces.

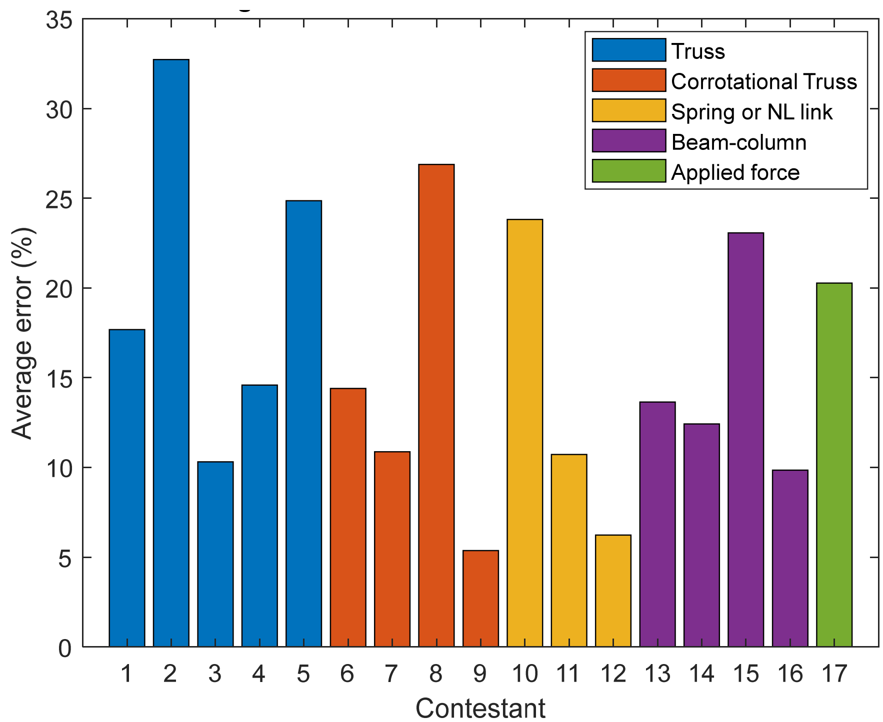

Figure 6.1 **Average error over nine ground motions in predicting largest post-tension bar force in Column 1 using four different element types and applied force.**

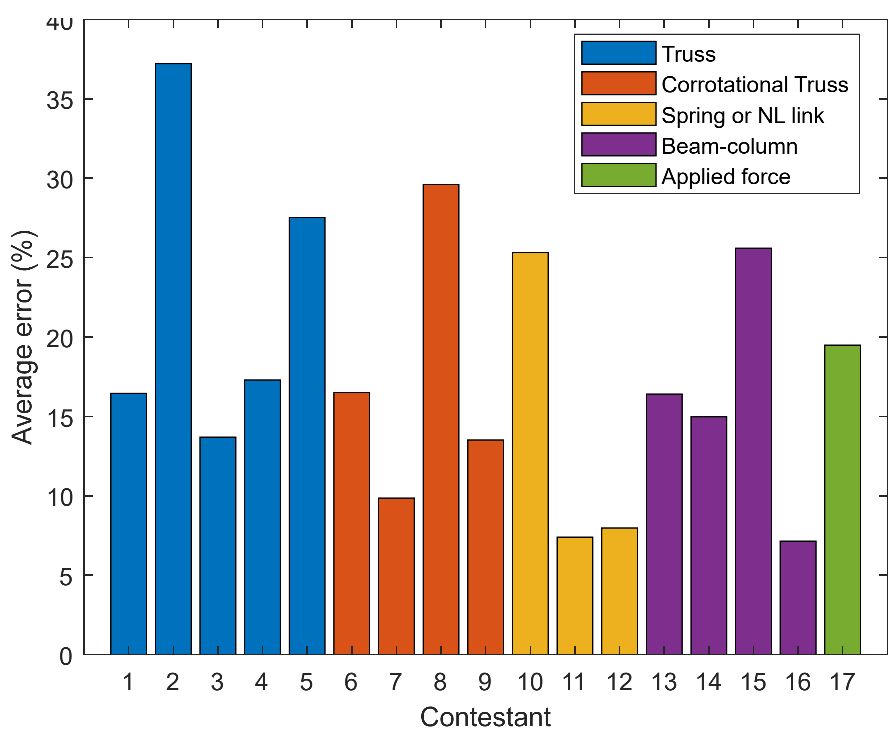

Figure 6.2 **Average error over nine ground motions in predicting largest post-tension bar force in Column 2 using four different element types and applied force.**

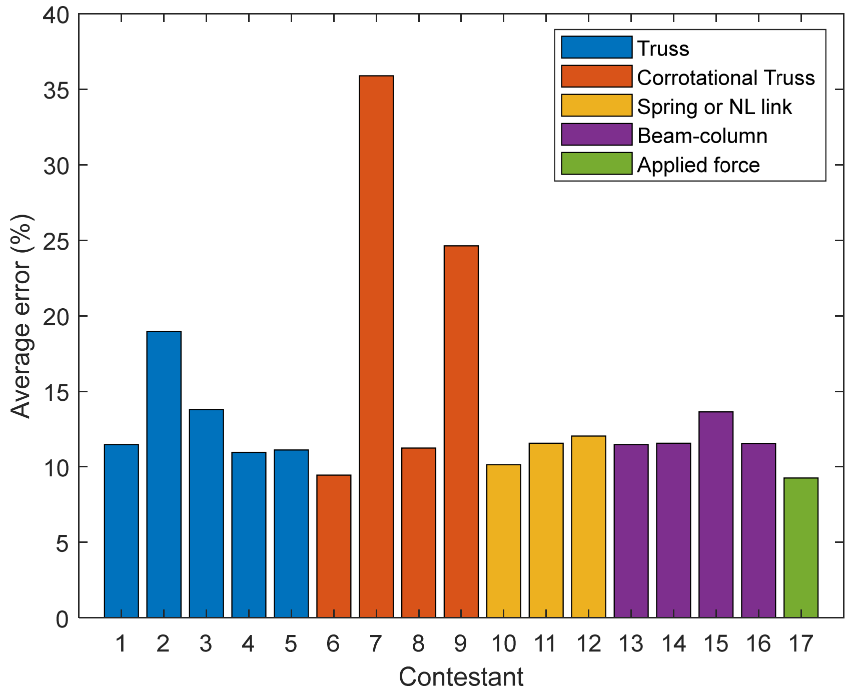

Figure 6.3 **Average error over nine ground motions in predicting residual post-tension bar force in Column 1 using four different element types and applied force.**

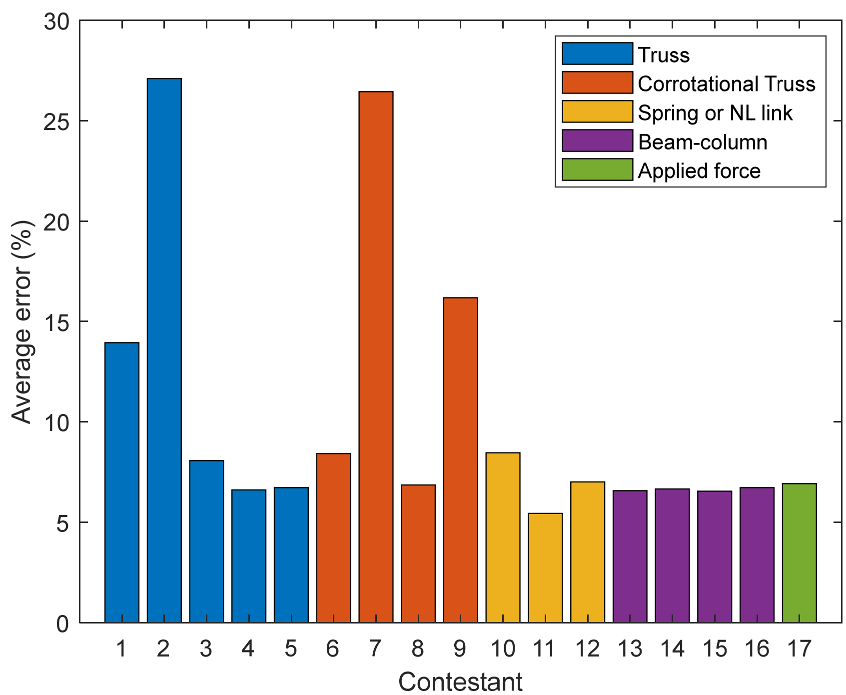

Figure 6.4 **Average error over nine ground motions in predicting residual post-tension bar force in Column 2 using four different element types and applied force.**

6.2 DAMPING MODEL

Utilized damping models can affect the results. For example, it is known that Rayleigh damping models that use initial stiffness can lead to spurious forces in the inelastic range and can lead to misleading results [Chopra and McKenna 2016]. The effect of the utilized damping model on the accuracy of predicted accelerations is investigated in Figure 6.5–Figure 6.7. As expected, Rayleigh damping with initial stiffness led to larger errors for horizontal and vertical inertia forces.

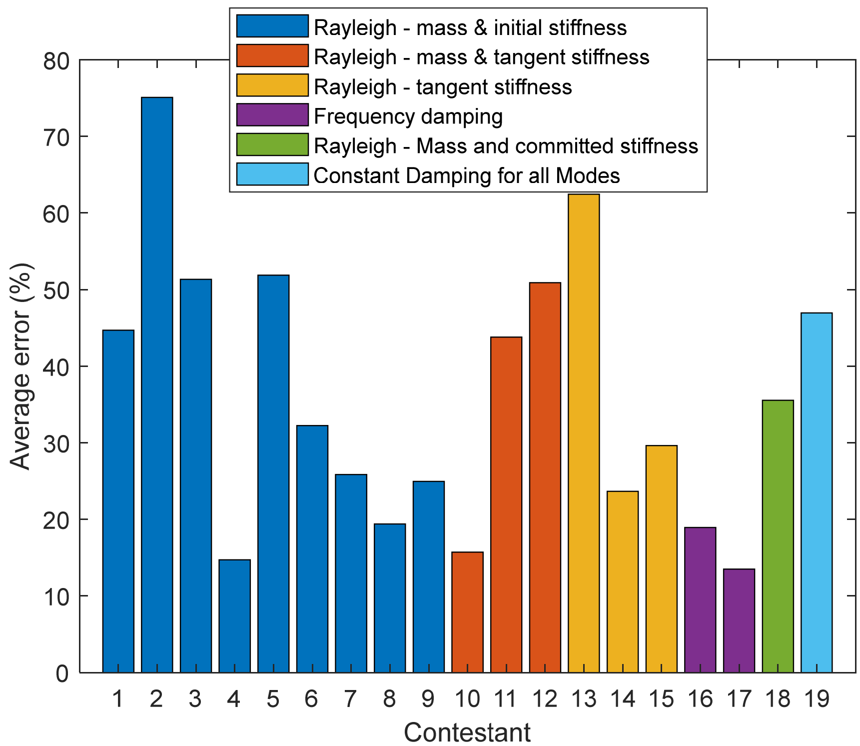

Figure 6.5 **Average error over nine ground motions in predicting maximum lateral inertia force using different damping models.**

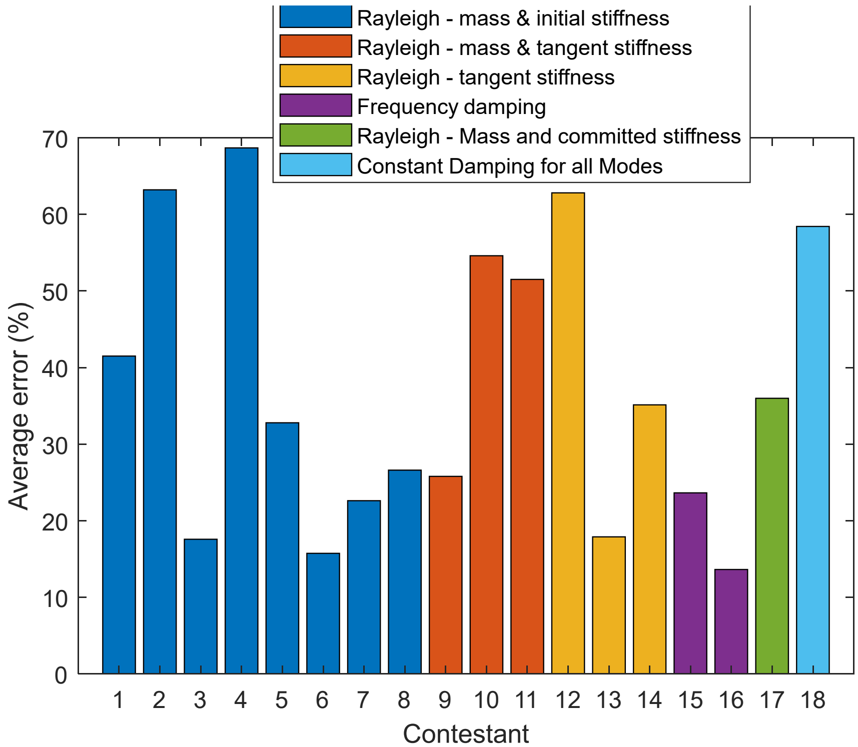

Figure 6.6 **Average error over nine ground motions in predicting minimum lateral inertia force using different damping models.**

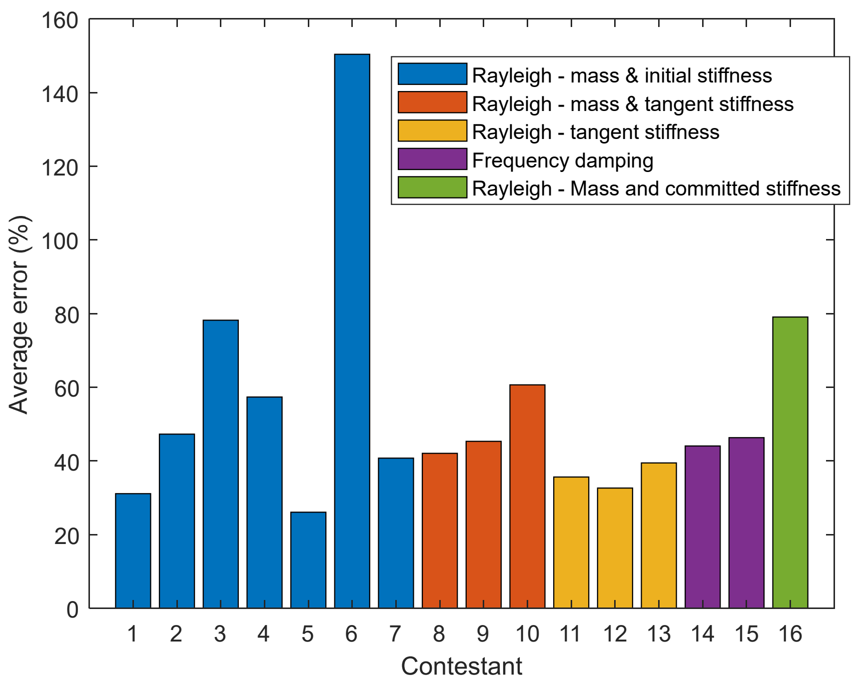

Figure 6.7 **Average error over nine ground motions in predicting minimum lateral inertia force using different damping models.**

7 Summary and Conclusions

Based on the analysis of thirteen (13) predictions of the bridge-bent peak responses subjected to nine (9) consecutive ground motions, the following conclusions are drawn:

1. In general, forces were predicted better than displacements. The post-tension bar forces were predicted with the best accuracy. This is followed by the vertical inertia force and the maximum lateral inertia forces and the overturning moments. The peak and residual displacements were predicted with the least accuracy. These results indicate that the accelerations and forces were predicted better than the displacements.
2. The inaccuracy of the displacement predictions is a concern for the performance-based evaluation of this type of resilient systems as the displacement is a good indicator of the column response and damage.
3. It is observed that some of the quantities were predicted with COV values larger than 50% including the vertical inertia force, maximum horizontal displacement, vertical uplift, and the residual displacement. However, in general, it can be stated that the scatter in the predictions of different teams is not significantly large.
4. Displacements were systematically underpredicted by almost every team. Errors were also typically underestimated, especially in displacements. These results suggest that there is a general problem either in the assumptions made or the models used to simulate the response of this type of bridge bent.
5. For the elastic response predictions, any small error in the period or damping values result in large errors, this is mainly due to the shape of the response spectrum of several ground motions.
6. To identify the source of errors in a more systematic way in the future blind predictions, it is recommended to add the natural periods to the list of predicted quantities. Also, the damping ratios in the elastic range should be provided to the contestants.
7. It is observed that GM1 was the largest contributor to the displacement error for most of the teams, while GM7 was the largest contributor to the force (hence the acceleration) error. The reason for the large contribution of GM1 to the displacement error is the elastic response in GM1 and the errors due to the incorrect estimation of the period and damping ratio. The contribution of GM7

to the force error can be explained by the errors in the estimation of the base-shear capacity.

8. The announced winners predicted all column responses better than average; notwithstanding their good performance relative to other teams, some of their predictions were greatly inaccurate. To identify the winner, the four best predictions were awarded 8, 5, 3, and 1 points (8 for the best prediction) for each of 117 entries, all points were then totaled, and the team with the greatest total was declared a winner. The same weight was given to each response quantity. Giving points to only four best predictions and not penalizing poor predictions might have skewed the results.

9. The properties of submitted models were also studied to enhance understanding of different modeling parameters on the accuracy of predictions. It was observed that teams that used springs or NL link (nonlinear link) elements had the smallest error for largest and residual post-tension bar forces. Teams that used truss elements had the biggest errors for the largest forces, and teams that used corotational truss elements had the biggest errors for the residual forces. As expected, Rayleigh damping with initial stiffness led to larger errors. The engineering community would benefit from learning more about the approach of the best teams and the factors causing the models of the other teams to fail to produce similarly good results.

10. The results of this blind prediction contest provide data regarding the modeling uncertainty of bridge bents with resilient features for use within performance-based earthquake evaluations. More than anything, these results stress the need for a comprehensive analytical study with the goal of producing assessment and design guidelines to reduce the uncertainty in the modeling of bridge columns with resilient features.

11. Blind prediction contests provide (1) very useful information regarding areas where current numerical models might be improved, and (2) quantitative data regarding the uncertainty of analytical models for use in performance-based earthquake evaluations. Such blind prediction contest should be encouraged for other experimental tests and are planned to be conducted annually by the PEER Center.

REFERENCES

AASHTO (2012). *AASHTO LRFD Bridge Design Specifications*, 7th ed., The American Association of State Highway and Transportation Officials, Washington DC.

ACI 318 (2011). *Building Code Requirements for Structural Concrete and Commentary, ACI 318*, American Concrete Institute, Farmington Hills, MI.

Caltrans (2013). *Seismic Design Criteria*, v. 1.7, California Department of Transportation, Sacramento, CA.

Chopra A.K., McKenna, F. (2016). Modeling viscous damping in nonlinear response history analysis of buildings for earthquake excitation. *Earthq. Eng. Struct. Dyn*., 45(2): 193–211.

Guerrini G., Restrepo J.I. (2013). Seismic response of composite concrete-dual steel shell columns for accelerated bridge construction, *Proceedings, 7th National Seismic Conf. on Bridges and Highways*, Oakland, CA.

Guerrini G., Restrepo J.I., Vervelidis A., Massari M. (2015). Self-centering precast concrete dual-steel-shell columns for accelerated bridge construction: seismic performance, analysis, *PEER Report No. 2015/13*, Pacific Earthquake Engineering Research Center, University of California, Berkeley, CA.

Nema A. (2018). *Development of Low Seismic Damage Structural Systems*, PhD Dissertation, Department of Structural Engineering, University of California, San Diego, CA.

Palermo A., Pampanin S. (2008). Enhanced seismic performance of hybrid bridge systems: Comparison with traditional monolithic solutions, *J. Earthq. Eng*., 12(8): 1267–1295.

Restrepo J.I., Tobolski M.J., Matsumoto E.E. (2011). Development of a precast bent cap system for seismic regions, *NCHRP Report 681*, Washington, DC: The National Academies Press, *https://doi.org/10.17226/14484*.

Terzic V., Schoettler M.J., Restrepo J.I., Mahin S.A. (2015). Concrete column blind prediction contest 2010, *PEER Report No. 2015/01*, Pacific Earthquake Engineering Research Center, University of California, Berkeley, CA.

PEER REPORTS

PEER reports are available as a free PDF download from https://peer.berkeley.edu/peer-reports. In addition, printed hard copies of PEER reports can be ordered directly from our printer by following the instructions at https://peer.berkeley.edu/peer-reports. For other related questions about the PEER Report Series, contact the Pacific Earthquake Engineering Research Center, 325 Davis Hall, Mail Code 1792, Berkeley, CA 94720. Tel.: (510) 642-3437; and Email: peer_center@berkeley.edu.

PEER 2020/08 *PEER Activities Report 2018_2020.* Khalid M. Mosalam and Amarnath Kasalanati, November 2020.

PEER 2020/07 *Comparison of NGA-Sub Ground-Motion Models.* Nicholas Gregor, Kofi Addo, Linda Al Atik, David M. Boore, Yousef Bozorgnia, Kenneth W. Campbell, Brian S.-J. Choiu, Zeynep Gülerce, Behzad Hassani, Tadahiro Kishida, Nico Kuehn, Saburoh Midorikawa, Silvia Mazzoni, Grace A. Parker, Hongjun Si, Jonathan P. Stewart, and Robert R. Youngs. November 2020.

PEER 2020/06 *Development of NGA-Sub Ground-Motion Model of 5%-Damped Pseudo-Spectral Acceleration based on Database for Subduction Earthquakes in Japan.* Hongjun Si, Saburoh Midorikawa, and Tadahiro Kishida. November 2020.

PEER 2020/05 *Conditional Ground-Motion Model for Peak Ground Velocity for Active Crustal Regions.* Norman A. Abrahamson and Sarabjot Bhasin. October 2020.

PEER 2020/05 *Conditional Ground-Motion Model for Peak Ground Velocity for Active Crustal Regions.* Norman A. Abrahamson and Sarabjot Bhasin. October 2020.

PEER 2020/04 *Partially Non-Ergodic Ground-Motion Model for Subduction Regions using the NGA-Subduction Database.* Nicolas Kuehn, Yousef Bozognia, Kenneth W. Campbell, and Nicholas Gregor. September 2020.

PEER 2020/03 *NGA-Subduction Global Ground-Motion Models with Regional Adjustment Factors.* Grace A. Parker, Jonathan P. Stewart, David M. Boore, Gail M. Atkinson, and Behzad Hassani. September 2020.

PEER 2020/02 *Data Resources for NGA-Subduction Project.* Yousef Bozorgnia (PI) and Jonathan P. Stewart (Editor). March 2020.

PEER 2020/01 *Modeling Viscous Damping in Nonlinear Response History Analysis for Steel Moment-Frame Buildings.* Xin Qian, Anil K. Chopra, and Frank McKenna. June 2020.

PEER 2019/09 Seismic Behavior of Special Concentric Braced Frames under Short- and Long-Duration Ground Motions. Ali Hammad and Mohamed A. Moustafa. December 2019.

PEER 2019/08 Influence of Vertical Ground Motion on Bridges Isolated with Spherical Sliding Bearings. Rushil Mojidra and Keri L. Ryan. December 2019.

PEER 2019/07 *PEER Hub ImageNet* (ϕ-Net): *A Large-Scale Multi-Attribute Benchmark Dataset of Structural Images*. Yuqing Gao, and Khalid. M. Mosalam. November 2019.

PEER 2019/06 *Fluid-Structure Interaction and Python-Scripting Capabilities in OpenSees*. Minjie Zhu and Michael H. Scott. August 2019.

PEER 2019/05 *Expected Earthquake Performance of Buildings Designed to the California Building Code (California Alfred E. Alquist Seismic Safety Publication 19-01).* Grace S. Kang, Sifat Muin, Jorge Archbold, Bitanoosh Woods, and Khalid Mosalam. July 2019.

PEER 2019/04 *Aftershock Seismic Vulnerability and Time-Dependent Risk Assessment of Bridges*. Sujith Mangalathu, Mehrdad Shokrabadi, and Henry V. Burton. May 2019.

PEER 2019/03 *Ground-Motion Directivity Modeling for Seismic Hazard Applications.* Jennifer L. Donahue, Jonathan P. Stewart, Nicolas Gregor, and Yousef Bozorgnia. Review Panel: Jonathan D. Bray, Stephen A. Mahin, I. M. Idriss, Robert W. Graves, and Tom Shantz. May 2019.

PEER 2019/02 *Direct-Finite-Element Method for Nonlinear Earthquake Analysis of Concrete Dams Including Dam–Water–Foundation Rock Interaction.* Arnkjell Løkke and Anil K. Chopra. March 2019.

PEER 2019/01 *Flow-Failure Case History of the Las Palmas, Chile, Tailings Dam.* R. E. S. Moss, T. R. Gebhart, D. J. Frost, and C. Ledezma. January 2019.

PEER 2018/08 *Central and Eastern North America Ground-Motion Characterization: NGA-East Final Report.* Christine Goulet, Yousef Bozorgnia, Norman Abrahamson, Nicolas Kuehn, Linda Al Atik, Robert Youngs, Robert Graves, and Gail Atkinson. December 2018.

PEER 2018/07 *An Empirical Model for Fourier Amplitude Spectra using the NGA-West2 Database*. Jeff Bayless, and Norman A. Abrahamson. December 2018.

PEER 2018/06 *Estimation of Shear Demands on Rock-Socketed Drilled Shafts subjected to Lateral Loading*. Pedro Arduino, Long Chen, and Christopher R. McGann. December 2018.

PEER 2018/05 *Selection of Random Vibration Procedures for the NGA-East Project*. Albert Kottke, Norman A. Abrahamson, David M. Boore, Yousef Bozorgnia, Christine Goulet, Justin Hollenback, Tadahiro Kishida, Armen Der Kiureghian, Olga-Joan Ktenidou, Nicolas Kuehn, Ellen M. Rathje, Walter J. Silva, Eric Thompson, and Xiaoyue Wang. December 2018.

PEER 2018/04 *Capturing Directivity Effects in the Mean and Aleatory Variability of the NGA-West 2 Ground Motion Prediction Equations*. Jennie A. Watson-Lamprey. November 2018.

PEER 2018/03 *Probabilistic Seismic Hazard Analysis Code Verification*. Christie Hale, Norman Abrahamson, and Yousef Bozorgnia. July 2018.

PEER 2018/02 *Update of the BCHydro Subduction Ground-Motion Model using the NGA-Subduction Dataset.* Norman Abrahamson, Nicolas Kuehn, Zeynep Gulerce, Nicholas Gregor, Yousef Bozorgnia, Grace Parker, Jonathan Stewart, Brian Chiou, I. M. Idriss, Kenneth Campbell, and Robert Youngs. June 2018.

PEER 2018/01 *PEER Annual Report 2017–2018*. Khalid Mosalam, Amarnath Kasalanati, and Selim Günay. June 2018.

PEER 2017/12 *Experimental Investigation of the Behavior of Vintage and Retrofit Concentrically Braced Steel Frames under Cyclic Loading*. Barbara G. Simpson, Stephen A. Mahin, and Jiun-Wei Lai, December 2017.

PEER 2017/11 *Preliminary Studies on the Dynamic Response of a Seismically Isolated Prototype Gen-IV Sodium-Cooled Fast Reactor* (*PGSFR*). Benshun Shao, Andreas H. Schellenberg, Matthew J. Schoettler, and Stephen A. Mahin. December 2017.

PEER 2017/10 *Development of Time Histories for IEEE693 Testing and Analysis (including Seismically Isolated Equipment).* Shakhzod M. Takhirov, Eric Fujisaki, Leon Kempner, Michael Riley, and Brian Low. December 2017.

PEER 2017/09 *“”R” Package for Computation of Earthquake Ground-Motion Response Spectra.* Pengfei Wang, Jonathan P. Stewart, Yousef Bozorgnia, David M. Boore, and Tadahiro Kishida. December 2017.

PEER 2017/08 *Influence of Kinematic SSI on Foundation Input Motions for Bridges on Deep Foundations*. Benjamin J. Turner, Scott J. Brandenberg, and Jonathan P. Stewart. November 2017.

PEER 2017/07 *A Nonlinear Kinetic Model for Multi-Stage Friction Pendulum Systems*. Paul L. Drazin and Sanjay Govindjee. September 2017.

PEER 2017/06 *Guidelines for Performance-Based Seismic Design of Tall Buildings, Version 2.02*. TBI Working Group led by co-chairs Ron Hamburger and Jack Moehle: Jack Baker, Jonathan Bray, C.B. Crouse, Greg Deierlein, John Hooper, Marshall Lew, Joe Maffei, Stephen Mahin, James Malley, Farzad Naeim, Jonathan Stewart, and John Wallace. May 2017.

PEER 2017/05 *Recommendations for Ergodic Nonlinear Site Amplification in Central and Eastern North America*. Youssef M.A. Hashash, Joseph A. Harmon, Okan Ilhan, Grace A. Parker, and Jonathan P. Stewart. March 2017.

PEER 2017/04 *Expert Panel Recommendations for Ergodic Site Amplification in Central and Eastern North America*. Jonathan P. Stewart, Grace A. Parker, Joseph P. Harmon, Gail M. Atkinson, David M. Boore, Robert B. Darragh, Walter J. Silva, and Youssef M.A. Hashash. March 2017.

PEER 2017/03 *NGA-East Ground-Motion Models for the U.S. Geological Survey National Seismic Hazard Maps*. Christine A. Goulet, Yousef Bozorgnia, Nicolas Kuehn, Linda Al Atik, Robert R. Youngs, Robert W. Graves, and Gail M. Atkinson. March 2017.

PEER 2017/02 *U.S.–New Zealand–Japan Workshop: Liquefaction-Induced Ground Movements Effects, University of California, Berkeley, California, 2–4 November 2016*. Jonathan D. Bray, Ross W. Boulanger, Misko Cubrinovski, Kohji Tokimatsu, Steven L. Kramer, Thomas O'Rourke, Ellen Rathje, Russell A. Green, Peter K. Robinson, and Christine Z. Beyzaei. March 2017.

PEER 2017/01 *2016 PEER Annual Report*. Khalid M. Mosalam, Amarnath Kasalanati, and Grace Kang. March 2017.

PEER 2016/10 *Performance-Based Robust Nonlinear Seismic Analysis with Application to Reinforced Concrete Bridge Systems*. Xiao Ling and Khalid M. Mosalam. December 2016.

PEER 2017/09 *Detailing Requirements for Column Plastic Hinges subjected to Combined Flexural, Axial, and Torsional Seismic Loading.* Gabriel Hurtado and Jack P. Moehle. December 2016.

PEER 2016/08 *Resilience of Critical Structures, Infrastructure, and Communities*. Gian Paolo Cimellaro, Ali Zamani-Noori, Omar Kamouh, Vesna Terzic, and Stephen A. Mahin. December 2016.

PEER 2016/07 *Hybrid Simulation Theory for a Classical Nonlinear Dynamical System*. Paul L. Drazin and Sanjay Govindjee. September 2016.

PEER 2016/06 *California Earthquake Early Warning System Benefit Study*. Laurie A. Johnson, Sharyl Rabinovici, Grace S. Kang, and Stephen A. Mahin. July 2006.

PEER 2016/05 *Ground-Motion Prediction Equations for Arias Intensity Consistent with the NGA-West2 Ground-Motion Models.* Charlotte Abrahamson, Hao-Jun Michael Shi, and Brian Yang. July 2016.

PEER 2016/04 *The M_W 6.0 South Napa Earthquake of August 24, 2014: A Wake-Up Call for Renewed Investment in Seismic Resilience Across California.* Prepared for the California Seismic Safety Commission, Laurie A. Johnson and Stephen A. Mahin. May 2016.

PEER 2016/03 *Simulation Confidence in Tsunami-Driven Overland Flow*. Patrick Lynett. May 2016.

PEER 2016/02 *Semi-Automated Procedure for Windowing time Series and Computing Fourier Amplitude Spectra for the NGA-West2 Database.* Tadahiro Kishida, Olga-Joan Ktenidou, Robert B. Darragh, and Walter J. Silva. May 2016.

PEER 2016/01 *A Methodology for the Estimation of Kappa (κ) from Large Datasets: Example Application to Rock Sites in the NGA-East Database and Implications on Design Motions.* Olga-Joan Ktenidou, Norman A. Abrahamson, Robert B. Darragh, and Walter J. Silva. April 2016.

PEER 2015/13 *Self-Centering Precast Concrete Dual-Steel-Shell Columns for Accelerated Bridge Construction: Seismic Performance, Analysis, and Design*. Gabriele Guerrini, José I. Restrepo, Athanassios Vervelidis, and Milena Massari. December 2015.

PEER 2015/12 *Shear-Flexure Interaction Modeling for Reinforced Concrete Structural Walls and Columns under Reversed Cyclic Loading*. Kristijan Kolozvari, Kutay Orakcal, and John Wallace. December 2015.

PEER 2015/11 *Selection and Scaling of Ground Motions for Nonlinear Response History Analysis of Buildings in Performance-Based Earthquake Engineering*. N. Simon Kwong and Anil K. Chopra. December 2015.

PEER 2015/10 *Structural Behavior of Column-Bent Cap Beam-Box Girder Systems in Reinforced Concrete Bridges Subjected to Gravity and Seismic Loads. Part II: Hybrid Simulation and Post-Test Analysis.* Mohamed A. Moustafa and Khalid M. Mosalam. November 2015.

PEER 2015/09 *Structural Behavior of Column-Bent Cap Beam-Box Girder Systems in Reinforced Concrete Bridges Subjected to Gravity and Seismic Loads. Part I: Pre-Test Analysis and Quasi-Static Experiments*. Mohamed A. Moustafa and Khalid M. Mosalam. September 2015.

PEER 2015/08 *NGA-East: Adjustments to Median Ground-Motion Models for Center and Eastern North America*. August 2015.

PEER 2015/07 *NGA-East: Ground-Motion Standard-Deviation Models for Central and Eastern North America*. Linda Al Atik. June 2015.

PEER 2015/06 *Adjusting Ground-Motion Intensity Measures to a Reference Site for which V_{S30} = 3000 m/sec*. David M. Boore. May 2015.

PEER 2015/05 *Hybrid Simulation of Seismic Isolation Systems Applied to an APR-1400 Nuclear Power Plant.* Andreas H. Schellenberg, Alireza Sarebanha, Matthew J. Schoettler, Gilberto Mosqueda, Gianmario Benzoni, and Stephen A. Mahin. April 2015.

PEER 2015/04 *NGA-East: Median Ground-Motion Models for the Central and Eastern North America Region*. April 2015.

PEER 2015/03 *Single Series Solution for the Rectangular Fiber-Reinforced Elastomeric Isolator Compression Modulus*. James M. Kelly and Niel C. Van Engelen. March 2015.

PEER 2015/02 *A Full-Scale, Single-Column Bridge Bent Tested by Shake-Table Excitation.* Matthew J. Schoettler, José I. Restrepo, Gabriele Guerrini, David E. Duck, and Francesco Carrea. March 2015.

PEER 2015/01 *Concrete Column Blind Prediction Contest 2010: Outcomes and Observations.* Vesna Terzic, Matthew J. Schoettler, José I. Restrepo, and Stephen A Mahin. March 2015.

PEER 2014/20 *Stochastic Modeling and Simulation of Near-Fault Ground Motions for Performance-Based Earthquake Engineering*. Mayssa Dabaghi and Armen Der Kiureghian. December 2014.

PEER 2014/19 *Seismic Response of a Hybrid Fiber-Reinforced Concrete Bridge Column Detailed for Accelerated Bridge Construction*. Wilson Nguyen, William Trono, Marios Panagiotou, and Claudia P. Ostertag. December 2014.

PEER 2014/18 *Three-Dimensional Beam-Truss Model for Reinforced Concrete Walls and Slabs Subjected to Cyclic Static or Dynamic Loading*. Yuan Lu, Marios Panagiotou, and Ioannis Koutromanos. December 2014.

PEER 2014/17 *PEER NGA-East Database*. Christine A. Goulet, Tadahiro Kishida, Timothy D. Ancheta, Chris H. Cramer, Robert B. Darragh, Walter J. Silva, Youssef M.A. Hashash, Joseph Harmon, Jonathan P. Stewart, Katie E. Wooddell, and Robert R. Youngs. October 2014.

PEER 2014/16 *Guidelines for Performing Hazard-Consistent One-Dimensional Ground Response Analysis for Ground Motion Prediction*. Jonathan P. Stewart, Kioumars Afshari, and Youssef M.A. Hashash. October 2014.

PEER 2014/15 *NGA-East Regionalization Report: Comparison of Four Crustal Regions within Central and Eastern North America using Waveform Modeling and 5%-Damped Pseudo-Spectral Acceleration Response*. Jennifer Dreiling, Marius P. Isken, Walter D. Mooney, Martin C. Chapman, and Richard W. Godbee. October 2014.

PEER 2014/14 *Scaling Relations between Seismic Moment and Rupture Area of Earthquakes in Stable Continental Regions*. Paul Somerville. August 2014.

PEER 2014/13 *PEER Preliminary Notes and Observations on the August 24, 2014, South Napa Earthquake*. Grace S. Kang and Stephen A. Mahin, Editors. September 2014.

PEER 2014/12 *Reference-Rock Site Conditions for Central and Eastern North America: Part II – Attenuation (Kappa) Definition*. Kenneth W. Campbell, Youssef M.A. Hashash, Byungmin Kim, Albert R. Kottke, Ellen M. Rathje, Walter J. Silva, and Jonathan P. Stewart. August 2014.

PEER 2014/11 *Reference-Rock Site Conditions for Central and Eastern North America: Part I - Velocity Definition*. Youssef M.A. Hashash, Albert R. Kottke, Jonathan P. Stewart, Kenneth W. Campbell, Byungmin Kim, Ellen M. Rathje, Walter J. Silva, Sissy Nikolaou, and Cheryl Moss. August 2014.

PEER 2014/10 *Evaluation of Collapse and Non-Collapse of Parallel Bridges Affected by Liquefaction and Lateral Spreading*. Benjamin Turner, Scott J. Brandenberg, and Jonathan P. Stewart. August 2014.

PEER 2014/09 *PEER Arizona Strong-Motion Database and GMPEs Evaluation*. Tadahiro Kishida, Robert E. Kayen, Olga-Joan Ktenidou, Walter J. Silva, Robert B. Darragh, and Jennie Watson-Lamprey. June 2014.

PEER 2014/08 *Unbonded Pretensioned Bridge Columns with Rocking Detail*. Jeffrey A. Schaefer, Bryan Kennedy, Marc O. Eberhard, and John F. Stanton. June 2014.

PEER 2014/07 *Northridge 20 Symposium Summary Report: Impacts, Outcomes, and Next Steps*. May 2014.

PEER 2014/06 *Report of the Tenth Planning Meeting of NEES/E-Defense Collaborative Research on Earthquake Engineering*. December 2013.

PEER 2014/05 *Seismic Velocity Site Characterization of Thirty-One Chilean Seismometer Stations by Spectral Analysis of Surface Wave Dispersion*. Robert Kayen, Brad D. Carkin, Skye Corbet, Camilo Pinilla, Allan Ng, Edward Gorbis, and Christine Truong. April 2014.

PEER 2014/04 Effect of Vertical Acceleration on Shear Strength of Reinforced Concrete Columns. Hyerin Lee and Khalid M. Mosalam. April 2014.

PEER 2014/03 *Retest of Thirty-Year-Old Neoprene Isolation Bearings*. James M. Kelly and Niel C. Van Engelen. March 2014.

PEER 2014/02 *Theoretical Development of Hybrid Simulation Applied to Plate Structures*. Ahmed A. Bakhaty, Khalid M. Mosalam, and Sanjay Govindjee. January 2014.

PEER 2014/01 *Performance-Based Seismic Assessment of Skewed Bridges.* Peyman Kaviani, Farzin Zareian, and Ertugrul Taciroglu. January 2014.

PEER 2013/26 *Urban Earthquake Engineering*. Proceedings of the U.S.-Iran Seismic Workshop. December 2013.

PEER 2013/25 *Earthquake Engineering for Resilient Communities: 2013 PEER Internship Program Research Report Collection.* Heidi Tremayne (Editor), Stephen A. Mahin (Editor), Jorge Archbold Monterossa, Matt Brosman, Shelly Dean, Katherine deLaveaga, Curtis Fong, Donovan Holder, Rakeeb Khan, Elizabeth Jachens, David Lam, Daniela Martinez Lopez, Mara Minner, Geffen Oren, Julia Pavicic, Melissa Quinonez, Lorena Rodriguez, Sean Salazar, Kelli Slaven, Vivian Steyert, Jenny Taing, and Salvador Tena. December 2013.

PEER 2013/24 *NGA-West2 Ground Motion Prediction Equations for Vertical Ground Motions*. September 2013.

PEER 2013/23 *Coordinated Planning and Preparedness for Fire Following Major Earthquakes*. Charles Scawthorn. November 2013.

PEER 2013/22 *GEM-PEER Task 3 Project: Selection of a Global Set of Ground Motion Prediction Equations*. Jonathan P. Stewart, John Douglas, Mohammad B. Javanbarg, Carola Di Alessandro, Yousef Bozorgnia, Norman A. Abrahamson, David M. Boore, Kenneth W. Campbell, Elise Delavaud, Mustafa Erdik, and Peter J. Stafford. December 2013.

PEER 2013/21 *Seismic Design and Performance of Bridges with Columns on Rocking Foundations*. Grigorios Antonellis and Marios Panagiotou. September 2013.

PEER 2013/20 *Experimental and Analytical Studies on the Seismic Behavior of Conventional and Hybrid Braced Frames*. Jiun-Wei Lai and Stephen A. Mahin. September 2013.

PEER 2013/19 *Toward Resilient Communities: A Performance-Based Engineering Framework for Design and Evaluation of the Built Environment.* Michael William Mieler, Bozidar Stojadinovic, Robert J. Budnitz, Stephen A. Mahin, and Mary C. Comerio. September 2013.

PEER 2013/18 *Identification of Site Parameters that Improve Predictions of Site Amplification*. Ellen M. Rathje and Sara Navidi. July 2013.

PEER 2013/17 *Response Spectrum Analysis of Concrete Gravity Dams Including Dam-Water-Foundation Interaction*. Arnkjell Løkke and Anil K. Chopra. July 2013.

PEER 2013/16 *Effect of Hoop Reinforcement Spacing on the Cyclic Response of Large Reinforced Concrete Special Moment Frame Beams*. Marios Panagiotou, Tea Visnjic, Grigorios Antonellis, Panagiotis Galanis, and Jack P. Moehle. June 2013.

PEER 2013/15 *A Probabilistic Framework to Include the Effects of Near-Fault Directivity in Seismic Hazard Assessment*. Shrey Kumar Shahi, Jack W. Baker. October 2013.

PEER 2013/14 *Hanging-Wall Scaling using Finite-Fault Simulations*. Jennifer L. Donahue and Norman A. Abrahamson. September 2013.

PEER 2013/13 *Semi-Empirical Nonlinear Site Amplification and its Application in NEHRP Site Factors*. Jonathan P. Stewart and Emel Seyhan. November 2013.

PEER 2013/12 *Nonlinear Horizontal Site Response for the NGA-West2 Project.* Ronnie Kamai, Norman A. Abramson, Walter J. Silva. May 2013.

PEER 2013/11 *Epistemic Uncertainty for NGA-West2 Models*. Linda Al Atik and Robert R. Youngs. May 2013.

PEER 2013/10 *NGA-West 2 Models for Ground-Motion Directionality*. Shrey K. Shahi and Jack W. Baker. May 2013.

PEER 2013/09 *Final Report of the NGA-West2 Directivity Working Group*. Paul Spudich, Jeffrey R. Bayless, Jack W. Baker, Brian S.J. Chiou, Badie Rowshandel, Shrey Shahi, and Paul Somerville. May 2013.

PEER 2013/08 *NGA-West2 Model for Estimating Average Horizontal Values of Pseudo-Absolute Spectral Accelerations Generated by Crustal Earthquakes*. I. M. Idriss. May 2013.

PEER 2013/07 *Update of the Chiou and Youngs NGA Ground Motion Model for Average Horizontal Component of Peak Ground Motion and Response Spectra*. Brian Chiou and Robert Youngs. May 2013.

PEER 2013/06 *NGA-West2 Campbell-Bozorgnia Ground Motion Model for the Horizontal Components of PGA, PGV, and 5%-Damped Elastic Pseudo-Acceleration Response Spectra for Periods Ranging from 0.01 to 10 sec.* Kenneth W. Campbell and Yousef Bozorgnia. May 2013.

PEER 2013/05 *NGA-West 2 Equations for Predicting Response Spectral Accelerations for Shallow Crustal Earthquakes*. David M. Boore, Jonathan P. Stewart, Emel Seyhan, and Gail M. Atkinson. May 2013.

PEER 2013/04 *Update of the AS08 Ground-Motion Prediction Equations Based on the NGA-West2 Data Set*. Norman Abrahamson, Walter Silva, and Ronnie Kamai. May 2013.

PEER 2013/03 *PEER NGA-West2 Database*. Timothy D. Ancheta, Robert B. Darragh, Jonathan P. Stewart, Emel Seyhan, Walter J. Silva, Brian S.J. Chiou, Katie E. Wooddell, Robert W. Graves, Albert R. Kottke, David M. Boore, Tadahiro Kishida, and Jennifer L. Donahue. May 2013.

PEER 2013/02 *Hybrid Simulation of the Seismic Response of Squat Reinforced Concrete Shear Walls*. Catherine A. Whyte and Bozidar Stojadinovic. May 2013.

PEER 2013/01 *Housing Recovery in Chile: A Qualitative Mid-program Review*. Mary C. Comerio. February 2013.

PEER 2012/08 *Guidelines for Estimation of Shear Wave Velocity*. Bernard R. Wair, Jason T. DeJong, and Thomas Shantz. December 2012.

PEER 2012/07 *Earthquake Engineering for Resilient Communities: 2012 PEER Internship Program Research Report Collection.* Heidi Tremayne (Editor), Stephen A. Mahin (Editor), Collin Anderson, Dustin Cook, Michael Erceg, Carlos Esparza, Jose Jimenez, Dorian Krausz, Andrew Lo, Stephanie Lopez, Nicole McCurdy, Paul Shipman, Alexander Strum, Eduardo Vega. December 2012.

PEER 2012/06 *Fragilities for Precarious Rocks at Yucca Mountain.* Matthew D. Purvance, Rasool Anooshehpoor, and James N. Brune. December 2012.

PEER 2012/05 *Development of Simplified Analysis Procedure for Piles in Laterally Spreading Layered Soils.* Christopher R. McGann, Pedro Arduino, and Peter Mackenzie–Helnwein. December 2012.

PEER 2012/04 *Unbonded Pre-Tensioned Columns for Bridges in Seismic Regions.* Phillip M. Davis, Todd M. Janes, Marc O. Eberhard, and John F. Stanton. December 2012.

PEER 2012/03 *Experimental and Analytical Studies on Reinforced Concrete Buildings with Seismically Vulnerable Beam-Column Joints*. Sangjoon Park and Khalid M. Mosalam. October 2012.

PEER 2012/02 *Seismic Performance of Reinforced Concrete Bridges Allowed to Uplift during Multi-Directional Excitation*. Andres Oscar Espinoza and Stephen A. Mahin. July 2012.

PEER 2012/01 *Spectral Damping Scaling Factors for Shallow Crustal Earthquakes in Active Tectonic Regions.* Sanaz Rezaeian, Yousef Bozorgnia, I. M. Idriss, Kenneth Campbell, Norman Abrahamson, and Walter Silva. July 2012.

PEER 2011/10 *Earthquake Engineering for Resilient Communities: 2011 PEER Internship Program Research Report Collection.* Heidi Faison and Stephen A. Mahin, Editors. December 2011.

PEER 2011/09 *Calibration of Semi-Stochastic Procedure for Simulating High-Frequency Ground Motions*. Jonathan P. Stewart, Emel Seyhan, and Robert W. Graves. December 2011.

PEER 2011/08 *Water Supply in regard to Fire Following Earthquake*. Charles Scawthorn. November 2011.

PEER 2011/07 *Seismic Risk Management in Urban Areas*. Proceedings of a U.S.-Iran-Turkey Seismic Workshop. September 2011.

PEER 2011/06 *The Use of Base Isolation Systems to Achieve Complex Seismic Performance Objectives*. Troy A. Morgan and Stephen A. Mahin. July 2011.

PEER 2011/05 *Case Studies of the Seismic Performance of Tall Buildings Designed by Alternative Means*. Task 12 Report for the Tall Buildings Initiative. Jack Moehle, Yousef Bozorgnia, Nirmal Jayaram, Pierson Jones, Mohsen Rahnama, Nilesh Shome, Zeynep Tuna, John Wallace, Tony Yang, and Farzin Zareian. July 2011.

PEER 2011/04 *Recommended Design Practice for Pile Foundations in Laterally Spreading Ground.* Scott A. Ashford, Ross W. Boulanger, and Scott J. Brandenberg. June 2011.

PEER 2011/03 *New Ground Motion Selection Procedures and Selected Motions for the PEER Transportation Research Program.* Jack W. Baker, Ting Lin, Shrey K. Shahi, and Nirmal Jayaram. March 2011.

PEER 2011/02 *A Bayesian Network Methodology for Infrastructure Seismic Risk Assessment and Decision Support*. Michelle T. Bensi, Armen Der Kiureghian, and Daniel Straub. March 2011.

PEER 2011/01 *Demand Fragility Surfaces for Bridges in Liquefied and Laterally Spreading Ground.* Scott J. Brandenberg, Jian Zhang, Pirooz Kashighandi, Yili Huo, and Minxing Zhao. March 2011.

PEER 2010/05 *Guidelines for Performance-Based Seismic Design of Tall Buildings*. Developed by the Tall Buildings Initiative. November 2010.

PEER 2010/04 *Application Guide for the Design of Flexible and Rigid Bus Connections between Substation Equipment Subjected to Earthquakes*. Jean-Bernard Dastous and Armen Der Kiureghian. September 2010.

PEER 2010/03 *Shear Wave Velocity as a Statistical Function of Standard Penetration Test Resistance and Vertical Effective Stress at Caltrans Bridge Sites*. Scott J. Brandenberg, Naresh Bellana, and Thomas Shantz. June 2010.

PEER 2010/02 *Stochastic Modeling and Simulation of Ground Motions for Performance-Based Earthquake Engineering.* Sanaz Rezaeian and Armen Der Kiureghian. June 2010.

PEER 2010/01 *Structural Response and Cost Characterization of Bridge Construction Using Seismic Performance Enhancement Strategies*. Ady Aviram, Božidar Stojadinović, Gustavo J. Parra-Montesinos, and Kevin R. Mackie. March 2010.

PEER 2009/03 *The Integration of Experimental and Simulation Data in the Study of Reinforced Concrete Bridge Systems Including Soil-Foundation-Structure Interaction.* Matthew Dryden and Gregory L. Fenves. November 2009.

PEER 2009/02 *Improving Earthquake Mitigation through Innovations and Applications in Seismic Science, Engineering, Communication, and Response*. Proceedings of a U.S.-Iran Seismic Workshop. October 2009.

PEER 2009/01 *Evaluation of Ground Motion Selection and Modification Methods: Predicting Median Interstory Drift Response of Buildings*. Curt B. Haselton, Editor. June 2009.

PEER 2008/10 *Technical Manual for Strata.* Albert R. Kottke and Ellen M. Rathje. February 2009.

PEER 2008/09 *NGA Model for Average Horizontal Component of Peak Ground Motion and Response Spectra.* Brian S.-J. Chiou and Robert R. Youngs. November 2008.

PEER 2008/08 *Toward Earthquake-Resistant Design of Concentrically Braced Steel Structures*. Patxi Uriz and Stephen A. Mahin. November 2008.

PEER 2008/07 *Using OpenSees for Performance-Based Evaluation of Bridges on Liquefiable Soils*. Stephen L. Kramer, Pedro Arduino, and HyungSuk Shin. November 2008.

PEER 2008/06 *Shaking Table Tests and Numerical Investigation of Self-Centering Reinforced Concrete Bridge Columns*. Hyung IL Jeong, Junichi Sakai, and Stephen A. Mahin. September 2008.

PEER 2008/05 *Performance-Based Earthquake Engineering Design Evaluation Procedure for Bridge Foundations Undergoing Liquefaction-Induced Lateral Ground Displacement*. Christian A. Ledezma and Jonathan D. Bray. August 2008.

PEER 2008/04 *Benchmarking of Nonlinear Geotechnical Ground Response Analysis Procedures*. Jonathan P. Stewart, Annie On-Lei Kwok, Youssef M. A. Hashash, Neven Matasovic, Robert Pyke, Zhiliang Wang, and Zhaohui Yang. August 2008.

PEER 2008/03 *Guidelines for Nonlinear Analysis of Bridge Structures in California.* Ady Aviram, Kevin R. Mackie, and Božidar Stojadinović. August 2008.

PEER 2008/02 *Treatment of Uncertainties in Seismic-Risk Analysis of Transportation Systems*. Evangelos Stergiou and Anne S. Kiremidjian. July 2008.

PEER 2008/01 *Seismic Performance Objectives for Tall Buildings.* William T. Holmes, Charles Kircher, William Petak, and Nabih Youssef. August 2008.

PEER 2007/12 *An Assessment to Benchmark the Seismic Performance of a Code-Conforming Reinforced Concrete Moment-Frame Building.* Curt Haselton, Christine A. Goulet, Judith Mitrani-Reiser, James L. Beck, Gregory G. Deierlein, Keith A. Porter, Jonathan P. Stewart, and Ertugrul Taciroglu. August 2008.

PEER 2007/11 *Bar Buckling in Reinforced Concrete Bridge Columns.* Wayne A. Brown, Dawn E. Lehman, and John F. Stanton. February 2008.

PEER 2007/10 *Computational Modeling of Progressive Collapse in Reinforced Concrete Frame Structures*. Mohamed M. Talaat and Khalid M. Mosalam. May 2008.

PEER 2007/09 *Integrated Probabilistic Performance-Based Evaluation of Benchmark Reinforced Concrete Bridges*. Kevin R. Mackie, John-Michael Wong, and Božidar Stojadinović. January 2008.

PEER 2007/08 *Assessing Seismic Collapse Safety of Modern Reinforced Concrete Moment-Frame Buildings*. Curt B. Haselton and Gregory G. Deierlein. February 2008.

PEER 2007/07 *Performance Modeling Strategies for Modern Reinforced Concrete Bridge Columns*. Michael P. Berry and Marc O. Eberhard. April 2008.

PEER 2007/06 *Development of Improved Procedures for Seismic Design of Buried and Partially Buried Structures*. Linda Al Atik and Nicholas Sitar. June 2007.

PEER 2007/05 *Uncertainty and Correlation in Seismic Risk Assessment of Transportation Systems*. Renee G. Lee and Anne S. Kiremidjian. July 2007.

PEER 2007/04 *Numerical Models for Analysis and Performance-Based Design of Shallow Foundations Subjected to Seismic Loading.* Sivapalan Gajan, Tara C. Hutchinson, Bruce L. Kutter, Prishati Raychowdhury, José A. Ugalde, and Jonathan P. Stewart. May 2008.

PEER 2007/03 *Beam-Column Element Model Calibrated for Predicting Flexural Response Leading to Global Collapse of RC Frame Buildings*. Curt B. Haselton, Abbie B. Liel, Sarah Taylor Lange, and Gregory G. Deierlein. May 2008.

PEER 2007/02 *Campbell-Bozorgnia NGA Ground Motion Relations for the Geometric Mean Horizontal Component of Peak and Spectral Ground Motion Parameters*. Kenneth W. Campbell and Yousef Bozorgnia. May 2007.

PEER 2007/01 *Boore-Atkinson NGA Ground Motion Relations for the Geometric Mean Horizontal Component of Peak and Spectral Ground Motion Parameters*. David M. Boore and Gail M. Atkinson. May 2007.

PEER 2006/12 Societal Implications of Performance-Based Earthquake Engineering. Peter J. May. May 2007.

PEER 2006/11 *Probabilistic Seismic Demand Analysis Using Advanced Ground Motion Intensity Measures, Attenuation Relationships, and Near-Fault Effects*. Polsak Tothong and C. Allin Cornell. March 2007.

PEER 2006/10 *Application of the PEER PBEE Methodology to the I-880 Viaduct*. Sashi Kunnath. February 2007.

PEER 2006/09 *Quantifying Economic Losses from Travel Forgone Following a Large Metropolitan Earthquake*. James Moore, Sungbin Cho, Yue Yue Fan, and Stuart Werner. November 2006.

PEER 2006/08 *Vector-Valued Ground Motion Intensity Measures for Probabilistic Seismic Demand Analysis*. Jack W. Baker and C. Allin Cornell. October 2006.

PEER 2006/07 *Analytical Modeling of Reinforced Concrete Walls for Predicting Flexural and Coupled–Shear-Flexural Responses*. Kutay Orakcal, Leonardo M. Massone, and John W. Wallace. October 2006.

PEER 2006/06 *Nonlinear Analysis of a Soil-Drilled Pier System under Static and Dynamic Axial Loading*. Gang Wang and Nicholas Sitar. November 2006.

PEER 2006/05 *Advanced Seismic Assessment Guidelines*. Paolo Bazzurro, C. Allin Cornell, Charles Menun, Maziar Motahari, and Nicolas Luco. September 2006.

PEER 2006/04 *Probabilistic Seismic Evaluation of Reinforced Concrete Structural Components and Systems*. Tae Hyung Lee and Khalid M. Mosalam. August 2006.

PEER 2006/03 *Performance of Lifelines Subjected to Lateral Spreading.* Scott A. Ashford and Teerawut Juirnarongrit. July 2006.

PEER 2006/02 *Pacific Earthquake Engineering Research Center Highway Demonstration Project.* Anne Kiremidjian, James Moore, Yue Yue Fan, Nesrin Basoz, Ozgur Yazali, and Meredith Williams. April 2006.

PEER 2006/01 *Bracing Berkeley. A Guide to Seismic Safety on the UC Berkeley Campus*. Mary C. Comerio, Stephen Tobriner, and Ariane Fehrenkamp. January 2006.

PEER 2005/17 *Earthquake Simulation Tests on Reducing Residual Displacements of Reinforced Concrete Bridges*. Junichi Sakai, Stephen A Mahin, and Andres Espinoza. December 2005.

PEER 2005/16 *Seismic Response and Reliability of Electrical Substation Equipment and Systems*. Junho Song, Armen Der Kiureghian, and Jerome L. Sackman. April 2006.

PEER 2005/15 *CPT-Based Probabilistic Assessment of Seismic Soil Liquefaction Initiation.* R. E. S. Moss, R. B. Seed, R. E. Kayen, J. P. Stewart, and A. Der Kiureghian. April 2006.

PEER 2005/14 *Workshop on Modeling of Nonlinear Cyclic Load-Deformation Behavior of Shallow Foundations*. Bruce L. Kutter, Geoffrey Martin, Tara Hutchinson, Chad Harden, Sivapalan Gajan, and Justin Phalen. March 2006.

PEER 2005/13 *Stochastic Characterization and Decision Bases under Time-Dependent Aftershock Risk in Performance-Based Earthquake Engineering*. Gee Liek Yeo and C. Allin Cornell. July 2005.

PEER 2005/12 *PEER Testbed Study on a Laboratory Building: Exercising Seismic Performance Assessment*. Mary C. Comerio, Editor. November 2005.

PEER 2005/11 *Van Nuys Hotel Building Testbed Report: Exercising Seismic Performance Assessment*. Helmut Krawinkler, Editor. October 2005.

PEER 2005/10 *First NEES/E-Defense Workshop on Collapse Simulation of Reinforced Concrete Building Structures*. September 2005.

PEER 2005/09 *Test Applications of Advanced Seismic Assessment Guidelines*. Joe Maffei, Karl Telleen, Danya Mohr, William Holmes, and Yuki Nakayama. August 2006.

PEER 2005/08 *Damage Accumulation in Lightly Confined Reinforced Concrete Bridge Columns*. R. Tyler Ranf, Jared M. Nelson, Zach Price, Marc O. Eberhard, and John F. Stanton. April 2006.

PEER 2005/07 *Experimental and Analytical Studies on the Seismic Response of Freestanding and Anchored Laboratory Equipment.* Dimitrios Konstantinidis and Nicos Makris. January 2005.

PEER 2005/06 *Global Collapse of Frame Structures under Seismic Excitations*. Luis F. Ibarra and Helmut Krawinkler. September 2005.

PEER 2005//05 *Performance Characterization of Bench- and Shelf-Mounted Equipment.* Samit Ray Chaudhuri and Tara C. Hutchinson. May 2006.

PEER 2005/04 *Numerical Modeling of the Nonlinear Cyclic Response of Shallow Foundations.* Chad Harden, Tara Hutchinson, Geoffrey R. Martin, and Bruce L. Kutter. August 2005.

PEER 2005/03 *A Taxonomy of Building Components for Performance-Based Earthquake Engineering.* Keith A. Porter. September 2005.

PEER 2005/02 *Fragility Basis for California Highway Overpass Bridge Seismic Decision Making*. Kevin R. Mackie and Božidar Stojadinović. June 2005.

PEER 2005/01 *Empirical Characterization of Site Conditions on Strong Ground Motion.* Jonathan P. Stewart, Yoojoong Choi, and Robert W. Graves. June 2005.

PEER 2004/09 *Electrical Substation Equipment Interaction: Experimental Rigid Conductor Studies.* Christopher Stearns and André Filiatrault. February 2005.

PEER 2004/08 *Seismic Qualification and Fragility Testing of Line Break 550-kV Disconnect Switches*. Shakhzod M. Takhirov, Gregory L. Fenves, and Eric Fujisaki. January 2005.

PEER 2004/07 *Ground Motions for Earthquake Simulator Qualification of Electrical Substation Equipment.* Shakhzod M. Takhirov, Gregory L. Fenves, Eric Fujisaki, and Don Clyde. January 2005.

PEER 2004/06 *Performance-Based Regulation and Regulatory Regimes.* Peter J. May and Chris Koski. September 2004.

PEER 2004/05 *Performance-Based Seismic Design Concepts and Implementation: Proceedings of an International Workshop.* Peter Fajfar and Helmut Krawinkler, Editors. September 2004.

PEER 2004/04 *Seismic Performance of an Instrumented Tilt-up Wall Building.* James C. Anderson and Vitelmo V. Bertero. July 2004.

PEER 2004/03 *Evaluation and Application of Concrete Tilt-up Assessment Methodologies.* Timothy Graf and James O. Malley. October 2004.

PEER 2004/02 *Analytical Investigations of New Methods for Reducing Residual Displacements of Reinforced Concrete Bridge Columns.* Junichi Sakai and Stephen A. Mahin. August 2004.

PEER 2004/01 *Seismic Performance of Masonry Buildings and Design Implications.* Kerri Anne Taeko Tokoro, James C. Anderson, and Vitelmo V. Bertero. February 2004.

PEER 2003/18 *Performance Models for Flexural Damage in Reinforced Concrete Columns.* Michael Berry and Marc Eberhard. August 2003.

PEER 2003/17 *Predicting Earthquake Damage in Older Reinforced Concrete Beam-Column Joints.* Catherine Pagni and Laura Lowes. October 2004.

PEER 2003/16 *Seismic Demands for Performance-Based Design of Bridges.* Kevin Mackie and Božidar Stojadinović. August 2003.

PEER 2003/15 *Seismic Demands for Nondeteriorating Frame Structures and Their Dependence on Ground Motions.* Ricardo Antonio Medina and Helmut Krawinkler. May 2004.

PEER 2003/14 *Finite Element Reliability and Sensitivity Methods for Performance-Based Earthquake Engineering*. Terje Haukaas and Armen Der Kiureghian. April 2004.

PEER 2003/13 *Effects of Connection Hysteretic Degradation on the Seismic Behavior of Steel Moment-Resisting Frames.* Janise E. Rodgers and Stephen A. Mahin. March 2004.

PEER 2003/12 *Implementation Manual for the Seismic Protection of Laboratory Contents: Format and Case Studies*. William T. Holmes and Mary C. Comerio. October 2003.

PEER 2003/11 *Fifth U.S.-Japan Workshop on Performance-Based Earthquake Engineering Methodology for Reinforced Concrete Building Structures*. February 2004.

PEER 2003/10 *A Beam-Column Joint Model for Simulating the Earthquake Response of Reinforced Concrete Frames.* Laura N. Lowes, Nilanjan Mitra, and Arash Altoontash. February 2004.

PEER 2003/09 *Sequencing Repairs after an Earthquake: An Economic Approach.* Marco Casari and Simon J. Wilkie. April 2004.

PEER 2003/08 *A Technical Framework for Probability-Based Demand and Capacity Factor Design (DCFD) Seismic Formats.* Fatemeh Jalayer and C. Allin Cornell. November 2003.

PEER 2003/07 *Uncertainty Specification and Propagation for Loss Estimation Using FOSM Methods.* Jack W. Baker and C. Allin Cornell. September 2003.

PEER 2003/06 *Performance of Circular Reinforced Concrete Bridge Columns under Bidirectional Earthquake Loading.* Mahmoud M. Hachem, Stephen A. Mahin, and Jack P. Moehle. February 2003.

PEER 2003/05 *Response Assessment for Building-Specific Loss Estimation.* Eduardo Miranda and Shahram Taghavi. September 2003.

PEER 2003/04 *Experimental Assessment of Columns with Short Lap Splices Subjected to Cyclic Loads*. Murat Melek, John W. Wallace, and Joel Conte. April 2003.

PEER 2003/03 *Probabilistic Response Assessment for Building-Specific Loss Estimation*. Eduardo Miranda and Hesameddin Aslani. September 2003.

PEER 2003/02 *Software Framework for Collaborative Development of Nonlinear Dynamic Analysis Program*. Jun Peng and Kincho H. Law. September 2003.

PEER 2003/01 *Shake Table Tests and Analytical Studies on the Gravity Load Collapse of Reinforced Concrete Frames.* Kenneth John Elwood and Jack P. Moehle. November 2003.

PEER 2002/24 *Performance of Beam to Column Bridge Joints Subjected to a Large Velocity Pulse.* Natalie Gibson, André Filiatrault, and Scott A. Ashford. April 2002.

PEER 2002/23 *Effects of Large Velocity Pulses on Reinforced Concrete Bridge Columns.* Greg L. Orozco and Scott A. Ashford. April 2002.

PEER 2002/22 *Characterization of Large Velocity Pulses for Laboratory Testing.* Kenneth E. Cox and Scott A. Ashford. April 2002.

PEER 2002/21 *Fourth U.S.-Japan Workshop on Performance-Based Earthquake Engineering Methodology for Reinforced Concrete Building Structures*. December 2002.

PEER 2002/20 *Barriers to Adoption and Implementation of PBEE Innovations.* Peter J. May. August 2002.

PEER 2002/19 *Economic-Engineered Integrated Models for Earthquakes: Socioeconomic Impacts.* Peter Gordon, James E. Moore II, and Harry W. Richardson. July 2002.

PEER 2002/18 *Assessment of Reinforced Concrete Building Exterior Joints with Substandard Details.* Chris P. Pantelides, Jon Hansen, Justin Nadauld, and Lawrence D. Reaveley. May 2002.

PEER 2002/17 *Structural Characterization and Seismic Response Analysis of a Highway Overcrossing Equipped with Elastomeric Bearings and Fluid Dampers: A Case Study*. Nicos Makris and Jian Zhang. November 2002.

PEER 2002/16 *Estimation of Uncertainty in Geotechnical Properties for Performance-Based Earthquake Engineering.* Allen L. Jones, Steven L. Kramer, and Pedro Arduino. December 2002.

PEER 2002/15 *Seismic Behavior of Bridge Columns Subjected to Various Loading Patterns*. Asadollah Esmaeily-Gh. and Yan Xiao. December 2002.

PEER 2002/14 *Inelastic Seismic Response of Extended Pile Shaft Supported Bridge Structures.* T.C. Hutchinson, R.W. Boulanger, Y.H. Chai, and I.M. Idriss. December 2002.

PEER 2002/13 *Probabilistic Models and Fragility Estimates for Bridge Components and Systems.* Paolo Gardoni, Armen Der Kiureghian, and Khalid M. Mosalam. June 2002.

PEER 2002/12 *Effects of Fault Dip and Slip Rake on Near-Source Ground Motions: Why Chi-Chi Was a Relatively Mild M7.6 Earthquake*. Brad T. Aagaard, John F. Hall, and Thomas H. Heaton. December 2002.

PEER 2002/11 *Analytical and Experimental Study of Fiber-Reinforced Strip Isolators*. James M. Kelly and Shakhzod M. Takhirov. September 2002.

PEER 2002/10 *Centrifuge Modeling of Settlement and Lateral Spreading with Comparisons to Numerical Analyses***.** Sivapalan Gajan and Bruce L. Kutter. January 2003.

PEER 2002/09 *Documentation and Analysis of Field Case Histories of Seismic Compression during the 1994 Northridge, California, Earthquake*. Jonathan P. Stewart, Patrick M. Smith, Daniel H. Whang, and Jonathan D. Bray. October 2002.

PEER 2002/08 *Component Testing, Stability Analysis and Characterization of Buckling-Restrained Unbonded Braces^{TM}*. Cameron Black, Nicos Makris, and Ian Aiken. September 2002.

PEER 2002/07 *Seismic Performance of Pile-Wharf Connections.* Charles W. Roeder, Robert Graff, Jennifer Soderstrom, and Jun Han Yoo. December 2001.

PEER 2002/06 *The Use of Benefit-Cost Analysis for Evaluation of Performance-Based Earthquake Engineering Decisions*. Richard O. Zerbe and Anthony Falit-Baiamonte. September 2001.

PEER 2002/05 *Guidelines, Specifications, and Seismic Performance Characterization of Nonstructural Building Components and Equipment*. André Filiatrault, Constantin Christopoulos, and Christopher Stearns. September 2001.

PEER 2002/04 *Consortium of Organizations for Strong-Motion Observation Systems and the Pacific Earthquake Engineering Research Center Lifelines Program: Invited Workshop on Archiving and Web Dissemination of Geotechnical Data, 4–5 October 2001*. September 2002.

PEER 2002/03 *Investigation of Sensitivity of Building Loss Estimates to Major Uncertain Variables for the Van Nuys Testbed*. Keith A. Porter, James L. Beck, and Rustem V. Shaikhutdinov. August 2002.

PEER 2002/02 *The Third U.S.-Japan Workshop on Performance-Based Earthquake Engineering Methodology for Reinforced Concrete Building Structures*. July 2002.

PEER 2002/01 *Nonstructural Loss Estimation: The UC Berkeley Case Study.* Mary C. Comerio and John C. Stallmeyer. December 2001.

PEER 2001/16 *Statistics of SDF-System Estimate of Roof Displacement for Pushover Analysis of Buildings*. Anil K. Chopra, Rakesh K. Goel, and Chatpan Chintanapakdee. December 2001.

PEER 2001/15 *Damage to Bridges during the 2001 Nisqually Earthquake.* R. Tyler Ranf, Marc O. Eberhard, and Michael P. Berry. November 2001.

PEER 2001/14 *Rocking Response of Equipment Anchored to a Base Foundation.* Nicos Makris and Cameron J. Black. September 2001.

PEER 2001/13 *Modeling Soil Liquefaction Hazards for Performance-Based Earthquake Engineering*. Steven L. Kramer and Ahmed-W. Elgamal. February 2001.

PEER 2001/12 *Development of Geotechnical Capabilities in OpenSees*. Boris Jeremić. September 2001.

PEER 2001/11 *Analytical and Experimental Study of Fiber-Reinforced Elastomeric Isolators*. James M. Kelly and Shakhzod M. Takhirov. September 2001.

PEER 2001/10 *Amplification Factors for Spectral Acceleration in Active Regions*. Jonathan P. Stewart, Andrew H. Liu, Yoojoong Choi, and Mehmet B. Baturay. December 2001.

PEER 2001/09 *Ground Motion Evaluation Procedures for Performance-Based Design*. Jonathan P. Stewart, Shyh-Jeng Chiou, Jonathan D. Bray, Robert W. Graves, Paul G. Somerville, and Norman A. Abrahamson. September 2001.

PEER 2001/08 *Experimental and Computational Evaluation of Reinforced Concrete Bridge Beam-Column Connections for Seismic Performance*. Clay J. Naito, Jack P. Moehle, and Khalid M. Mosalam. November 2001.

PEER 2001/07 *The Rocking Spectrum and the Shortcomings of Design Guidelines*. Nicos Makris and Dimitrios Konstantinidis. August 2001.

PEER 2001/06 *Development of an Electrical Substation Equipment Performance Database for Evaluation of Equipment Fragilities*. Thalia Agnanos. April 1999.

PEER 2001/05 *Stiffness Analysis of Fiber-Reinforced Elastomeric Isolators*. Hsiang-Chuan Tsai and James M. Kelly. May 2001.

PEER 2001/04 *Organizational and Societal Considerations for Performance-Based Earthquake Engineering*. Peter J. May. April 2001.

PEER 2001/03 *A Modal Pushover Analysis Procedure to Estimate Seismic Demands for Buildings: Theory and Preliminary Evaluation*. Anil K. Chopra and Rakesh K. Goel. January 2001.

PEER 2001/02 *Seismic Response Analysis of Highway Overcrossings Including Soil-Structure Interaction*. Jian Zhang and Nicos Makris. March 2001.

PEER 2001/01 *Experimental Study of Large Seismic Steel Beam-to-Column Connections*. Egor P. Popov and Shakhzod M. Takhirov. November 2000.

PEER 2000/10 *The Second U.S.-Japan Workshop on Performance-Based Earthquake Engineering Methodology for Reinforced Concrete Building Structures*. March 2000.

PEER 2000/09 *Structural Engineering Reconnaissance of the August 17, 1999 Earthquake: Kocaeli (Izmit), Turkey*. Halil Sezen, Kenneth J. Elwood, Andrew S. Whittaker, Khalid Mosalam, John J. Wallace, and John F. Stanton. December 2000.

PEER 2000/08 *Behavior of Reinforced Concrete Bridge Columns Having Varying Aspect Ratios and Varying Lengths of Confinement*. Anthony J. Calderone, Dawn E. Lehman, and Jack P. Moehle. January 2001.

PEER 2000/07 *Cover-Plate and Flange-Plate Reinforced Steel Moment-Resisting Connections*. Taejin Kim, Andrew S. Whittaker, Amir S. Gilani, Vitelmo V. Bertero, and Shakhzod M. Takhirov. September 2000.

PEER 2000/06 *Seismic Evaluation and Analysis of 230-kV Disconnect Switches*. Amir S. J. Gilani, Andrew S. Whittaker, Gregory L. Fenves, Chun-Hao Chen, Henry Ho, and Eric Fujisaki. July 2000.

PEER 2000/05 *Performance-Based Evaluation of Exterior Reinforced Concrete Building Joints for Seismic Excitation*. Chandra Clyde, Chris P. Pantelides, and Lawrence D. Reaveley. July 2000.

PEER 2000/04 *An Evaluation of Seismic Energy Demand: An Attenuation Approach*. Chung-Che Chou and Chia-Ming Uang. July 1999.

PEER 2000/03 *Framing Earthquake Retrofitting Decisions: The Case of Hillside Homes in Los Angeles*. Detlof von Winterfeldt, Nels Roselund, and Alicia Kitsuse. March 2000.

PEER 2000/02 *U.S.-Japan Workshop on the Effects of Near-Field Earthquake Shaking*. Andrew Whittaker, Editor. July 2000.

PEER 2000/01 *Further Studies on Seismic Interaction in Interconnected Electrical Substation Equipment*. Armen Der Kiureghian, Kee-Jeung Hong, and Jerome L. Sackman. November 1999.

PEER 1999/14 *Seismic Evaluation and Retrofit of 230-kV Porcelain Transformer Bushings*. Amir S. Gilani, Andrew S. Whittaker, Gregory L. Fenves, and Eric Fujisaki. December 1999.

PEER 1999/13 *Building Vulnerability Studies: Modeling and Evaluation of Tilt-up and Steel Reinforced Concrete Buildings*. John W. Wallace, Jonathan P. Stewart, and Andrew S. Whittaker, Editors. December 1999.

PEER 1999/12 *Rehabilitation of Nonductile RC Frame Building Using Encasement Plates and Energy-Dissipating Devices*. Mehrdad Sasani, Vitelmo V. Bertero, James C. Anderson. December 1999.

PEER 1999/11 *Performance Evaluation Database for Concrete Bridge Components and Systems under Simulated Seismic Loads*. Yael D. Hose and Frieder Seible. November 1999.

PEER 1999/10 *U.S.-Japan Workshop on Performance-Based Earthquake Engineering Methodology for Reinforced Concrete Building Structures*. December 1999.

PEER 1999/09 *Performance Improvement of Long Period Building Structures Subjected to Severe Pulse-Type Ground Motions*. James C. Anderson, Vitelmo V. Bertero, and Raul Bertero. October 1999.

PEER 1999/08 *Envelopes for Seismic Response Vectors*. Charles Menun and Armen Der Kiureghian. July 1999.

PEER 1999/07 *Documentation of Strengths and Weaknesses of Current Computer Analysis Methods for Seismic Performance of Reinforced Concrete Members*. William F. Cofer. November 1999.

PEER 1999/06 *Rocking Response and Overturning of Anchored Equipment under Seismic Excitations*. Nicos Makris and Jian Zhang. November 1999.

PEER 1999/05 *Seismic Evaluation of 550 kV Porcelain Transformer Bushings*. Amir S. Gilani, Andrew S. Whittaker, Gregory L. Fenves, and Eric Fujisaki. October 1999.

PEER 1999/04 *Adoption and Enforcement of Earthquake Risk-Reduction Measures.* Peter J. May, Raymond J. Burby, T. Jens Feeley, and Robert Wood. August 1999.

PEER 1999/03 *Task 3 Characterization of Site Response General Site Categories*. Adrian Rodriguez-Marek, Jonathan D. Bray and Norman Abrahamson. February 1999.

PEER 1999/02 *Capacity-Demand-Diagram Methods for Estimating Seismic Deformation of Inelastic Structures: SDF Systems*. Anil K. Chopra and Rakesh Goel. April 1999.

PEER 1999/01 *Interaction in Interconnected Electrical Substation Equipment Subjected to Earthquake Ground Motions*. Armen Der Kiureghian, Jerome L. Sackman, and Kee-Jeung Hong. February 1999.

PEER 1998/08 *Behavior and Failure Analysis of a Multiple-Frame Highway Bridge in the 1994 Northridge Earthquake*. Gregory L. Fenves and Michael Ellery. December 1998.

PEER 1998/07 *Empirical Evaluation of Inertial Soil-Structure Interaction Effects*. Jonathan P. Stewart, Raymond B. Seed, and Gregory L. Fenves. November 1998.

PEER 1998/06 *Effect of Damping Mechanisms on the Response of Seismic Isolated Structures*. Nicos Makris and Shih-Po Chang. November 1998.

PEER 1998/05 *Rocking Response and Overturning of Equipment under Horizontal Pulse-Type Motions*. Nicos Makris and Yiannis Roussos. October 1998.

PEER 1998/04 *Pacific Earthquake Engineering Research Invitational Workshop Proceedings, May 14–15, 1998: Defining the Links between Planning, Policy Analysis, Economics and Earthquake Engineering*. Mary Comerio and Peter Gordon. September 1998.

PEER 1998/03 *Repair/Upgrade Procedures for Welded Beam to Column Connections*. James C. Anderson and Xiaojing Duan. May 1998.

PEER 1998/02 *Seismic Evaluation of 196 kV Porcelain Transformer Bushings*. Amir S. Gilani, Juan W. Chavez, Gregory L. Fenves, and Andrew S. Whittaker. May 1998.

PEER 1998/01 *Seismic Performance of Well-Confined Concrete Bridge Columns*. Dawn E. Lehman and Jack P. Moehle. December 2000.

PEER REPORTS: ONE HUNDRED SERIES

PEER 2012/103 *Performance-Based Seismic Demand Assessment of Concentrically Braced Steel Frame Buildings.* Chui-Hsin Chen and Stephen A. Mahin. December 2012.

PEER 2012/102 *Procedure to Restart an Interrupted Hybrid Simulation: Addendum to PEER Report 2010/103.* Vesna Terzic and Bozidar Stojadinovic. October 2012.

PEER 2012/101 *Mechanics of Fiber Reinforced Bearings.* James M. Kelly and Andrea Calabrese. February 2012.

PEER 2011/107 *Nonlinear Site Response and Seismic Compression at Vertical Array Strongly Shaken by 2007 Niigata-ken Chuetsu-oki Earthquake.* Eric Yee, Jonathan P. Stewart, and Kohji Tokimatsu. December 2011.

PEER 2011/106 *Self Compacting Hybrid Fiber Reinforced Concrete Composites for Bridge Columns.* Pardeep Kumar, Gabriel Jen, William Trono, Marios Panagiotou, and Claudia Ostertag. September 2011.

PEER 2011/105 *Stochastic Dynamic Analysis of Bridges Subjected to Spacially Varying Ground Motions.* Katerina Konakli and Armen Der Kiureghian. August 2011.

PEER 2011/104 *Design and Instrumentation of the 2010 E-Defense Four-Story Reinforced Concrete and Post-Tensioned Concrete Buildings.* Takuya Nagae, Kenichi Tahara, Taizo Matsumori, Hitoshi Shiohara, Toshimi Kabeyasawa, Susumu Kono, Minehiro Nishiyama (Japanese Research Team) and John Wallace, Wassim Ghannoum, Jack Moehle, Richard Sause, Wesley Keller, Zeynep Tuna (U.S. Research Team). June 2011.

PEER 2011/103 *In-Situ Monitoring of the Force Output of Fluid Dampers: Experimental Investigation.* Dimitrios Konstantinidis, James M. Kelly, and Nicos Makris. April 2011.

PEER 2011/102 *Ground-Motion Prediction Equations 1964–2010.* John Douglas. April 2011.

PEER 2011/101 *Report of the Eighth Planning Meeting of NEES/E-Defense Collaborative Research on Earthquake Engineering.* Convened by the Hyogo Earthquake Engineering Research Center (NIED), NEES Consortium, Inc. February 2011.

PEER 2010/111 *Modeling and Acceptance Criteria for Seismic Design and Analysis of Tall Buildings.* Task 7 Report for the Tall Buildings Initiative - Published jointly by the Applied Technology Council. October 2010.

PEER 2010/110 *Seismic Performance Assessment and Probabilistic Repair Cost Analysis of Precast Concrete Cladding Systems for Multistory Buildlings.* Jeffrey P. Hunt and Božidar Stojadinovic. November 2010.

PEER 2010/109 *Report of the Seventh Joint Planning Meeting of NEES/E-Defense Collaboration on Earthquake Engineering. Held at the E-Defense, Miki, and Shin-Kobe, Japan, September 18–19, 2009.* August 2010.

PEER 2010/108 *Probabilistic Tsunami Hazard in California.* Hong Kie Thio, Paul Somerville, and Jascha Polet, preparers. October 2010.

PEER 2010/107 *Performance and Reliability of Exposed Column Base Plate Connections for Steel Moment-Resisting Frames.* Ady Aviram, Božidar Stojadinovic, and Armen Der Kiureghian. August 2010.

PEER 2010/106 *Verification of Probabilistic Seismic Hazard Analysis Computer Programs.* Patricia Thomas, Ivan Wong, and Norman Abrahamson. May 2010.

PEER 2010/105 *Structural Engineering Reconnaissance of the April 6, 2009, Abruzzo, Italy, Earthquake, and Lessons Learned.* M. Selim Günay and Khalid M. Mosalam. April 2010.

PEER 2010/104 *Simulating the Inelastic Seismic Behavior of Steel Braced Frames, Including the Effects of Low-Cycle Fatigue.* Yuli Huang and Stephen A. Mahin. April 2010.

PEER 2010/103 *Post-Earthquake Traffic Capacity of Modern Bridges in California.* Vesna Terzic and Božidar Stojadinović. March 2010.

PEER 2010/102 *Analysis of Cumulative Absolute Velocity (CAV) and JMA Instrumental Seismic Intensity (I_{JMA}) Using the PEER–NGA Strong Motion Database.* Kenneth W. Campbell and Yousef Bozorgnia. February 2010.

PEER 2010/101 *Rocking Response of Bridges on Shallow Foundations.* Jose A. Ugalde, Bruce L. Kutter, and Boris Jeremic. April 2010.

PEER 2009/109 *Simulation and Performance-Based Earthquake Engineering Assessment of Self-Centering Post-Tensioned Concrete Bridge Systems.* Won K. Lee and Sarah L. Billington. December 2009.

PEER 2009/108 *PEER Lifelines Geotechnical Virtual Data Center.* J. Carl Stepp, Daniel J. Ponti, Loren L. Turner, Jennifer N. Swift, Sean Devlin, Yang Zhu, Jean Benoit, and John Bobbitt. September 2009.

PEER 2009/107 *Experimental and Computational Evaluation of Current and Innovative In-Span Hinge Details in Reinforced Concrete Box-Girder Bridges: Part 2: Post-Test Analysis and Design Recommendations.* Matias A. Hube and Khalid M. Mosalam. December 2009.

PEER 2009/106 *Shear Strength Models of Exterior Beam-Column Joints without Transverse Reinforcement.* Sangjoon Park and Khalid M. Mosalam. November 2009.

PEER 2009/105 *Reduced Uncertainty of Ground Motion Prediction Equations through Bayesian Variance Analysis.* Robb Eric S. Moss. November 2009.

PEER 2009/104 *Advanced Implementation of Hybrid Simulation.* Andreas H. Schellenberg, Stephen A. Mahin, Gregory L. Fenves. November 2009.

PEER 2009/103 *Performance Evaluation of Innovative Steel Braced Frames.* T. Y. Yang, Jack P. Moehle, and Božidar Stojadinovic. August 2009.

PEER 2009/102 *Reinvestigation of Liquefaction and Nonliquefaction Case Histories from the 1976 Tangshan Earthquake.* Robb Eric Moss, Robert E. Kayen, Liyuan Tong, Songyu Liu, Guojun Cai, and Jiaer Wu. August 2009.

PEER 2009/101 *Report of the First Joint Planning Meeting for the Second Phase of NEES/E-Defense Collaborative Research on Earthquake Engineering.* Stephen A. Mahin et al. July 2009.

PEER 2008/104 *Experimental and Analytical Study of the Seismic Performance of Retaining Structures.* Linda Al Atik and Nicholas Sitar. January 2009.

PEER 2008/103 *Experimental and Computational Evaluation of Current and Innovative In-Span Hinge Details in Reinforced Concrete Box-Girder Bridges. Part 1: Experimental Findings and Pre-Test Analysis.* Matias A. Hube and Khalid M. Mosalam. January 2009.

PEER 2008/102 *Modeling of Unreinforced Masonry Infill Walls Considering In-Plane and Out-of-Plane Interaction.* Stephen Kadysiewski and Khalid M. Mosalam. January 2009.

PEER 2008/101 *Seismic Performance Objectives for Tall Buildings.* William T. Holmes, Charles Kircher, William Petak, and Nabih Youssef. August 2008.

PEER 2007/101 *Generalized Hybrid Simulation Framework for Structural Systems Subjected to Seismic Loading.* Tarek Elkhoraibi and Khalid M. Mosalam. July 2007.

PEER 2007/100 *Seismic Evaluation of Reinforced Concrete Buildings Including Effects of Masonry Infill Walls.* Alidad Hashemi and Khalid M. Mosalam. July 2007.

The Pacifi c Earthquake Engineering Research Center (PEER) is a multi-institutional research and education center with headquarters at the University of California, Berkeley. Investigators from over 20 universities, several consulting companies, and researchers at various state and federal government agencies contribute to research programs focused on performance-based earthquake engineering.

These research programs aim to identify and reduce the risks from major earthquakes to life safety and to the economy by including research in a wide variety of disciplines including structural and geotechnical engineering, geology/seismology, lifelines, transportation, architecture, economics, risk management, and public policy.

PEER is supported by federal, state, local, and regional agencies, together with industry partners.

PEER Core Institutions

University of California, Berkeley (Lead Institution)
California Institute of Technology
Oregon State University
Stanford University
University of California, Davis
University of California, Irvine
University of California, Los Angeles
University of California, San Diego
University of Nevada, Reno
University of Southern California
University of Washington

PEER reports can be ordered at https://peer.berkeley.edu/peer-reports or by contacting

Pacific Earthquake Engineering Research Center
University of California, Berkeley
325 Davis Hall, Mail Code 1792
Berkeley, CA 94720-1792
Tel: 510-642-3437
Email: peer_center@berkeley.edu

ISSN 2770-8314
https://doi.org/10.55461/SVKS9397